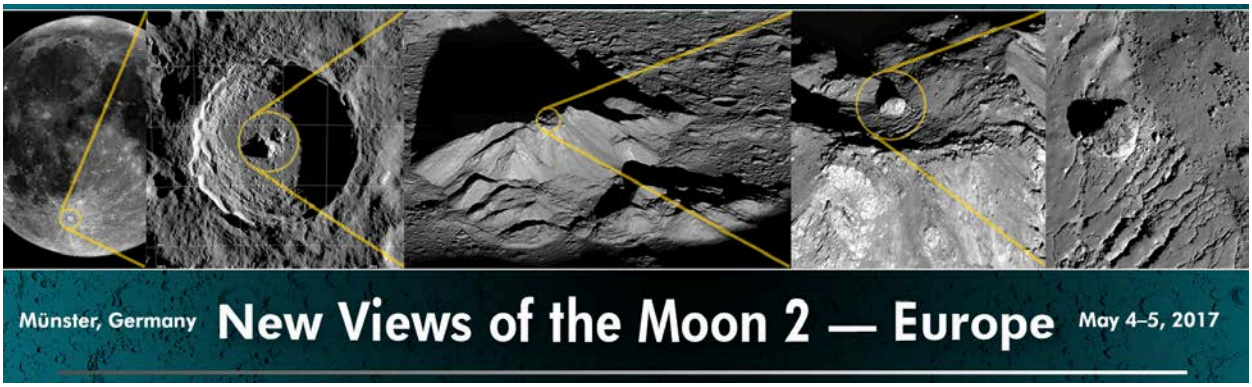

Program and Abstracts

LUNAR AND PLANETARY INSTITUTE

USRA

New Views of the Moon 2 — Europe

May 4–5, 2017 • Münster, Germany

Organizers

Lunar and Planetary Institute
University of Münster

Conveners

Clive Neal
University of Notre Dame

Harald Hiesinger
Westfälische Wilhelms-Universität, Institut für Planetologie, University of Münster

Organizing Committee

Lisa Gaddis, *U.S. Geological Survey*
Bradley Jolliff, *Washington University*
Samuel Lawrence, *NASA Johnson Space Center*
Steve Mackwell, *Universities Space Research Association*
Clive Neal, *University of Notre Dame*
Chip Shearer, *University of New Mexico*

Lunar and Planetary Institute 3600 Bay Area Boulevard Houston TX 77058-1113

Abstracts for this workshop are available via the workshop website at

www.hou.usra.edu/meetings/newviews2017/

Abstracts can be cited as

Author A. B. and Author C. D. (2016) Title of abstract. In *New Views of the Moon 2 – Europe,* Abstract #XXXX. LPI Contribution No. 1988, Lunar and Planetary Institute, Houston.

Guide to Sessions

Thursday, May 4, 2017

8:30 a.m.	Aula Conference Room	Origin, Differentiation, Structure, Meteorites
10:45 a.m.	Aula Conference Room	Lunar Magmatism
1:30 p.m.	Aula Conference Room	Lunar Crust and Tectonics
3:45 p.m.	Aula Conference Room	Lunar Volatiles
5:30 p.m.	Foyer	Poster Session

Friday, May 5, 2017

8:30 a.m.	Aula Conference Room	Impact Features, Processes, Chronology
10:45 a.m.	Aula Conference Room	Lunar Exosphere and Space Weathering
1:30 p.m.	Aula Conference Room	Lunar Resources, Surface Operations, Regolith
3:15 p.m.	Aula Conference Room	Lunar Magnetism

Program

Thursday, May 4, 2017
ORIGIN, DIFFERENTIATION, STRUCTURE, METEORITES
8:30 a.m. Aula Conference Room

Topics include discussion of the origin, differentiation, and structure of the Moon and chapter summaries covering these topics and lunar meteorites.

Chairs: **Carle Pieters**
Jeffrey Andrews-Hanna

8:30 a.m. Magna T. * Dauphas N. Righter K. Camp R.
Stable Isotope Constraints on the Formation of Moon **[#6044]**
The development of high-precision techniques to measure stable isotope compositions of a number of elements which, in the past, were considered homogeneous, implicated a new fresh look at the origin of Moon.

8:45 a.m. Kleine T. * Kruijer T. S. Burkhardt C.
Isotopic Constraints on the Origin of the Moon **[#6028]**
Isotopic constraints on the origin of the Moon will be reviewed, with a focus on 182W. Explaining the Earth-Moon similarity in 182W is a challenge to current lunar formation models.

9:00 a.m. Righter K. * Canup R. M. Dauphas N. Magna T.
Impact Origin of the Moon: New Data, New Models, and New Challenges **[#6042]**
We review the new data, models, and challenges for the origin of the Moon.

9:15 a.m. Andrews-Hanna J. C. * Weber R. C. Ishihara Y. Kamata S. Keane J. Kiefer W. S. Matsuyama I. Siegler M. Warren P.
Structure and Evolution of the Lunar Interior **[#6039]**
Recent significant improvements in both data and analysis techniques have yielded fundamental advances in our understanding of the structure and evolution of the lunar interior.

9:30 a.m. Ohtake M. O. * Yamamoto S. Y. Uemoto K. U. Ishihara Y. I.
Distribution and Composition of the Lunar Mantle Material and Its Implication **[#6016]**
We analyzed exposures of possible mantle material to identify their origin. Result indicates that vertical heterogeneity (olivine dominant and low-Ca pyroxene dominant layers) of the lunar mantle, which apparently correspond to the original depth.

9:45 a.m. Pieters C. M. *
Do the Olivine-Plagioclase Observations at Basins Imply Lunar Mantle Overturn? **[#6032]**
If the olivine at basins didn't come from the mantle directly, how DID it become associated with plagioclase in the lower crust?

10:00 a.m. BREAK

10:15 a.m. Gaffney A. M. * Warren P. H. Borg L. E. Draper D. S. Dygert N. Elkins-Tanton L. T. Joy K. Prissel T. Rapp J. Steenstra E. S. van Westrenen W.
Magmatic Evolution 1: Initial Differentiation **[#6040]**
This presentation is summary of the material that will be reviewed and synthesized in the Magmatic Evolution 1: Initial Differentiation chapter of the NVM2 volume.

10:30 a.m. Zeigler R. A. * Joy K. H. Arai T. Gross J. Korotev R. L. McCubbin F. M.
Lunar Meteorites: A Global Geochemical Dataset **[#6047]**
A summary of the status of the chapter on Lunar Meteorites.

Thursday, May 4, 2017
LUNAR MAGMATISM
10:45 a.m. Aula Conference Room

Topics include discussion of the magmatism of the Moon and chapter summaries covering this topic.

Chair: Clive Neal

10:45 a.m. Glotch T. D. * Elder C. M. Hayne P. O. Greenhagen B. T. Dhingra D. Kiefer W. S.
Overview of Silicic Magmatic Activity on the Moon **[#6052]**
We provide an overview of silicic volcanic activity on the Moon, as constrained by Diviner, M3, and GRAIL.

11:00 a.m. Demidova S. I. * Brandstätter F. Ntaflos Th. Kononkova N. N.
P-Bearing Olivines in Lunar Rocks: A New View on Lunar Phosphorus **[#6010]**
We report about finding of P-bearing olivines in lunar samples of Luna 16, 20, Apollo 14, and in Dhofar 025, 961, 287 lunar meteorites and discuss their implications for lunar petrology and geochemistry.

11:15 a.m. Shearer C. K. * Neal C. R. Gaddis L. Jolliff B. L. Head J. Hiesinger H. Bell A. S. Taylor G. J. Glotch T. D. Simon J. I. Prissel T. C. Magna T.
Magmatic Evolution 2: A New View of Post-Differentiation Magmatism **[#6045]**
This presentation involves the post-differentiation magmatism for the Moon.

11:30 a.m. DISCUSSION

Thursday, May 4, 2017
LUNAR CRUST AND TECTONICS
1:30 p.m. Aula Conference Room

Topics include discussion of the crust and tectonics of the Moon and chapter summaries covering these topics.

Chair: Amanda Nahm

1:30 p.m. Donaldson Hanna K. L. * Cheek L. C. Pieters C. M. Mustard J. F. Greenhagen B. T. Bowles N. E.
Remote Sensing Constraints on the Formation and Evolution of the Moon's Anorthositic Crust **[#6031]**
Remote sensing observations place important constraints on the formation and evolution of the Moon's anorthositic crust.

1:45 p.m. Clark J. D. * van der Bogert C. H. Hiesinger H.
Advances in Understanding the Formation, Distribution, and Ages of Lunar Lobate Scarps **[#6024]**
We applied crater counting methods on 40 lobate scarps, to investigate the range and distribution of scarp ages, and the effects of seismic shaking.

2:00 p.m. Nahm A. L. * Chierici V. R.
Ages of Dike Intrusions on the Moon **[#6007]**
The ages of dike-induced graben identified by Klimczak [2014] are determined through geologic mapping and crater counting to be as recent as 3.3 Ga.

2:15 p.m. Garrick-Bethell I. *
Long Wavelength Structure of the Lunar Crust: Tidal-Rotational Origins and Implications for True Polar Wander **[#6033]**
Understanding the origin and structure of the lunar crust at long wavelengths would help constrain the Moon's thermal history and orbital evolution. I present a review of work on these problems and future research directions.

2:30 p.m. Nahm A. L. * Johnson C. L.
Lunar Tectonics Chapter in the Updated New Views of the Moon 2 Volume **[#6021]**
We discuss the lunar tectonics chapter to be included in the New Views of the Moon 2 volume.

2:45 p.m. DISCUSSION

3:15 p.m. BREAK

Thursday, May 4, 2017
LUNAR VOLATILES
3:45 p.m. Aula Conference Room

Topics include discussion of lunar volatiles and a chapter summary covering this topic.

Chairs: **Dana Hurley**
Francis McCubbin

3:45 p.m. Anand M. *
An Integrated View of the History and Evolution of Volatiles in the Moon **[#6050]**
This abstract provides an integrated view of lunar interior volatiles based on recent data acquired on lunar samples and their implications for understanding the history and evolution of volatiles in the Moon.

4:00 p.m. Grumpe A. Wöhler C. * Berezhnoy A. A. Shevchenko V. V.
Daytime Dependence of the Near-Infrared Lunar Water/Hydroxyl Absorption Depth **[#6018]**
The daytime dependence of the lunar near-3-μm water/hydroxyl absorption depth is analyzed based on Moon Mineralogy Mapper (M3) data for a set of highland regions with available M3 data acquired at 4-8 different local daytimes.

4:15 p.m. Hurley D. M. * Siegler M. A.
Surface Volatiles Chapter Update **[#6029]**
This is the chapter status and summary report for the Surface Volatiles chapter.

4:30 p.m. McCubbin F. M. * Liu Y. Barnes J. J. Boyce J. W. Day J. M. D. Elardo S. M. Hui H. Magna T. Ni P. Tartèse R. Vander Kaaden K. E.
Endogenous Lunar Volatiles **[#6046]**
This abstract summarizes the contents that will be covered in the Endogenous Volatiles chapter of the forthcoming New Views of the Moon 2 RiMG volume.

4:45 p.m. DISCUSSION

Thursday, May 4, 2017
POSTER SESSION
5:30 p.m. Foyer

Gaddis L. R. Bennett K. Horgan B. McBride M. Stopar J. Lawrence S. Gustafson J. O. Giguere T.
Complex Volcanism at Lunar Floor-Fractured Crater Oppenheimer U **[#6012]**
Here we examine the floor of Oppenheimer U Crater and show evidence for multiple eruptive episodes, resulting in a pyroclastic deposit with compositional diversity within a single floor-fractured crater.

Assis Fernandes V. Burgess R. Cooper L. Czaja P. Khan A. Liebske C. Neal C.
Sliwinski J. Zhu M.-H.
Type, Chemistry, Ar-Isotopes and Magma Generation of New Apollo 17 Basaltic Regolith Fragments **[#6011]**
Six new Apollo 17 regolith basaltic fragments: Petrology, bulk composition, Ar-Ar and CRE age, magma generation, and initial comparison with orbital data.

Lemelin M. Lucey P. G. Crites S. T. Jha K.
Mineralogy and Iron Content of the Lunar Polar Regions Using the Kaguya Spectral Profiler and the Lunar Orbiter Laser Altimeter **[#6005]**
We use reflectance data from LOLA and reflectance ratio from SP to derive FeO maps of the polar regions at 1 km per pixel and compare them with lunar propector-derived abundances. We model mineral abundances using SP data and FeO as a constraint.

Vanderliek D. M. Becker H. Rocholl A.
Petrologic Context and Dating of 4.2 Ga Old Zircon in Lunar Impactites — 67955 Revisited **[#6026]**
New U-Pb data for zircons from different lithologies of impactite 67955 confirm the occurrence of one or several large impacts at 4.2 Ga. The importance of textural and compositional information will be discussed.

Varatharajan I. Sruthi U.
Impact Geology of Fresh Simple Craters on Moon **[#6015]**
Detailed morphologic and mineralogical mapping of impact features of fresh simple craters on Moon using high resolution datasets and their relationship to Earth's Lonar Crater.

Anderson F. S. Whitaker T. J. Wiesendanger R. Wurz P. Beck S. Levine J.
Revising Lunar History with In-Situ Dating of the Moon **[#6030]**
We have developed a mission concept to address ±1 Ga year uncertainties in the history of the Moon by obtaining 10 or more Rb-Sr and Pb-Pb radiometric dates in-situ, ultimately constraining the age of the surface to well within ±200 Ma (2-σ).

Lawrence S. J. Gaddis L. R. Joy K. H. Petro N. E.
Lunar Exploration Missions Since 2006 **[#6051]**
Here, we describe the vision for the Recent Lunar Missions chapter, which will tersely summarize missions that have explored the Moon between 2006 and 2017.

Weitz C. M. Staid M. I. Gaddis L. R. Besse S. Sunshine J. M.
Investigation of Lunar Spinels at Sinus Aestuum **[#6003]**
We have analyzed Moon Mineralogy Mapper (M3) data of spinels at Sinus Aestuum. Our results indicate that Fe- or Cr-spinels with 0.7 μm absorptions are mixed into most of the DMD across the Sinus Aestuum highlands. Cr-spinels with 0.7 μm absorptions are mixed into most of the dark mantle deposit (DMD) across the Sinus Aestuum highlands.

Friday, May 5, 2017
IMPACT FEATURES, PROCESSES, CHRONOLOGY
8:30 a.m. Aula Conference Room

Topics include discussion of lunar impact features, processes of formation and evolution, and chronology, as well as chapter summaries covering these topics.

Chairs: **Carolyn van der Bogert**
Harald Hiesinger

8:30 a.m. Gleißner P. * Becker H.
Late Accreted Material on the Lunar Surface: Constraints from Highly Siderophile and Chalcophile Elements in Ancient Lunar Impactites **[#6020]**
Abundances of HSE, Te, Se, and S in ancient lunar impactites constrain accretion of differentiated and primitive material (including carbonaceous chondrite-like material) and variable mixing of their compositions on the lunar surface.

8:45 a.m. Neumann G. A. * Goossens S. Head J. W. Mazarico E. Melosh H. J. Smith D. E. Wieczorek M. A. Zuber M. T. LOLA and GRAIL Science Teams
Lunar Impact Basin Population and Origins Revealed by LOLA and GRAIL **[#6037]**
The inventory and sizes of large lunar impact basins, some obscured by superposed cratering and volcanism, together with better understanding of the factors that control basin size, will help constrain models of the original impactor population.

9:00 a.m. Huang Y.-H. * Minton D. A. Hirabayashi M. Elliott J. R. Richardson J. E. Fassett C. I. Zellner N. E. B.
Heterogeneous Impact Transport on the Moon **[#6013]**
Both distal ejecta and proximal ejecta are important to material transport on the Moon, and the patchy nature of ejecta may have resulted in a spatial heterogeneity of exotic material seen in some lunar samples.

9:15 a.m. Mazrouei S. * Ghent R. R.
Towards an Understanding of Initial Crater Rock Populations: Copernicus Crater vs. Avery Crater **[#6038]**
Boulder distribution around Copernicus Crater and Avery Crater, in pursuit of understanding boulder survival times based on crater size, age, and terrain.

9:30 a.m. van der Bogert C. H. * Hiesinger H. Spudis P.
The Age of the Crisium Impact Basin **[#6009]**
CSFD measurements of newly discovered Crisium impact melt remnants give absolute model ages consistent with radiometric ages of Luna 20 samples. Our new Crisium N(1) fits the lunar chronology function better than the previous value.

9:45 a.m. Hiesinger H. * van der Bogert C. H. Plescia J. B. Robinson M. S. Robbins S. Michael G. Schmedemann N. Ivanov B. Hartmann W. Ostrach L. Williams J.-P. Zanetti M. Speyerer E. Werner S.
Lunar Impact Chronology: Status, Advancements, Implications, and Things to Consider **[#6023]**
We will present the outline of the chronology chapter of the New Views of the Moon 2 book and will present recent progress with respect to the lunar chronology.

10:00 a.m. BREAK

10:15 a.m. DISCUSSION

Friday, May 5, 2017
LUNAR EXOSPHERE AND SPACE WEATHERING
10:45 a.m. Aula Conference Room

Topics include discussion of the lunar exosphere and space weathering on the Moon and chapter summaries covering these topics.

Chair: Brett Denevi

10:45 a.m. Stickle A. M. * Cahill J. T. S. Grier J. A. Greenhagen B. Patterson G. W.
New Views of Lunar Surface Maturity Using LRO Data from UV to Radar **[#6017]**
Lunar soil ages / Across the wavelengths of light / Do we see a trend? / Can we tell the differences / Across the wavelengths?

11:00 a.m. Wu Y. Z. * Wang Z. C. Lu Y.
New Results from the Chang'E-3 Optical Instruments **[#6006]**
New results (in situ space weathering and young tectonism) derived from Chang'E-3 were shown.

11:15 a.m. Denevi B. W. * Noble S. K. Blewett D. T. Christoffersen R. Gillis-Davis J. J. Greenhagen B. T. Hendrix A. R. Hurley D. M. Keller L. P. Thompson M. S.
Space Weathering and Exosphere–Surface Interactions **[#6027]**
Summary of our plans for the chapter on advances in our understanding of space weathering.

11:30 a.m. DISCUSSION

Friday, May 5, 2017
LUNAR RESOURCES, SURFACE OPERATIONS, REGOLITH
1:30 p.m. Aula Conference Room

Topics include discussion of lunar resources, surface operations, the lunar regolith, and chapter summaries covering these topics.

Chair: Clive Neal

1:30 p.m. Kołodziejczyk A. * Vos H. C. Harasymczuk M. Kraiński M. Foing B. H.
Using Lunar Regolith for Organics: Plant Growth Test Using Soil Analogues **[#6041]**
Plant development depends on environmental factors such light, humidity and temperature, seed quality, contaminations, and soil type. We study the use of lunar regolith simulants from Eifel volcanic region on the growth of plants.

1:45 p.m. Foing B. H. *
Update from Moon Village Workshops and Studies **[#6043]**
We report on Moon Village workshops that gathered multi-disciplinary professionals to discuss Moon habitat design, science and technology potentials of the Moon Village, and engaging stakeholders. We also report studies and activities that followed.

2:00 p.m. Eppler D. * Bleacher J. Bell E. Cohen B. Deans M. Evans C. Graff T. Head J. Helper M. Hodges K. Hurtado J. Klaus K. Kring D. Schmitt H. Skinner J. Spudis P. Tewksbury B. Young K. Yingst A.
A Framework for Lunar Surface Science Exploration **[#6022]**
Successful lunar science will be dependent on mission concept, mobility, robotic/human assets, crew training, field tools, and IT assets. To achieve good science return, element integration must be considered at the start of any exploration program.

2:15 p.m. Plescia J. B. * Robinson M. S. Kramer G.
Lunar Regolith — New Views **[#6048]**
The regolith presented is viewed as a much more complicated system than previously recognized.

2:30 p.m. Plescia J. B. * Robinson M. S. Clegg-Watkins R. Fa W. Ghent R. Harayuma J. Hiesinger H. Hirata N. Kramer G. Lawrence S. Mahanti P. Ostrach L.
Patterson W. Spudis P. Stopar J. Siegler M. Speyerer E. Stickle A. Williams j. P. Zanetti M. Zellner N.
Surface Processes **[#6049]**
The Surface Processes chapter will provide an update on our current understanding of surface processes.

2:45 p.m. DISCUSSION

3:00 p.m. BREAK

Friday, May 5, 2017
LUNAR MAGNETISM
3:15 p.m. Aula Conference Room

Topics include discussion of lunar impact magnetism and a chapter summary covering this topic.

Chairs: **Mark Wieczorek**
Sonia Tikoo

3:15 p.m. Laneuville M. * Taylor J. Wieczorek M.
Distribution of Radioactive Heat Sources and Magnetic Field **[#6019]**
We consider updated distributions of heat sources based on GRAIL results to understand the structure of the PKT. The remanent magnetization pattern suggests an inhomogeneous distribution within the PKT, which has implication for the global evolution.

3:30 p.m. Tikoo S. M. * Weiss B. P. Shuster D. L. Suavet C. Wang H. Grove T. L.
A Three-Billion-Year History for the Lunar Dynamo **[#6025]**
The paleomagnetic record of young regolith breccia 15498 suggests that the lunar core dynamo may have persisted beyond 2.5 Ga.

3:45 p.m. Oran R. * Weiss B. P.
Impact-Amplified Magnetic Fields as a Possible Source of Crustal Magnetization **[#6014]**
Latest advancements in testing the hypothesis that crustal magnetization can be explained by impact-amplified magnetic fields in basin antipodes.

4:00 p.m. Rückriemen T. * Breuer D. Spohn T.
Compositional Convection in a Fe-FeS Core of the Moon **[#6035]**
We investigate dynamo lifetimes associated with bottom-up and top-down crystallization in a Fe-FeS lunar core. To do so we employ a 1D thermo-chemical evolution model. The resulting dynamo lifetimes are too short to explain the observations.

4:15 p.m. Wieczorek M. A. * Weiss B. P. Breuer D. Fuller M. Gattacceca J. Halekas J. Hood L. Nimmo F. Oran R. Purucker M. Soderlund K. Tikoo S.
Recent Advances in Lunar Magnetism **[#6036]**
In this contribution, our current understanding of lunar magnetism will be reviewed. Advances made in the past decade since the publication of the first New Views of the Moon book will be emphasized.

4:30 p.m. DISCUSSION

PRINT ONLY

Head J. W. Hiesinger H. van der Bogert C. Gaddis L. Haruyama J. Hurwitz D. Jozwiak L. Morota T. Pieters C. M. Prisell T. Wilson L. Whitten J.
New Views of the Moon 2: Lunar Volcanism (Volcanic Features and Processes) **[#6034]**
New Views of the Moon 2 provides a unique opportunity to synthesize the important developments of the last decade in our understanding of lunar volcanism and its implications for lunar petrology and the thermal evolution.

AN INTEGRATED VIEW OF THE HISTORY AND EVOLUTION OF VOLATILES IN THE MOON. M. Anand[1,2], [1]Planetary and Space Sciences, The Open University, Milton Keynes, MK7 6AA, UK; [2]Department of Earth Sciences, The Natural History Museum, London, SW7 5BD, UK Affiliation (Mahesh.Anand@open.ac.uk).

Introduction: The last decade has witnessed an unprecedented growth in lunar volatiles research, which has revealed a complex history of volatiles in the lunar interior. A range of volatile elements and their isotopes (e.g. H, C, N, O, Cl, K, Zn) have been measured in lunar samples exploiting latest advancements afforded by modern analytical instrumentation, confirming not only a significant presence of volatiles in the lunar interior but also highlighting an array of complex physico-chemical processes that might have influenced the volatile inventory of the Moon. Such processes range from interaction of solar wind with lunar melts to degassing of magma during and upon eruption to shock-induced volatile redistribution in volatile-bearing minerals/phases. Furthermore, the variety of data that has been acquired on lunar interior volatiles can now be brought to bear on various hypothesis testing a genetic connection between the Earth and the Moon as well as the evolution of the Lunar Magma Ocean (LMO) that formed in the aftermath of lunar accretion.

Recent dataset: Recent measurements have targeted bulk-samples, individual mineral phases such as apatite and plagioclase feldspar, and melt-inclusions in lunar samples returned by the Apollo missions and lunar meteorites [e.g., 1-4]. As a result of these recent efforts, there now exists a considerable dataset for volatile elements in lunar samples but to a large extent, integration of different dataset has been lacking. This is critical for fully understanding the history and evolution of lunar volatiles since the accretion of the Moon until the present day. Such an approach is also essential for reconciling various lunar formation theories (several new models for the origin of the Moon have been proposed recently) and in developing a coherent view of the timing of delivery, sources and distribution of volatiles in the lunar interior [e.g., 5-7]. Furthermore, a comprehensive understanding of the inventory of various volatiles in lunar material would facilitate in developing appropriate *in-situ* resource utilisation (ISRU) applications on the Moon – an increasing possibility in light of the emergence of new space faring nations and private entities intrested in space exploration.

Future prospects: Recent efforts have already resulted in several new discoveries about the Moon, one of which has been an unambiguous detection and quantification of water in lunar samples. Nevertheless, our understanding of complex physico-chemical processes influencing the volatile inventory of lunar samples is relatively poor. Future analytical work using a multi-proxy approach and targeting a range of lunar samples, minerals and other analogue materials will lead to new discoveries and better understanding of the abundance, distribution and sources of volatiles in the Moon. As the next phase of planetary sample return missions is unfolding, an integrated view of lunar volatiles would be instrumental in guiding/informing not only future lunar sample return missions but also missions to other target bodies such as Mars, asteroids, and beyond.

References: [1] Anand, M. et al. (2014) *Phil. Trans Royal Soc. A*, Article ID 20130254. **[2]** McCubbin, F.M. et al. (2015) *Am. Min.*, 100 (8-9) pp. 1668-1707. **[3]** Hauri, E.H. et al. (2017). *Ann. Rev. Earth and Planet. Sci.* 45(1). *In Press*. **[4]** Mortimer, J.I. et al. (2016) *GCA*, 193 pp. 36–53. **[5]** Barnes, J.J. et al (2016) *Nat. Comm.* 7, article no. 11684 **[6]** Hauri, E.H. et al. (2015) *EPS*L. 409, 252–264. **[7]** Canup, R. et al. (2015) *Nat Geo*. 8, 918-921.

Acknowledgements: The author wishes to thank the UK Science and Technology Facilities Council (STFC), The European Commission (EC), and the European Space Agency (ESA) for providing research funding, NASA CAPTEM for the allocation of Apollo samples, and a number of PhD students, Postdocs and co-workers who have worked in his research team over the last decade on the topic of lunar volatiles.

REVISING LUNAR HISTORY WITH IN-SITU DATING OF THE MOON. F. S. Anderson[1] , T. J. Whitaker[1], R. Wiesendanger[2], P. Wurz[2], S. Beck[3], J. Levine[4], [1]Southwest Research Institute, 1050 Walnut St, Suite 300, Boulder, CO (anderson@boulder.swri.edu), [2]Physikalisches Institut, University of Bern, Bern, Switzerland, [3]The Aerospace Corporation, Los Angeles, CA, [4]Department of Physics and Astronomy, Colgate University, New York, USA.

Introduction: The chronology of the inner solar system is built on crater flux models extrapolated from the relationship between lunar crater densities and radiometric dates of well-provenanced lunar samples [e.g., 1, 2]. The modeled flux primarily constrain the era between 3.5 and 4.2 Ga, as well as the very recent past [2]. These results have been extrapolated to Mars, and throughout the solar system [3-8]. However, a comparison of numerous lunar chronology models illustrates differences between the models of up to one billion years for the period between ~2.8 to 3.3 Ga [2]. For the Moon and Mars, this period is geologically rich, including the cessation of abundant volcanism, and, for Mars, the apparent termination of volatile production and formation of hydrated minerals [e.g., 9, 10, 11]. Under the new chronology functions, these processes could have lasted for a billion additional years, undermining models for thermal evolution of the Moon [12]; similarly, Mars would have undergone a longer epoch of voluminous, shield-forming volcanism and associated mantle evolution, as well as a longer era of abundant volatiles and hence potential habitability.

These differences are in part due to different estimates of crater densities observed in Lunar Reconnaissance Orbiter data, and a lack of samples from terrains with N(1) crater densities of ~0.0015 km^{-2} to 0.0025 km^{-2}. Thus, the most straightforward part of the chronology curve to refine is associated with previously unsampled Eratosthenian near-side terrains, such as the Aristarchus basalts. Large lava flows in the Schiaparelli region could be readily targeted for future missions. Similar regions could be identified for Mars, and used as a constraint on models relating cratering rates to the Moon, and hence the lunar chronology.

A Near-Side Lunar Mission: We have developed a mission concept [13-16] to address one billion year uncertainties in the history of the Moon [2] by landing on a large, homogenous lava flow of 2.5-3.5 Ga, obtaining 20 or more Rb-Sr and Pb-Pb radiometric dates, ultimately constraining the age of the surface to well within ±200 Ma (2-σ) [13, 17, 18]. Our lander would use an arm with a gripper and rake to reveal and acquire a sample [16]. This rock would be imaged with both the camera and NIR/IR spectrometer, before having a flat ground onto it's face. It would then be re-imaged, and assessed for dating suitability. If the rock is a basalt appropriate for measurement, it is presented to our Chemistry, Organics, and Dating EXperiment (CODEX) for analysis. CODEX uses: a) laser ablation to vaporize a small amount of material from a sample surface, b) resonance ionization spectroscopy to provide selective, efficient ionization of the desired element, and c) mass spectrometry to provide isotopic information. The mass spectrometer is based on a TRL-8 reflectron time-of-flight (RTOF) unit designed and constructed by the University of Bern for the Luna-Resurs lunar mission. We have engaged in a half-decade of international cooperation, culminating in the delivery of a similar RTOF from the Bern group that is presently undergoing tests in our research facility.

CODEX rasters over hundreds of points to create an elemental and isotopic abundance image. These data points are used to produce isochrons, and place every point in context [17-19]. We have previously published Rb-Sr results for the Mars meteorite Zagami, and the Duluth Gabbro, a lunar analog [17, 18], and demonstrated that we can obtain Rb-Sr dates with accuracy better than ±200 Ma (1-σ). We have recently expanded our approach to include Pb-Pb [13], enabling tests of concordance, and with accuracy as good as ±50 Ma on zircons, up to ±90 Ma for difficult, low Pb abundance samples like lunar meteorite MIL 05035 (1-σ). We plan to make at least three, likely 10, and potentially up to 20 measurements of the lava flow, enabling us to obtain dates well-within ±200 Ma at 2-σ.

Conclusion: New radiometric constraints provided by CODEX will be used to reduce the ±1.1 Ga uncertainties in the crater flux models, and provide insight into terrains with N(1) crater densities of ~0.0015 km^{-2} to 0.0025 km^{-2}.

References: [1] S. Marchi et al. *Astron. Journal* **137**, 4936 (2009). [2] S. J. Robbins. *EPSL* **403**, 188 (2014). [3] R. A. Grieve *et al.*, *The record of past impacts on Earth*. (1994). [4] W. K. Hartmann *et al. SSR* **96**, 165 (April 1, 2001, 2001). [5] D. Korycansky et al. *PSS* **53**, 695 (2005). [6] C. I. Fassett et al. *GRL* **38**, (2011). [7] M. Le Feuvre *et al. Icarus* **214**, 1 (2011). [8] S. Marchi *et al. Nature* **499**, 59 (2013). [9] C. I. Fassett *et al. Icarus* **195**, 61 (2008). [10] S. C. Werner. *Icarus* **201**, 44 (2009). [11] B. L. Ehlmann *et al. Nature* **479**, 53 (2011). [12] T. Spohn *et al. Icarus* **149**, 54 (2001). [13] F. S. Anderson et al. *LPSC* **1246**, 2 (2017). [14] F. S. Anderson et al. *LPSC* **2957**, 2 (2017). [15] S. M. Beck et al. *LPSC* **3001**, 2 (2017). [16] T. J. Whitaker et al. *LPSC* **2328**, 2 (2017). [17] F. S. Anderson et al. *RCMS* **29**, 1 (2015). [18] F. S. Anderson et al. *RCMS* **29**, 191 (2015). [19] S. Foster et al., in *LPSC* (2016).

STRUCTURE AND EVOLUTION OF THE LUNAR INTERIOR. J. C. Andrews-Hanna[1], R. C. Weber[2], Y. Ishihara[3], S. Kamata[4], J. Keane[1], W. S. Kiefer[5], I. Matsuyama[1], M. Siegler[6], and P. Warren[7]. [1]Lunar and Planetary Laboratory, University of Arizona, Tucson, AZ, USA (jcahanna@lpl.arizona.edu), [2]Marshall Spaceflight Center, Huntsville, AL, USA (renee.c.weber@nasa.gov),.[3]Japanese Aerospace Exploration Agency, Japan, [4]Hokkaido University, Hokaido, Japan, [5]Lunar and Planetary Institute, Houston, TX, USA [6]Planetary Science Institute, Tucson, AZ, USA, [7]Institute for Geophysics and Planetary Physics, UCLA, Los Angeles, CA, USA.

Introduction: Early in its evolution, the Moon underwent a magma ocean phase leading to its differentiation into a feldspathic crust, cumulate mantle, and iron core. However, far from the simplest view of a uniform plagioclase flotation crust, the present-day crust of the Moon varies greatly in thickness, composition, and physical properties. Recent significant improvements in both data and analysis techniques have yielded fundamental advances in our understanding of the structure and evolution of the lunar interior. The structure of the crust is revealed by gravity, topography, magnetics, seismic, radar, electromagnetic, and VNIR remote sensing data. The mantle structure of the Moon is revealed primarily by seismic and laser ranging data. Together, this data paints a picture of a Moon that is heterogeneous in all directions and across all scales, whose structure is a result of its unique formation, differentiation, and subsequent evolution. This brief review highlights a small number of recent advances in our understanding of lunar structure.

Shallow structure: Crust and upper mantle. The surface varies in composition on both local and regional scales [1], including the concentration of incompatible elements within the Procellarum KREEP terrane (PKT) [2]. Remote sensing data show that pure anorthosite is limited to rare small outcrops [3], while much of the upper crust outside the maria is dominated by a mixed feldspathic layer [4].

Gravity data reveal large variations in crustal thickness, primarily associated with impact basins and the nearside-farside asymmetry [5,6]. The upper crust has a mean density of ~2550 kg/m^3 and porosity of 12% [5], with an increase in density with depth [7]. A wide range of smaller structures exist within the crust including linear dike-like intrusions [8], ring-dikes around basins, a quasi-rectangular pattern of structures surrounding the PKT [9], magma chambers beneath volcanoes [10], density anomalies beneath craters [11], and pervasive small-scale density anomalies [12].

Seismic data show a low velocity and low density megaregolith, overlying a higher velocity and density crust. The strongest seismic constraints on crustal structure come from analysis of the signals generated by the crash landings of the lunar module ascent stages and the Saturn S-IVB booster stages, resulting in crustal thickness estimates of ~30-35 km in mare regions, and 40-50 km in highland regions [13].

Deep structure: Mantle and core. Exposures in impact basins indicate that the uppermost mantle is rich in either orthopyroxene (representing the top layer of magma ocean cumulates) [14] or olivine (representing the post-overturn mantle) [15]. Constraints from joint consideration of the mean density and Love numbers (GRAIL) and the moment of inertia (Lunar Laser Ranging) of the Moon result in a family of models which support the presence of a solid inner and liquid outer core [16], and possibly a deep mantle low shear velocity zone interpreted as partial melt [17]. Deep seismic reflections also support a partial melt layer overlaying a fluid outer core and solid inner core, with radii of ~480, 330, and 240 km, respectively [18]. The Lunar Prospector magnetometer detected an induced moment in the Earth's geomagnetic tail, supporting the existence of a conducting metallic core of radius 340+90 km [19], or 1 to 3% of the lunar mass.

Thermal evolution and geodynamics. The early thermal and geodynamic evolution was dominated by the equilibration and loss of accretionary heat, leading to early global expansion followed by contraction [8]. Subsequent evolution has been heavily affected by the concentration of heat producing elements in the Procellarum KREEP terrane [20] and the secular decline in radiogenic heat, resulting in relaxation of ancient basins [21] and declining rates of volcanism [20].

References: [1] Cahill, J. T. S. et al. (2009) *JGR* 114 1–17. [2] Jolliff B. L. et al. (2000) *JGR* 105 4197-4216. [3] Ohtake M. et al. (2009) *Nature* 461 236–240. [4] Hawke B. R. (2003) *JGR* 108 doi:10.1029/2002JE001890. [5] Wieczorek M. A. et al. (2013) *Science* 339 671–675. [6] Neumann G. A. et al. (2015) *Sci. Adv.* 1 1:e1500852. [7] Besserer J. et al. (2014) *GRL* 41 5771–5777. [8] Andrews-Hanna J. C. et al. (2013) *Science* 339 675–678. [9] Andrews-Hanna J. C. et al. (2014) *Nature* 514 68–71. [10] Kiefer W. S. et al. (2013) *JGR* doi:10.1029/2012 JE004111. [11] Soderblom J. M. et al. (2015) *GRL* 42 6939–6944. [12] Jansen J. C. et al. (2014) *LPSC* 45 Abstract 2730. [13] Chenet H. et al. (2006) *EPSL* 243 1–14. [14] Nakamura R. et al. (2012) *Nat. Geosci.* 5 775–778. [15] Yamamoto S. et al. (2010) *Nat. Geosci.* 3 533–536. [16] Matsuyama I. et al. (2016) *GRL*. 43 8365–8375. [17] Williams J. G. et al. (2014) *JGR* 119 1546–1578. [18] Weber R. C. et al. (2011) *Science* 331 309–312. [19] Hood L. et al. (1999) *GRL*. 26 2327–2330. [20] Laneuville M. et al. (2013) *JGR* 118 1435–1452. [21] Kamata S. et al. (2013) *JGR* 118 398–415.

TYPE, CHEMISTRY, AR-ISOTOPES AND MAGMA GENERATION OF NEW APOLLO 17 BASALTIC REGOLITH FRAGMENTS V. A. Fernandes[1,2], R. Burgess[2], L. Cooper[3] P. Czaja[1], A. Khan[4], C. Liebske[3], C. Neal[5], J. Sliwinski[3], and M.-H. Zhu[1,6], [1]Museum für Naturkunde, Berlin, Germany, [2]SEES, Univ. Manchester, UK, veraafernandes@yahoo.com, [3]Inst. Geochemisty and Petrology, ETH-Zürich, Switzerland, [4]Inst. Geophysics, ETH-Zürich, Switzerland, [5]Dept. Civil & Env. Eng. & Earth Sci., Univ. Notre Dame, Indiana, U.S.A., [6]Space Science Inst., Macau Univ. of Science and Technology, Macau, China.

Introduction: Many of the larger basins of the Moon are filled with different lava flows. The Serenitatis basin presents 29 spectrally different compositions on its surface [1], but the chemical diversity of the lava flows below is not known. Thus, a complete understanding of chemical and isotopic mantle evolution beneath this basin cannot yet be constrained. Apollo 17 basalts are divided into high- & very-low-Ti compositions with the high-Ti representing the majority. The range in ages for volcanic samples is 3.75-3.65 Ga [2] and from cratering statistics volcanism occurred between ~3.9 and 3.6 Ga [1]. Acquiring chemical composition, mineralogic and chronologic data from different lava types is needed. Here we present textural, chemical composition and isotopic ages of 6 Apollo 17 2-4 mm regolith fragments collected from impact ejecta of Shorty, Steno and Camelot craters. Ejecta from these small craters come from depths greater than any of the Apollo 17 drill-cores. Hence, these fragments potentially sampled material from underlying lava flows and intercalated regolith that probably included local and regional material (from other flows within Mare Serenitatis). The results obtained using different analytical techniques are compared with remote sensing and literature data to evaluate mantle source(s) evolution under the Serenitatis Basin.

Type and chemical composition:
74244,12 pyroxene-porphyritic high-Ti basalt, pyroxene ($En_{31-46}Wo_{27-46}Fs_{16-42}$), plagioclase ($An_{81-85}$) & ilmenite with armalcolite cores; 75063,13 olivine-porphyritic high-Ti basalt, sub-variolitic texture, contains olivine (Fo_{69-73}), plagioclase (An_{85-88}) & ilmenite of various sizes; 71063,7 high-Ti dolerite (phases >1mm), olivine (Fo_{56-71}), pyroxene (En_{36-69} $Wo_{6-26}Fs_{25-41}$), plagioclase (An_{93-96}) & ilmenite; 75063,5 high-Ti olivine dolerite with 2 size domains. Phases in the coarser domain are 0.5-1 mm Ø, composed of plagioclase (An_{89-92}), olivine (Fo_{33-52}), pyroxene ($En_{32-45}Wo_{9-35}Fs_{33-53}$) & ilmenite; 71064,12 vitrophyric high-Ti basaltic melt with 50-200 µm olivine crystals (Fo_{72-76}) & ~10 µm chromite; 74243,41 vitrophyric high-Ti basalt with olivine (Fo_{64-73}) & armalcolite phenocrysts. Potentially an impact melt composed of mare material. All samples show the same depletion in the LREE and a relative enrichment in the HREE as in literature data [3]. Fragments 71064,12 and 74243,41 show a negative Eu-anomaly and a pattern similar to Apollo 17 types A and U [3]. Fragment 71063,7 shows a steeper LREE depletion and a very slight negative Eu-anomaly. Fragments 74244,12, 75065,5 and 75063,13 have similar REE pattern and a slight to positive Eu-anomaly.

^{40}Ar-^{39}Ar and CRE age: All data were corrected for blank, discrimination, decay of short-lived nucleogenic nuclides (^{37}Ar & ^{39}Ar), and where necessary cosmogenic and/or trapped Ar corrections were applied. Ages were obtained from Ar-release spectra, inverse or normal isochron. ^{40}Ar-^{39}Ar ages range from 3.96 to 3.68 Ga, extending the range previously determined for Apollo 17 basalts. CRE-ages define a range of 112-441 Ma.

Magma generation and source depth: initial modelling [4] using estimated bulk compositions gives primary pressure of 1.3-2.6 GPa and temperature of 1260-1400°C consistent with other Apollo 17 basalts [3]. Based on these P-T estimates, the thermodynamic model described in [5] was employed to convert to depth in the lunar mantle. Source depths were found to range from 240 to 480 km. There is no direct correlation between age and depth.

Preliminary sample bulk composition vs. remote sensing data: The mare units considered are the larger flows of [6]. FeO and TiO_2 values determined from Clementine data and K from CE-2 & LP. First results suggest the orbital data to have a higher K content than samples. This will be further assessed.

Summary: New basaltic regolith fragments show a chemical composition range similar to those reported earlier. Potentially some of the fragments represent lavas not identified before. Fragments 74244,12, 75065,5 and 75063,13 show a slight positive Eu-anomaly potentially indicative of a change in source region or note representative of whole rock. The ^{40}Ar-^{39}Ar age range suggests a longer volcanic period. The non-correlation between age and magma generation depth suggest that heating of the lunar mantle is heterogeneous [e.g. 7]

References: [1] Hiesinger et al. (2011) Geol. Soc. of America Sp. Pap. 477, 1-51. [2] Paces et al. (1991) GCA 55, 2025-2053. [3] Mare Basalt DB http://www3.nd.edu/~cneal/Lunar-L/. [4] Lee et al. (2009) EPSL 279, 20-33. [5] Khan et al. (2014) JGR 119, doi:10.1002/2014JE004661. [6] Hiesinger et al (2000) JGR 105, 29239-29275. [7] Laneuville et al. 118, 1435-1452.

Acknowledgements: Many thanks to: Apollo 17 astronauts, NASA-JSC Curatorial Staff, and K. Born (SEM) and H.-R. Knofler (thick sections) at MfN. VAF funded via a DFG-Eigenestelle FE 1523/3-1.

ADVANCES IN UNDERSTANDING THE FORMATION, DISTRIBUTION, AND AGES OF LUNAR LOBATE SCARPS. J. D. Clark[1], C. H. van der Bogert[1], and H. Hiesinger[1], [1]Institut für Planetologie, Westfälische Wilhelms-Universität, Wilhelm-Klemm-Str. 10, 49149 Münster, Germany (j.clark@uni-muenster.de).

Introduction: The Moon is covered by a wide suite of tectonic features, which is evidence of both ancient and recent activity. Long-term interior cooling, tidal stresses and contraction of the Moon resulted in compressional features called lobate scarps, the surface expression of low angle thrust faults [1-4]. Their fresh morphologies and the absence of large superimposed craters (> 400 m) are evidence that these features were created in the last (< 1 Ga) [5-7].

Early investigations of lobate scarps were conducted using images from the Apollo Panoramic Camera [8]; however, new high-resolution images obtained by the Lunar Reconnaissance Orbiter Camera (LROC) [9] allow the identification of smaller and more widely distributed scarps [4, 6]. [8] determined model ages for select scarps using crater degradation techniques. These model ages coupled with the fresh morphology of the scarps [6] attest to their late Copernican ages. More recently, using crater size-frequency distribution (CSFD) measurements [10,11], [12] showed that shaking during scarp formation seems to cause local resurfacing of the small craters and allows the derivation of absolute model ages for many scarps. We applied the technique on 40 lobate scarps, to investigate the range of scarp ages and the effects of seismic shaking.

Data and Methods: Using NAC (Narrow Angle Camera) image data from the Lunar Reconnaissance Orbiter [9] and applying the technique of [12], we generated count areas in ArcGIS and conducted CSFD measurements using CraterTools [13]. In Craterstats [14], we plotted and fit the CSFDs using the techniques described in [10]. Absolute model ages (AMAs) were derived based on the chronology function (CF) and production function (PF) of [11].

Discussion: *Global Distribution.* Our results show that lobate scarps formed in the last 700 Ma [15]. The global distribution of the scarps' AMAs is spatially random [15], which is in agreement with these small-scale features being mostly created in an isotropic stress field [4]. Such a stress field would generate a homogeneous distribution of thrust faults on the Moon [4].

Seismic Shaking Effects. Young ages derived for count areas proximal to scarps suggest that small craters are destroyed during scarp formation, therefore resetting the surface age. For example, at the Mandel'shtam hanging wall, craters ≥ 20 m in diameter exhibit significant degradation, whereas craters < 20 m have fresh crater morphologies. The small craters produce a CSFD that can be fit with the lunar PF. Therefore, the pre-existing population of small craters was likely erased by seismic activity associated with scarp formation. With increasing distance from the proximal hanging wall, the AMAs generally increase (Fig.1), as would be expected if localized seismic shaking causes resurfacing. The distal locations were less affected by seismicity, such that their ages were not completely reset. Variations in the degree of local seismic shaking would be expected to cause variations in the amount of alteration to the crater population.

Conclusion: Data sets provided by recent lunar missions have allowed significant advancement in the understanding of the formation, distribution, and ages of lunar lobate scarps.

References: [1] Hartmann W.K. and Davis D. (1975) *Icarus*, 24, 504-515. [2] Cameron A.G.W. and Ward W.A. (1976) Lunar Science VII, 120-122. [3] Binder A.B. (1982) *Moon and Planets*, 26, 117-133. [4] Watters et al., (2015) *Geology*, 43, 851-854. [5] Schultz (1976) *Moon Morphology*, Austin, TX. [6] Watters T.R. et al. (2010) *Science*, 329, 936-940. [7] Binder A.B. (1986) *Papers Presented to the Conference on the Origin of the Moon*, 425-433. [8] Binder A.B. and Gunga H. (1986) *Icarus*, 63, 421. [9] Robinson et al. (2010) *Space Sci. Rev*. 150, 55. [10] Neukum (1983) *Meteoritenbombardement und Datierung planetarer Oberflächen*, Habil. Thesis, Univ. Munich. [11] Neukum et al. (2001) *Space Sci. Rev*., 96, 55. [12] van der Bogert et al. (2012) *LPSC XLIII*, Abstract #1847. [13] Kneissl et al. (2011) *PSS*, 59. [14] Michael and Neukum (2010) *EPSL*, 294, 223. [15] Clark et al., (2016) *LPSC XLVII*, Abstract #1380.

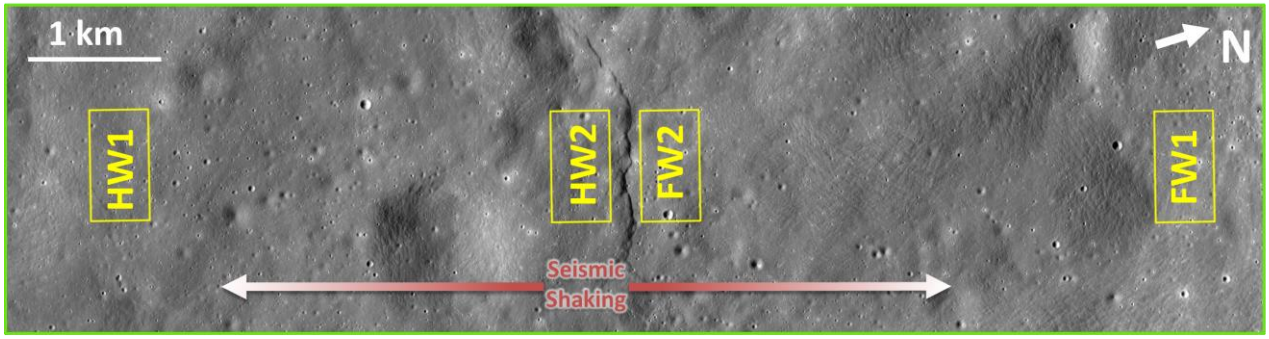

Figure 1. Location of count areas at Barrow scarp (69.9°N, 4.80°E) on NAC image pair M1116516111. The areas adjacent to the fault (HW2/FW2) typically experience more seismic shaking than their distal counterparts (HW1/FW1).

P-BEARING OLIVINES IN LUNAR ROCKS: A NEW VIEW ON LUNAR PHOSPHORUS. S. I. Demidova[1], F. Brandstätter[2], Th. Ntaflos[3], N. N. Kononkova[1], [1]Vernadsky Institute of Geochemistry and Analytical Chemistry, Kosygin St. 19, Moscow 119991, Russia, demidova.si@yandex.ru; [2]Naturhistorisches Museum, Burgring 7, 1010 Vienna, Austria; [3]Department für Lithosphärenforschung, Universität Wien, Althanstrasse 14, 1090 Wien, Austria.

Introduction: Phosphorus is the only highly incompatible element, which has a higher partition coefficient in olivine relative to pyroxene [1-4]. Extremely rare P-rich olivines (3-8 wt.% P_2O_5) were described in some unusual terrestrial and extraterrestrial associations. Their appearance is favored by a set of several factors, such as: low oxygen fugacity, high phosphorous and low silica activities, but a rapid growth of olivine from P-rich liquids is considered as a major factor of this enrichment. [e.g. 3 and references therein]. P-bearing olivine (up to 0.4 wt. % P_2O_5) has been described in typical olivine-bearing rocks such as terrestrial peridotites, basalts, andesites, dacites [3] and martian shergottites [5].

Phosphorus is an important minor element of lunar rocks. A highly differentiated igneous melt may produce phosphate minerals, typically merrillite and apatite. Schreibersite has also been reported as a trace mineral in some highland rocks [6]. Until recently these phases were supposed to be the main P repositories. However, after the finding of P-bearing olivines in the Luna 20 site and Dhofar 961 lunar meteorite [7,8] this assessment should be revised.

Results: Olivine with variable modal composition is present in highland anorthositic-noritic-troctolitic rocks (ANT) and rare ultramafic rocks (dunite-pyroxenite). It is also a major mineral of deep-seated crustal rocks - spinel cataclasites. Most mare basalts contain traces or even significant amounts of olivine [e.g. 6]. However in typical KREEP basalts (containing up to 0.7 wt.% P_2O_5 [9]) olivine is rare, which is thought to be a result of P enrichment [10].

We analyzed olivine with focus on its P-contain from the lunar samples of Luna 16 and 20, Apollo 14 and in Dhofar 025, 961, 287 lunar meteorites. The extremely rare olivine grains contain up to 0.5 wt.% P_2O_5. P-bearing olivine occurs in form of mineral fragments in breccias and in igneous rocks as well [8]. P content may vary in a single grain from below detection limit to tenths of a percent.

Three types of P-bearing olivines were observed. 1) P-bearing olivine (Fo_{51-88}) is present in rock and mineral fragments of anorthositic-noritic (gabbro-noritic)-troctolitic composition, which are enriched in incompatible elements. They are observed in Luna 20 [8], Luna 16, Apollo 14 sites and Dhofar 961 lunar meteorite. 2) P-bearing fayalite (Fo_{2-4}) was found in the late-stage mesostasis of Dhofar 287A basalt and in the Luna 16 coarse-grained anorthite-fayalite-Fe-rich pyroxene-silica rock. 3) Two large zoned olivine grains (Fo_{68-95}) with oriented enstatite inclusions were found in the Dho 025, 961 meteorites [7].

Implications for Lunar Petrology and Geochemistry:

Olivine is a common liquidus phase in lunar magmas. Slow diffusion rate of P in silicate melts and crystals [11] makes it promising indicator of magmatic processes. Once appearing, P zoning cannot be easily obliterated by subsequent annealing and may be used for estimation of the T-t history of the host olivine [12].

According to the known values of olivine/melt partition coefficient for phosphorus $D_P^{ol/melt}$ [e.g. 4] P-bearing olivines should crystallize from P-rich melts, which are not common among lunar rocks. However, it has been experimentally shown that $D_P^{ol/melt}$ increases under reduced conditions that might indicate the presence of P^{3+} [2]. This raises the question about mechanisms of P incorporation into lunar olivines. Along with the importance of oxygen fugacity, evaporation processes may influence the P behavior as well [13].

The source(s) of the P-bearing olivine may be both Fe-rich residues after mare basalts crystallization and highland Mg-rich melts of ANT composition enriched in KREEP. The source of the olivine-enstatite objects (type 3) is not clear yet however could be either of meteoritic [14] or lunar origin [7].

Acknowledgments: This study was supported by RFBR grant 16-05-00695 and Russian Academy of Sciences (Program №7).

References: [1] Brunet F. and Chazot G. (2001) *Chem. Geology* 176: 51-72. [2] Mallmann G. and O'Neill H. St. C. (2009) *J. Pet., 50,* 1765-1794. [3] Millman-Barris M. S. et al. (2008) *Contrib. Min. Pet., 155*, 739-765. [4] Grant T. B. and Kohn S. C. (2013) *Am. Min., 98,* 1860-1869. [5] Shearer C. K. et al. (2013) *GCA, 120*, 17-38. [6] Heiken G. H. et al. (1991) *Lunar sourcebook*. [7] Demidova S. I. et al. (2015) *Petrology, 23, 116-126*. [8] Demidova S. I. et al. (2017) *LPSC 48th,* Abstract #1409. [9] Rhodes J. M. and Hubbard N. J. (1973) *Proc. LPSC 4th,* 1127–1148. [10] Toplis et al. M. J. (1994) *GCA, 58,* 797-810. [11] Spandler C. et al. (2007) *Nature, 447,* 303–306. [12] Watson E. B. (2015) *Am. Min., 100*, 2053-2065. [13] Yakovlev O. I. et al. (2006) *Geochem. International, 44,* 847-854. [14] Joy K. et al. (2012) *Science, 336,* 1426-1429.

SPACE WEATHERING AND EXOSPHERE–SURFACE INTERACTIONS. Brett W. Denevi[1], Sarah K. Noble[2], David T. Blewett[1], Roy Christoffersen[3], Jeffrey J. Gillis-Davis[4], Benjamin T. Greenhagen[1], Amanda R. Hendrix[5], Dana M. Hurley[1], Lindsay P. Keller[3], and Michelle S. Thompson[3]. [1]Johns Hopkins Applied Physics Laboratory, Luarel, MD 20723, USA, [2]NASA Headquarters, Washington, DC 20546, USA, [3]NASA Johnson Space Center, Houston, TX 77058, USA, [4]University of Hawaii, Honolulu, HI 96822, USA, [5]Planetary Science Institute, Tucson, AZ 85719, USA.

Introduction: Advances in understanding space weathering and how exosphere–surface interactions alter the Moon's uppermost surface include both new laboratory work and new types of remote sensing measurements. The goal of this chapter will be to provide a broad overview of these innovations, as well as to integrate observations from the micro-scale (such as studies that focus on a single particle of soil) to the macro-scale (such as regional trends in space weathering). Since the Moon provides much of our foundational knowledge of space weathering processes, we aim to place our understanding of lunar space weathering in the context of recent advances elsewhere in the Solar System.

Chapter Outline: The chapter will start with an overview of the variety of processes that are included as part of space weathering, how the definition has changed and expanded, and a description of the significance of space weathering for wider lunar science questions. It will then cover recent laboratory advances, including analogs (e.g., studies of silica gels, laser, ion bombardment, and impact studies) and samples (e.g., single impacts, oxidation state of nanophase iron, agglutinates, and rates as inferred from solar-flare track densities). Recent remote sensing work both expands the wavelength range for examining space weathering (from the far-ultraviolet out to thermal infrared and even radar wavelengths), and provides new insight from high spatial- and spectral-resolution observations in the visible through near-infrared. Observations of space weathering trends in regions of reduced solar wind flux (magnetic anomalies, high latitudes) provide a means to understand the relative rates and influences of the solar wind and micrometeoroid bombardment. And finally new processes of space weathering have been proposed, such as dielectric breakdown that may occur in the poorly conducing regolith at cold temperatures. A synthesis of these topics will provide a means for evaluating important outstanding questions, such as the role of the solar wind, the origin of lunar swirls, rates of weathering, and paths forward for making significant progress toward a better understanding of space weathering across the Moon and across the Solar System.

Changes: Changes since the last New Views of the Moon 2 meeting include the addition several authors and minor updates to the outline.

IMPACT MELT COVER ON CENTRAL PEAKS OF COMPLEX CRATERS: IMPLICATIONS FOR DERIVING CRUSTAL COMPOSITION. Deepak Dhingra[1] and Carle M. Pieters[2], [1]Dept. of Physics, University of Idaho, Moscow, ID, USA (Email: deepdpes@gmail.com), [2]DEEPS, Brown University, Providence, RI, USA

Introduction: Central peaks of complex craters are believed to be the deepest crustal exposures (in some cases, possibly mantle) within a crater [e.g. 1]. This key attribute, along with their generally steep slopes (offering fresh surfaces) and prevalent occurrence of the complex craters, has enabled the extensive use of central peaks for determining crustal compositional trends [e.g. 2,3,4,5]. However, the occurrence of impact melt deposits on the peaks of several impact craters [e.g. 6,7,8,9] raises an important question: *whether the central-peak-derived mineralogy is representative of the crustal composition at depth?* To address this question, we have carried out coordinated 'geological mapping' & 'mineralogical assessment' at impact craters [10, 11] to enable mineralogical comparison of *impact melt-covered* vs *melt-free* regions on the peaks.

The Non-Unique Nature of Impact Melt: Impact melt deposits lack a unique mineralogical signature, meriting detailed evaluation to understand their influence on the central peak mineralogy. Impact melt can exhibit glassy to a completely crystalline texture [12] which directly affects the spectral properties. Further, we have documented examples of heterogeneous impact melt mineralogy within an impact crater [13, 14] as well as examples of homogeneous impact melt [11].

Impact Melt Studies at Crater Jackson: The central peaks of Jackson (Dia. 71 km) provide an excellent example to illustrate the potential influence of impact melt cover on the central peak mineralogy (Figure 1). The peaks are well-known for their exposures of crystalline plagioclase as well as a mafic unit which was suggested to be of potentially impact melt origin [6]. Our mapping of several additional impact melt exposures on the peak [10] and coordinated mineralogical assessment highlights some important aspects:

a) *Melt-covered peak regions exhibit heterogeneous mineralogy*: Impact melt on the peak exhibits contrasting composition with majority of the mapped melt having mafic mineralogy (Fig. 1b; green & red units) while some indicating a feldspathic affiliation (yellow unit). This compositional diversity *within* impact melt illustrates the strong influence of melt mineralogy on the central peaks and the need for such regions to be excluded before deriving any compositional estimates.

b) *Melt-free peak exposures could still be melt coated*: Although large sections of the peak lack any morphological evidence of impact melt, the rather seamless mineralogical continuity across some of these units and the nearby impact melt (regions marked with arrows in Fig. 1c) potentially indicates a thin veneer that cannot be directly detected but can possibly be inferred. Since remotely-derived mineralogy relies on the scattered light from the top few microns, such a coating might further limit the availability of pristine peak regions for deriving crustal composition at depth.

Summary: Central peak impact melt exposures may potentially influence peak mineralogical estimates and the inferred compositional trends of the lunar crust.

References: [1] Melosh (1982) *JGR*, **87**, 371-380 [2] Tompkins & Pieters (1999) *MAPS*, **34**, 25-41 [3] Cahill et al. (2009) *JGR*, **114**, doi:10.1029/2008JE003282 [4] Song et al. (2013) **118**, doi:10.1002/jgre.20065 [5] Lemelin et al. (2015) *JGR*, **120(5)**, 869-887 [6] Ohtake et al. (2008) *Nature*, **461**, 236-240 [7] Dhingra & Pieters (2011) LEAG Meeting, # 2025 [8] Kuriyama et al. (2013) *44th LPSC*, # 1402 [9] Dhingra R. D. et al. (2014) *45th LPSC*, # 1754 [10] Dhingra et al., (2017) *Icarus*, **283**, 268-281 [11] Dhingra (2014) *Ph.D. Thesis, Brown Univ.*, 523p. [12] Tompkins & Pieters (2010) *MAPS*, **45**, 1152-1169 [13] Dhingra et al. (2013) *GRL*, **40**, 1-6 [14] Dhingra et al. (2015) *EPSL*, **420**, 95-101

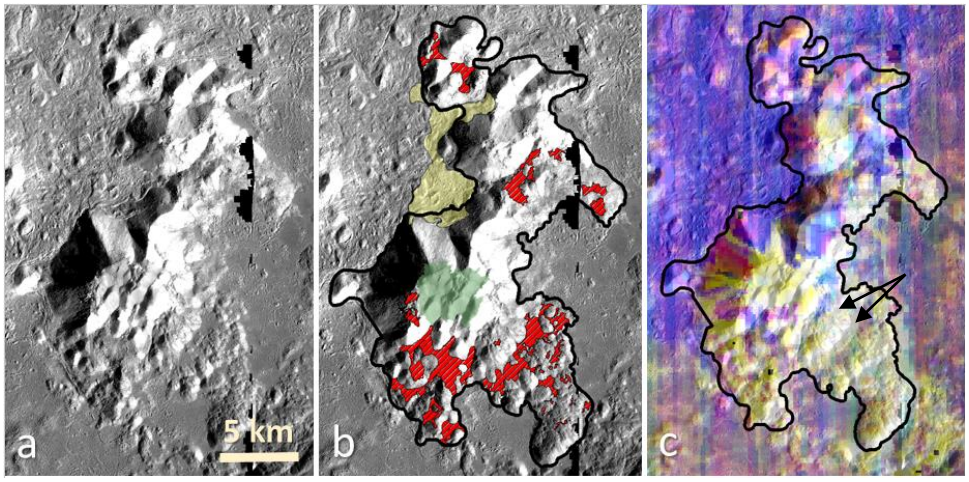

Figure 1 Assessment of impact melt cover on the central peaks of Jackson crater. (a) Kaguya TC context image of the central peaks. (b) Mapped impact melt units on the peak (modified from [10]). (c) Mineralogical color composite of the peaks and surroundings based on Moon Mineralogy Mapper (M^3) data. Red = 1 µm absorption band strength, Green = 2 µm absorption band strength, Blue = Albedo at 1489 nm.

REMOTE SENSING CONSTRAINTS ON THE FORMATION AND EVOLUTION OF THE MOON'S ANORTHOSITIC CRUST. K. L. Donaldson Hanna[1], L. C. Cheek[2], C. M. Pieters[3], J. F. Mustard[3], B. T. Greenhagen[4] and N. E. Bowles[1], [1]Atmospheric, Oceanic and Planetary Physics, University of Oxford, Oxford, UK (Kerri.DonaldsonHanna@physics.ox.ac.uk), [2]Austin, TX, USA, [3]Department of Earth, Environmental and Planetary Sciences, Brown University, Providence, RI, USA, and [4]Johns Hopkins Applied Physics Laboratory, Laurel, MD, USA.

Introduction: The formation of the Moon's primary anorthositic crust is still an outstanding science question as two major hypotheses have been suggested. The impetus for the hypothesis of a lunar magma ocean came from the analyses of pristine Apollo samples [e.g. 1-2] and suggests that the lunar primary crust was formed by the crystallization and flotation of plagioclase (anorthosite's most abundant mineral) in the late stages of a magma ocean. Serial magmatism models have also been suggested in which plagioclase crystallizes from several different plagioclase-rich diapirs and these models are based on the analyses of terrestrial anorthosites, lunar breccias, and feldspathic meteorites [e.g. 3-4]. Thus, examining the local and global distribution of anorthosite across the lunar surface and estimating its compositional variations is significant for better understanding lunar crustal formation processes. In this work we combine the strength of identifying Fe-bearing minerals in near infrared (NIR) remote sensing data with the strength of determining plagioclase composition using remote thermal infrared (TIR) observations to characterize the distribution of pure crystalline anorthosite and determine their composition.

Results: Analysis of Moon Mineralogy Mapper (M^3) NIR observations identified pure crystalline plagioclase (~99-100% plagioclase) widely distributed across the lunar surface. Spectrally pure, crystalline plagioclase was identified in the walls and ejecta of simple craters and in the walls, floors, central peaks, and ejecta of complex craters; most in association with the inner rings of near- and far-side impact basins [5]. While many of the anorthosite identifications are concentrated on the far-side and around impact basins, regions with the highest crustal thickness values [6], anorthosites are also identified within craters with intermediate and lower crustal thickness values [5]. Thus, pure anorthosite is found across large-scale surface features and throughout the crustal column suggesting large coherent zone(s) of anorthosite.

To better understand the compositional variability of plagioclase distributed across the lunar highlands, estimated Diviner Christensen Feature (CF, an emissivity maximum diagnostic of silicate mineralogy [7]) values were analyzed. A single distribution of CF values is observed with a mean CF value of 7.91 ± 0.05 μm suggesting that the average composition of plagioclase identified across the lunar highlands is similar [5]. The mean Diviner CF value can be compared to the wavelength position (7.84 μm) of the CF of high-Ca anorthite (An_{96}) measured under simulated lunar conditions to estimate the An# for the observed pure plagioclase units [5]. The mean Diviner CF value suggests the plagioclase composition across the highlands is relatively uniform in composition, highly calcic ($An_{\geq 96}$), and is consistent with plagioclase compositions found in the ferroan anorthosites ($An_{94\text{-}98}$) [e.g. 1-2] and feldspathic meteorites ($An_{95\text{-}97}$) [e.g. 4]. However, shorter CF values are observed in several craters, including Jackson crater, suggesting some anorthositic units may have less calic plagioclase corrobating earlier Diviner observations [8].

Conclusions: Our integrated remote sensing observations confirm that spectrally pure anorthosite is widely distributed across the lunar surface and most exposures of the primary anorthositic crust are concentrated in regions of thicker crust surrounding impact basins on the lunar near- and far-sides. The global nature of anorthosite identifications and the scale of the impact basins require a coherent zone of pure anorthosite of similar composition in the lunar crust. These considerations along with others including the (1) range in the ferroan anorthosites ages [e.g. 9], (2) geochemical differences observed in Apollo ferroan anorthosites and feldspathic meteorite anorthosites [e.g. 4, 10-11], and (3) the remotely observed differences in the Mg# on the near- and far-sides [e.g. 12-13] are important constraints to be considered in any model for the formation and evolution of the Moon's anorthositic crust.

References: [1] Wood J. A. et al. (1970), *Proc. Apollo 11 Lunar Sci. Conf., 1*, 965-988. [2] Warren P. H. (1985), *Ann. Rev. Earth Planet. Sci., 13*, 201-240. [3] Longhi J. (2003), *JGR, 108*, 2-1 – 2-16. [4] Korotev R. L. et al. (2003) *GCA, 67*, 4895-4923. [5] Donaldson Hanna K. L. et al. (2014) *JGR, 119*, doi:10.1002/2013JE004476. [6] Wieczorek M. A. et al. (2012) *Science,* 671-675. [7] Conel J. E. (1969) *JGR, 74*, 1614-1634. [8] Greenhagen B. T. et al. (2010) Science, 329, 1507-1509. [9] Borg, L. E. et al. (2011) *Nature, 47*, 70-72. [10] Gross J. et al. (2014) *EPSL, 388*, 318-428. [11] Russell S. S. et al. (2014) *Phil. Trans. R. Soc. A, 372*, 20130241. [12] Ohtake M. et al. (2012) *Nature Geosci., 5*, 384-388. [13] Crites S. T. and P J. Lucey (2015) *Am. Mineral., 100*, 973-982.

A FRAMEWORK FOR LUNAR SURFACE SCIENCE EXPLORATION D. Eppler[1], J. Bleacher[2], E. Bell[3], B. Cohen[2], M. Deans[4], C. Evans[5], T. Graff[5], J. Head[6], M. Helper[7], K. Hodges[8], J. Hurtado[9], K. Klaus[1], D. Kring[1], H. Schmitt[10], J. Skinner[11], P. Spudis[1], B. Tewksbury[12], K. Young[5], A. Yingst[13]. 1-Lunar & Planetary Institute, 3600 Bay Area Boulevard, Houston, TX, 77058, eppler@lpi.usra.edu; 2-Goddard Space Flight Center, Greenbelt, MD; 3-University of Maryland; 4-NASA-Ames Research Center; 5-Johnson Space Center; 6-Brown University; 7-University of Texas-Austin; 8-Arizona State University; 9-University of Texas-El Paso; 10-University of Wisconsin; 11-U.S.Geological Survey; 12-Hamilton College; 13-Planetary Science Institute.

Introduction: Successful lunar surface scientific exploration will be dependent on a number of different elements, including: mission concept; mobility; robotic and human crewmembers; crew makeup and training; and geologic field tools and IT assets that enable efficient data collection, sharing, and archiving. These key elements are not independent, and when they are developed together they become the foundation of successful and integrated mission operations. To achieve the best possible lunar surface science exploration, integration of these elements should start at the beginning of a mission concept, to include the development of mission hardware, crew training, and human and robotic operational concepts.

Mission Concepts: Different science problems call for different solutions, and in order to solve these problems, assets and operational approaches must be matched to the appropriate solution. We use the idea of mission concept to define the operational approaches that can be matched to a given solution. Of particular importance is matching the assets to the problem to be solved, so any given mission to the lunar surface has the right assets – robotic and/or human – to accomplish a given scientific activity. Insufficient or excessive assets applied to a problem either puts a given mission in jeopardy of failure, or wastes resources and needlessly increases the risks to human crews.

A Concept I mission involves either a simple sample return for geochemical and radiometric age determination or deployment of geophysical/space physics monitoring assets, and can be conducted robotically without requirements for extensive mobility. Concept II missions involve more detailed robotic rover exploration and sample return from a complex geological area. These missions would be executed over time periods greater than one day, with requirements for increased mobility and dexterity for the robotic asset. In a sense, these could be looked at similar to an Apollo J-mission executed by robots. A Concept III mission resembles an extended Apollo J-mission with as many as 4 crewmembers, duration of up to 14 days, mobility assets to allow a 10-20 km radius of exploration, and up to 150 kg of sample return capability. A Concept III mission could be sent to a site previously investigated by a Concept II robot, or it could be sent to a site where it is clear that human crewmembers will result in the best science return. A Concept IV mission involves advanced exploration capability, with durations longer than a Concept III mission and exploration around a semi-permanent outpost or on long (100s of km) surface traverses. These long traverses are likely to involve multiple small pressurized rovers that can, if necessary, be robotically pre-positioned into a potential exploration area prior to human crew arrival.

Chapter Approach: This chapter will have two sections. The initial section will establish the first order elements that will be needed to support future lunar exploration in four areas: (1) sample management and analysis; (2) surface measurements; (3) information assets and data management, including scientific record development and management, data dissemination, cartographic and photographic products, and geographic location knowledge requirements; and (4) robotic and human mission operations management, including operations approach, crew training, and operations team philosophy. The second section of the chapter will analyze the open questions developed by the each of the other chapter teams. The goal is to determine the different mission concepts will best satisfy each question and to assess the lunar exploration program implications in terms of developing the first order element to address each question.

Progress Since the First Workshop: Teams covering each of the four areas have been formed, and are in the process of developing the information that will be used to write the first section. In addition, a first draft of the mission concepts section has been written and is in review by the team. Once the other chapters in the volume produce their open science questions, the team will analyze these questions in light of the mission concept discussion, and propose mission sets that could be executed to answer a particular science mission.

UPDATES FROM MOON VILLAGE WORKSHOPS AND STUDIES.

B. Foing[1] et al [1]ESA/ESTEC & ILEWG (Bernard.Foing@esa.int)

Summary: We report on Moon Village workshops that gathered a multi-disciplinary group of professionals from all around the world to discuss their ideas about the concept. The workshop participants focussed on **Moon Habitat Design, science and technology potentials** of the Moon Village, and **engaging stakeholders**. We also report on technical and research studies, and activities that followed.

Introduction: The new DG of ESA, Jan Wörner, has expressed from the very beginning of his duty a clear ambition towards a Moon Village, where Europe could have a lead role. The concept of Moon Village is basically to develop a permanent station on the Moon with different countries and partners that can participate and contribute with different elements, experiments, technologies, and overall support.

ESA's DG has communicated about this programme and invited inputs from all the potential stakeholders, especially member states, engineers, industry, scientists, innovators and diverse representatives from the society. In order to fulfill this task, a series of Moon Village workshops have been organized first internally at ESA and then at international community events, and are also planned for the coming months, to gather stakeholders to present their ideas, their developments and their recommendations on how to put Moon Village into the minds of Europeans, international partners and prepare relevant actions for upcoming International Lunar Decade.

Workshop: Several Moon Village Workshops took place in ESTEC and other sites, organized by ILEWG & ESTEC. It gathered people coming from all around the world, with many young professionals involved, as well as senior experts and representatives, with a very well gender balanced and multidisciplinary group. Engineers, business experts, managers, scientists, architects, artists, students… presented their views and work done in the field of Lunar Exploration. Participants included colleagues from ESA, SGAC Space Generation Advisory Council, NASA, and industries such as OHB SE, TAS, Airbus DS, CGI, etc… and researchers or students from various Universities in Europe, America, and Asia.

The Workshops participants split in three working groups: **Moon Habitat Design, Science and Technology potentials on the Moon Village, and Engaging Stakeholders**. They were tasked to discuss ideas, and pilot projects with the aim to consolidate visions for Moon Village stakeholders and provide some recommendations to the ESA DG, Jan Wörner.

The **Moon Habitat Design** group discussed principles and concepts for a minimum base that would start with 4-10 crew, allowing a later evolution to 50 crew and elements contributed by Moon Village partners at large. Various aspects were assessed including habitats, laboratories, EVAs, pressurized vehicles, core modules, inflatable extensions, power systems, life support systems and bioreactors, ISRU using regolith, emergency, services, medical, escape, shelters.

The **Science and Technology** group analyzed the importance and readiness level of technologies needed for lunar robotic landers and for the Moon Village. The current ESA lunar exploration activities focus on the contribution within ISS operations barter of the ESA service module to bring Orion capsule to the Moon starting with an automatic demonstration in 2018. It is encouraged to consolidate this path for using the service module for crewed missions EM2 and EM3 giving also the possibility of an ESA astronaut, together with advanced technology, operations and science utilization. They noted the interesting contribution of instruments, drill, communications, and landing in support to Russian lunar polar lander missions Luna 27.

Building on previous studies (EuroMoon, lunar polar lander) ESA should develop a **mid-class lunar lander** (affordable in cost 300 Meu class), demonstrating the expertise at system level for a platform, that could carry innovative competitive robotic payload contributed and already with advance development from member states and international or commercial partners. With teleoperations from Earth and cis-lunar orbit, this will advance progress towards the next steps of Moon Village and beyond. We shall report on latest activities from these events, studies and field research.

References: [1] http://sci.esa.int/ilewg/ and https://ildwg.wordpress.com/

COMPLEX VOLCANISM AT LUNAR FLOOR-FRACTURED CRATER OPPENHEIMER U. L.R. Gaddis[1], K. Bennett[2], B. Horgan[3], Marie McBride[3], J. Stopar[4], S. Lawrence[5], J.O. Gustafson[6] and T. Giguere[7]. [1] U.S. Geological Survey, Astrogeology Science Center, , Flagstaff, AZ; [2]Northern Arizona Univ., Flagstaff, AZ; [3]Purdue Univ., West Lafayette, IN; [4]Lunar and Planetary Institute, Houston, TX; [5]Johnson Space Center, Houston, TX; [6]Cornell Univ., Ithaca, NY; [7]Univ. Hawaii, Honolulu, HI (lgaddis@usgs.gov).

Introduction: Complex volcanism is observed in floor-fractured crater (FFC) Oppenheimer U, located in the northwest floor of Oppenheimer crater (35.2°S, 166.3°W, 208 km dia., ***Figure 1***) on the lunar far side [1-3]. Fifteen sites of localized pyroclastic volcanism have been identified in the floor of Oppenheimer crater [4]. Studies with Moon Mineralogy Mapper data (M^3, 0.4-3 µm, 86 bands [5]) suggest that Oppenheimer U deposits show variable compositions and the most iron-rich volcanic glass thus far identified on the Moon. Here we examine the floor of Oppenheimer U and show evidence for possible multiple eruptive episodes.

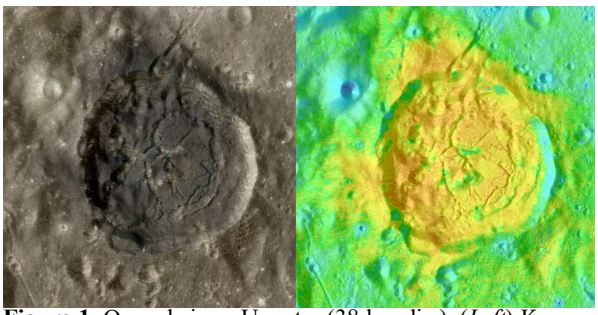

Figure 1. Oppenheimer U crater (38 km dia.). (*Left*) Kaguya MI mosaic (R=900 nm, G=750 nm, B=415 nm). (*Right*) Derived FeO (wt. %) [8].

Analysis: Data from the Lunar Reconnaissance Orbiter (LRO) Wide Angle Camera (WAC) [6] and mineral maps such as FeO derived from SELENE Kaguya Multiband Imager (MI) data [7, 8] for Oppenheimer U crater (***Figure 1***) show a flat floor with prominent fractures, especially on the east and central portions of the floor. Superimposed on those is a very dark pyroclastic mantle that covers much of the crater floor and extends up to 10 km to the west beyond the crater rim. The western floor of Oppenheimer U has a network of at least 6 irregular depressions (***Figures 1, 2, inset***). Topographic data (~60 m/pixel [9]) indicate that the depressions are ~2 to 4 km wide and up to 5.5 km long. The deepest of these depressions is ~1300 m, and it has an asymmetric profile with a steep (~ 35°) western edge and a more gently sloping interior margin (~27°). No raised rim is observed in association with any of these depressions.

A survey of LRO Narrow Angle Camera (NAC) [14] data for this area indicates that there are no small, cone-like features situated on fractures in the floor of Oppenheimer U. NAC data shows that (***Figure 2***) the pyroclastic deposit is a dark unit draped on the crater wall, with prominent dark streaks trending downslope toward the floor and possible cracks at slope breaks.

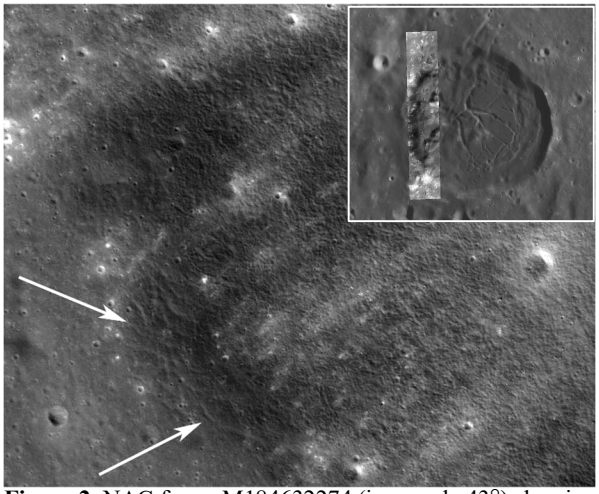

Figure 2. NAC frame M184632274 (inc. angle 43°) showing cracks (white arrows) in mantling material and streaks of low-albedo material trending downward (to the right) toward the crater floor.

Summary: These results suggest the presence of a widespread pyroclastic deposit in the floor of Oppenheimer U crater that erupted violently from multiple source vents, possibly in several episodes. The presence of multiple vents in the floor of Oppenheimer U crater, their association with relatively large irregular depressions, and possible cracks in the mantling deposit supports their origin via a fire-fountain style of eruption [2]. Such eruptions are associated with higher magmatic volatile contents and effusion rates than the Vulcanian-style eruptions observed in FFCs such as those at Alphonsus and elsewhere [e.g., 10]. These results support earlier analyses that indicated a more complex style of volcanism in Oppenheimer crater [2].

References: [1] Jawin, E.R. et al. (2015) JGR-P 120, 1310-1331. [2] Bennett, K. et al. (2016) Icarus 273, 296-314. [3] Gaddis, L. et al. (2014) 45th LPSC, #2383. [4] Gaddis, L. et al. (2013) 44th LPSC, #2262. [5] Pieters. C. et al. (2011) JGR, 116, 1-31. [6] Robinson, M. et al., 2010, Space Sci. Rev. 150, 81-124. [7] Ohtake, M. et al., 2010, Space Sci. Rev. 154, 57-77. [8] Lemelin, M. et al. (2016), 47th LPSC, #2994. [9] Barker, M. et al. (2015) Icarus 273, 346-355. [10] Gaddis, L. et al. (2016) 47th LPSC, #2065.

Magmatic Evolution 1: Initial Differentiation. A. M. Gaffney[1], P. H. Warren[2], L. E. Borg[1], D. S. Draper[3], N. Dygert[4], L. T. Elkins-Tanton[5], K. Joy[6], T. Prissel[7], J. Rapp[8], E. S. Steenstra[9], W. van Westrenen[8]. [1] Lawrence Livermore National Laboratory (gaffney1@llnl.gov), [2] University of California, Los Angeles (pwarren@g.ucla.edu), [3] NASA Johnson Space Center, [4] The University of Texas at Austin, [5] Arizona State University, [6] The University of Manchester, [7] Rutgers University, [9] VU University Amsterdam.

Introduction: The lunar samples retrieved by the Apollo 11 mission in 1969 provided the foundation for the magma ocean model for primordial differentiation of the Moon [1, 2]. Nearly 50 years later, this model remains the leading hypothesis describing the initial magmatic evolution of the Moon, including the formation of a widespread plagioclase-rich crust, the Eu-depleted mafic sources of lunar basalts, and urKREEP, the incompatible element enriched component. Over the past decade, testing of this hypothesis has continued, with investigations that focus on new meteorite samples or remote observations, as well as new experimental, geochemical, geophysical and chronological constraints on the timing of and key processes involved in the initial differentiation of the Moon. A central question of ongoing research continues to be whether the magma ocean remains the best model for early lunar history.

Chapter Summary: This chapter will review and synthesize recent advances on the following topics.

New observations. Anorthositic meteorites recently discovered and analyzed may represent further evidence for a global, extremely plagioclase rich crust with a potentially complex petrogenesis [e.g., 3]. Remote observations and compositional mapping may further reveal complexity in primordial and secondary crust [e.g., 4].

Experimental constraints on magma ocean crystallization. Experimental investigations have focused on evaluating the bulk composition and water content of the Moon, as well as crystallization mode, magma ocean depth and core size and composition [e.g., 5, 6]. The results of recent studies are also used to establish the potential crustal thickness that may result from magma ocean solidification, considering different processes of crystal segregation [e.g., 7].

Geophysical and geochemical models of magma ocean crystallization. Modeling has been employed to constrain the depth or thickness of crystallization products (crust, mantle, core), as well as the physical processes involved in crust formation, the parameters controlling overturn of magma ocean crystallization products and the timing of magma ocean solidification and cooling [e.g., 8, 9, 10].

Chronological constraints on lunar differentiation. Recent efforts have utilized refined analytical methods for measuring the ages of lunar crustal rocks and minerals, as well as determining model ages for the formation of lunar differentiation products including lunar basalt sources and urKREEP [e.g., 11, 12, 13]. Interpretation of lunar chronology is fundamentally linked to the magma ocean differentiation model derived from the combination of sample analyses, crystallization experiments and geophysical modeling.

References:

[1] Smith, J. V., *et al.* (1970) *Proc. A11 LSC* 1:897-925. [2] Wood, J. A., *et al.* (1970) *Proc. A11 LSC* 1:965-988. [3] Gross, J., *et al.* (2014) *EPSL* 388:318-328. [4] Yamamoto, S., *et al.* (2015) *JGR:Planets* 10.1002/2015JE004935. [5] Charlier, B., *et al.* (2015) *46th LPSC* Abstr. 1168. [6] Lin, Y. H., *et al.* (2016) *47th LPSC* Abstr. 1295. [7] Rapp, J. F. and Draper, D. S. (2016) *47th LPSC* Abstr. 2691. [8] Elkins-Tanton, L. T., *et al.* (2011) *EPSL* 304:326-336. [9] Steenstra, E. S., *et al.* (2016) *EPSL* 441:1-9. [10] Piskorz, J. and Stenvenson, D. J. (2014) *Icarus* 239: 238-243. [11] Borg, L. E., *et al.* (2011) *Nature* 477:70-73. [12] Gaffney, A. M. and Borg, L. E. (2014) *GCA* 140:227-240. [13] Nemchin, A., *et al.* (2009) *Nature Geo* 10.1038/NGEO417.

LLNL-ABS-872346.

LONG WAVELENGTH STRUCTURE OF THE LUNAR CRUST: TIDAL-ROTATIONAL ORIGINS AND IMPLICATIONS FOR TRUE POLAR WANDER. I. Garrick-Bethell[1,2], [1]Earth and Planetary Sciences, University of California, Santa Cruz (igarrick@ucsc.edu), [2]School of Space Research, Kyung Hee University, Korea.

Introduction: The origin of the Moon's shape and the structure of its crust at long wavelengths are some of the oldest puzzles in lunar science. Understanding the origins of these features would have implications for the Moon's thermal history, its orbital evolution, and its history of true polar wander. Here I review some of the historical and recent work in this area.

Background: Unlike the shape of the Earth, which is dominantly controlled by its spin, the shape of the Moon is not in hydrostatic equilibrium. That is, the Moon's shape is more distorted than would be expected if it was entirely controlled by tidal forces from the Earth and the Moon's own spin. Laplace was the first to notice this effect, when he inferred the Moon's moment of inertia differences from its precession rate. Historically, these moment of inertia differences were used to represent the distortions of the Moon, but in reality, they are distinct from the Moon's topographic shape – a distinction that becomes important in understanding its origin (below).

In the year 1898 Sedgwick offered an explanation for these moment of inertia differences: because the Moon was once closer to the Earth, it could have frozen in its shape during an epoch of stronger tidal and rotational deformation [1]. In particular, Sedgwick inferred that the freeze-in occurred at a semi-major axis between about 15 and 30 Earth radii. This idea became known as the fossil bulge hypothesis. However, a number of issues eventually arose with this idea. In particular, the ratios of the moment differences did not match those expected from theory, e.g. [2]. In the last few decades, proposals for reconciling the discrepancy suggested that some component of the lunar shape might be due to random geologic "noise" [3, 4].

New tidal-rotational models: A more recent proposal to reconcile the moment of inertia differences with a tidal-rotational shape model came about when it was realized that higher eccentricity orbits and spin-orbit resonances other than 1:1 would affect the moments of inertia differently during freeze-in [5]. The viability of this idea was subsequently deemed unlikely based on orbital evolution models [6].

A further limitation of the above study was that it only used the moments of inertia as a measure of the shape, when in fact the modern era of lunar observations has made available global maps of topography and gravity. The moment of inertia differences can be represented by the degree-2 spherical harmonic gravity coefficients. Garrick-Bethell et al. (2014) analyzed the Moon's topography and gravity together, outside of the largest basins, to infer that the Moon's shape was the sum of two tidal-rotational effects: a frozen fossil bulge, plus tidal heating in the crust [7]. The idea that the lunar crust could be tidally heated had been previously proposed [8], and was based on similar models for Europa's ice shell. Keane and Matsuyama studied the Moon's gravity after removing the effects of basins, but did not analyze the Moon's topography. They inferred that the moments of inertia were consistent with freeze-in during a synchronous orbit with eccentricity of ~0.2 [9].

Other models: Other early evolution models have been proposed to explain the structure of the crust without relying on tidal-rotational effects, e.g. [10].

True polar wander: The history of true polar wander is important for constraining the history of polar volatiles and density changes inside the Moon. The two studies above ([7, 9]) both inferred various degrees of polar wander, based on the orientation of the reference frame that contains the Moon's primordial tidal axis. However, the two inferred polar wander histories disagree with each other, and are in further disagreement with a variety of studies based on lunar magnetic anomalies. Runcorn suggested a pattern behind the Moon's magnetic paleopoles [11], but modern spacecraft data have increased their scatter [12, 13].

Interestingly, there is some degree of agreement between the Moon's "hydrogen paleopole" [14] and the topography paleopole of [7]: a great circle between them passes through the present poles and the center of the Procellarum KREEP Terrane [15]. Further modeling and data interpretation are required to reconcile the diverse paleopoles of the Moon, and better understand its orbital and thermal evolution.

References: [1] Sedgwick, W.F. (1898), *Messenger Math.* **27**, 159. [2] Jeffreys, H. (1937), *Geophys. Journal* **4**, 1. [3] Lambeck, K. & S. Pullan (1980), *PEPI* **22**, 29. [4] Stevenson, D.J. (2001), *LPSC* 32*,* abstract 1175. [5] Garrick-Bethell, I., et al. (2006) *Science* **313**, 652. [6] Meyer, J., L. et al. (2010), *Icarus* **208**, 1. [7] Garrick-Bethell, I., et al. (2014) *Nature* **512**, 181. [8] Garrick-Bethell, I., et al. (2010), *Science* **330**, 949. [9] Keane, J.T. & I. Matsuyama (2014), *GRL* **41**, 6610. [10] Wasson, J.T. & P.H. Warren (1980), *Icarus* **44**, 752. [11] Runcorn, S.K. (1983), *Nature* **304**, 589. [12] Nayak, M., D. J. Hemingway, I. Garrick-Bethell (2017), *Icarus* **286**, 153. [13] Oliveira, J. & M. Wieczorek (2017), *JGR,* in press. [14] Siegler, M. A., et al. (2016), *Nature* **531**, 480. [15] Garrick-Bethell, I. (2016), *LPSC*, 2874.

LATE ACCRETED MATERIAL ON THE LUNAR SURFACE: CONSTRAINTS FROM HIGHLY SIDEROPHILE AND CHALCOPHILE ELEMENTS IN ANCIENT LUNAR IMPACTITES. P. Gleißner[1] and H. Becker[1], [1]Freie Universität Berlin, Institut für Geologische Wissenschaften, Malteserstr. 74-100, 12249 Berlin, Germany (gleissner@zedat.fu-berlin.de).

Introduction: Knowledge of the composition and timing of late accretion onto terrestrial planets is crucial for our understanding of the latest stage of planetary accretion in general, but also its influence on some important compositional parameters (e.g., the arrival of volatiles). In principle ancient lunar impactites may provide constraints on the composition and timing of late accreted projectile populations. Yet, no consensus has been reached on the origin of variably fractionated highly siderophile element (HSE) patterns [1-4], their formation age and assignment to specific basin-forming events [e.g. 2-5].

The compositional range of HSE ratios in lunar impactites was either interpreted to reflect signatures of compositionally distinct basin forming impactors [1, 2] or to result from mixing of several ancient impactor compositions [3]. In either case, the nature of the putative impactors and the chemical variability of impacting populations with time remain not well understood [4]. Alternatively the observed range in HSE compositions may have been produced by large-scale metal-sulfide-silicate segregation in large impact melt sheets [6]. The impactite HSE signature would then reflect fractionation shortly after large impacts rather than processes on the parent bodies of the impactors.

Results and Discussion: Impactites from different landing sites display broadly linear correlations of $^{187}Os/^{188}Os$ (representing the long-term Re/Os ratio of the samples) and HSE ratios which range from chondritic to suprachondritic [1-4]. All impactites which exceed the chondritic range display peculiar high Ru/Pt ratios, a feature which is observed only in a limited number of differentiated metal-bearing meteorites [7]. Available data for siderophile volatile elements range from CI chondrite-like element ratios to strongly fractionated, exceeding the range of primitive meteorites [8].

If the observed spread in HSE ratios between 0.5-1 g samples of lunar impactites was caused by multiple impactors of distinct composition rather than mixing of chondritic with suprachondritic material, then the composition of most impactors was outside the range of known meteoritic compositions sampled on Earth. On the other hand, HSE ratios of all samples investigated by modern methods [1-4, 7] define correlation trends which can be satisfactorily explained by mixing of impactor compositions, similar to known meteorite compositions.

Many Apollo 16 impact melt rocks display sub-mm-scale Fe-Ni metal-schreibersite-troilite intergrowths. Modeling of solid metal-liquid metal partitioning in the Fe-Ni-P-S system indicates formation of these objects by closed system crystallization of solid metal from already fractionated metal melt compositions. Impactites with the highest proportion of metal usually display the most fractionated HSE pattern. The latter observation is inconsistent with fractionation of the HSE during large-scale fractional crystallization and metal segregation in impact melt sheets. Large-scale fractional crystallization of solid metal from S and P rich metallic melt with high P/S in planetesimal or embryo cores is currently the most likely process that may have produced the non-chondritic HSE compositions (including high Ru/Pt ratios) in lunar impactites [7].

The range of HSE ratios in ancient lunar impactites [7] and available impactite formation ages from internal isochron methods [3, 5] are consistent with accretion of chondrite-like and differentiated impactors at 4.2 Ga and variable mixing of their compositions on the lunar surface [3]. Se/Te and S/Se ratios in the range of CI chondrites were found recently in a Fe-Ni metal rich Apollo 16 impact melt rock displaying fractionated HSE patterns similar to volatile element depleted iron meteorites [8]. Impactites with slightly suprachondritic HSE ratios display S-Se-Te ratios suggestive of a predominance of primitive impactor compositions similar to carbonaceous and non-carbonaceous chondrites [3, 8]. These data are further evidence for large-scale mixing and remelting of impactites of different provenance (containing differentiated and primitive impactor material) on the lunar surface.

References: [1] Puchtel I. S. et al. (2008) *GCA 72,* 3022-3042. [2] Sharp M. et al. (2014) *GCA 131,* 62-80. [3] Fischer-Gödde M. and Becker H. (2012) *GCA 77,* 135-156. [4] Liu J. et al. (2015) *GCA 155,* 122-153. [5] Norman M. D. et al. (2016) *GCA 161,* 166-187. [6] Vaughan W. M. et al. (2013) *Icarus 223,* 749-765. [7] Gleißner P. and Becker H. (2017) *GCA 200,* 1-24. [8] Gleißner P. and Becker H. (2017) *LPSC 48,* #1380.

Acknowledgements: This work was funded by the Deutsche Forschungsgemeinschaft (Grant: Be1820/12-1, SFB-TRR 170, subproject B1) and samples were provided by NASA JSC.

OVERVIEW OF SILICIC MAGMATIC ACTIVITY ON THE MOON. T. D. Glotch[1] C. M. Elder[2], P. O. Hayne[2], B. T. Greenhagen3, D. Dhingra[4], and W. S. Kiefer[5], [1]Department of Geosciences, Stony Brook University (timothy.glotch@stonybrook.edu), [2]Jet Propulsion Laboratory, [3]Applied Physics Laboratory, [4]University of Idaho, [5]Lunar and Planetary Institute

Introduction: Lunar "red spots," originally recognized in the Apollo and post-Apollo era of lunar exploration, were thought to be examples of non-mare volcanism. This interpretation was based on the often rugged morphology associated with these features and characteristic featureless red slopes in visible and near-infrared (VNIR) spectra. The Diviner Lunar Radiometer Experiment onboard the Lunar Reconnaissance Orbiter has confirmed the hypothesis that at least some of the red spots are the product of silicic magmatic activity. Notable silicic regions on the Moon include the Gruithuisen domes, the Mairan domes, Hansteen Alpha, Lassell Massif, and Compton Belkovich. In addition, the detection of silicic material in the central peak and ejecta blanket of Aristarchus suggests the excavation of a silicic pluton. Some reported red spots, most notably the Helmet, apparently do not have silicic compositions.

Diviner Data: Diviner is an infrared radiometer that includes three narrow band channels centered at 7.8, 8.25, and 8.55 μm that are used to characterize the silicate Christiansen feature (CF), an emissivity maximum that is indicative of bulk silicate composition. The emissivities of these three "8 μm channels" are used to model the emissivity maximum as a parabola, the maximum of which is taken to be the CF position. Materials with high silica contents including SiO_2 polymorphs and alkali feldspars have CF positions outside of the region that can be characterized by the Diviner CF channels. Instead of defining a concave down parabola, the 8 μm channels display a concave-up spectral shape. Because the concave-up spectral shape is unique to highly silicic materials (with the notable exception of fayalitic olivine), we have defined an index to map the concavity of the Diviner 8 μm channels. So far, this work has focused on high spatial resolution (128-256 pixels per degree) analysis of known red spots, but current and future work is extending our range of analyses to global scales in an effort to identify additional compositionally unique lithologies.

In addition to the compositional information provided by daytime Diviner infrared measurements, Diviner nighttime temperature observations can be used to derive regolith properties including density and vertical variation. We assume regolith density follows an exponential vertical profile which increases with depth over a characteristic length scale, H. This H-parameter is representative of the thermophysical properties of the upper ~30 cm of regolith including rocks smaller than 1 m. Higher H-parameter values correspond to lower thermal inertia (lower density) of the uppermost regolith. Variations in H-parameter could correlate with variations in small rock fragment abundance, regolith porosity, or the crystallinity of the material.

Silicic regions on the Moon tend to be associated with a high H-parameter values, which correspond to a low thermal inertias. Previous work has shown that no clear relationship exists between thermal inertia and composition, so the low thermal inertia material at silicic regions may suggest pyroclastic deposits (containing small glass beads and fewer rock fragments than regolith) or a low-density material such as pumice.

GRAIL Data: Interestingly, Diviner H-parameter measurements at the silicic regions appear to correlate with low bulk densities based on models of Gravity Recovery and Interior Laboratory (GRAIL) data. Recent models of the Gruithuisen Delta dome suggest a bulk density of 2150 ± 150 kg m^{-3}. This is less than typical felsic materials, suggesting a high porosity. While a high primary porosity rock such as pumice is a reasonable candidate to explain the observations, secondary porosity between rhyolitic (or similar composition) rocks formed as materials are pushed away from the vent could also explain the observations. Diviner H-parameter and rock abundance data may help to distinguish between these two scenarios.

M^3 Data: Mg-spinel exposures are most commonly associated with iron-poor feldspathic lithologies and no detectable mafic minerals. The exposures of Mg-spinel at Hansteen Alpha are unique in terms of their association with a highly silicic lithology. Representative Mg-spinel spectra from the region show the typical absence of absorption band at 1 micron which is contrasted by a strong absorption near 2 micron. Work is ongoing to correlate M^3-derived Mg-spinel spectra with variability in mid-IR Diviner thermal emission spectra. This may shed more light on the provenance of the unique Mg-spinel lithology.

Summary: Data from the Diviner Lunar Radiometer, GRAIL, and M^3 all point to unique compositions for many previously recognized red spots. Work is ongoing to correlate these datasets and place additional constraints on the composition of these features. This work, combined with analysis of high resolution imagery and topography and crater counting can place these features in the broader context of lunar magmatic and volcanic history.

DAYTIME DEPENDENCE OF THE NEAR-INFRARED LUNAR WATER/HYDROXYL ABSORPTION DEPTH. A. Grumpe[1], C. Wöhler[1], A. A. Berezhnoy[2], V. V. Shevchenko[2], [1]Image Analysis Group, TU Dortmund University, Otto-Hahn-Str. 4, D-44227 Dortmund, Germany, {christian.woehler | arne.grumpe}@tu-dortmund.de, [2]Sternberg Astronomical Institute, Universitetskij pr., 13, Moscow State University, 119234 Moscow, Russia, {ber | shev}@sai.msu.ru.

Introduction: Analysis of the absorption band at wavelengths around 2.8-3.0 µm apparent in near-infrared spectral reflectance data of the Moon Mineralogy Mapper (M³) instrument [1, 2] has revealed the occurrence of lunar surficial water and/or hydroxyl (OH) [2]. Adsorption of protons from the solar wind and subsequent chemical reactions with oxygen atoms in the lunar surface material as proposed e.g. in [3, 4] are a widely accepted explanation of the origin of this surficial water/OH. An early description of daytime dependent variations of the water/OH absorption depth has been provided in [4].

In this study we analyze the daytime dependent behavior of the OH absorption depth for a set of lunar highland regions for which M³ data acquired at 4-8 different local daytimes are available. These regions are located both near the equator and at high latitudes. In particular, the latitude dependence of the pattern of the OH absorption depth variations during the lunar day is examined.

Data and Method: Based on the M³ level-1B spectral radiance data published on the PDS (pds-imaging.jpl.nasa.gov/volumes/m3.html) we constructed maps of the spectral reflectance for our study regions using the framework of [5].

The spectral radiances in the wavelength range covered by the lunar water/OH absorption are strongly affected by a thermal emission component, which needs to be removed based on an accurate estimation of the surface temperature. Since the thermal removal of the M³ level-2 spectral radiance data on the PDS, for which the well-known approach of [6] has been used [7], is meanwhile considered to be inaccurate (e.g. [8]), we applied the method introduced in [5]. This method extends the thermal equilibrium based approach of [9] by iteratively adjusting the surface temperature and spectral reflectance, and by providing a correction for the surface roughness similar to [10].

Based on the obtained normalized reflectance spectra, the OH band depth integrated over M³ channels 78-84 between 2697 and 2936 nm (here termed OHIBD) is computed [5]. For each study area we constructed a set of OHIBD maps for all daytimes with available corresponding M³ data.

Results and discussion: In highland regions located at moderate and high latitudes >45°, the maximal OHIBD is observed in the early morning around 06:00-08:00 local time. Already within the next 1-2 lunar hours the OHIBD decreases and reaches its minimum value around midday. Typically, the minimum OHIBD value amounts to less than 50% of the maximum value. In the afternoon the OHIBD tends to increase again, but since for only a few of our study regions M³ data acquired under local evening conditions are available, there is no clear evidence for the typical OHIBD level reached in the evening. A mechanism that might explain the observed behavior is the adsorption of solar wind protons [3, 4] reacting with oxygen atoms in the lunar surface minerals [3], counteracted by diffusion [3] and photolysis [5, 11] of the formed OH/water.

In contrast to e.g. [2], we observe also in highland regions located near the equator at low latitudes <20° a significant OHIBD level, in consistence with [8]. In this latitude range the OHIBD shows only insignificant variations with local time, where the OHIBD level is not far below the level observed at high latitudes.

Our observation that the OHIBD level never drops down to zero independent of the latitude suggests the presence of a spectrally detectable strongly bounded water/OH component as proposed e.g. in [8], which might add up with the variable, daytime-dependent component to generate the observed OHIBD behavior.

Acknowledgements: This work was supported by RFBR-DFG grant No. 15-52-12369 and RFBR-DFG grant No. WO 1800/7-1.

References: [1] Pieters, C. M. et al. (2009) *Current Science 96(4)*, 500-505. [2] Pieters, C. M. et al. (2009) *Science 326*, 568-572. [3] Starukhina, L. (2001) *JGR 106(E7)*, 14701-14710. [4] McCord, T. B. et al. (2011) *JGR 116 (E6)*, E00G05, doi:10.1029/2010JE003711. [5] Wöhler, C. et al. (2017) Icarus 285, 118-136. [6] Clark, R. N. et al. (2011) *JGR 116*, E00G16, doi: 10.1029/2010JE003751. [7] Isaacson et al. (2011) M³ Data Tutorial, http://pds-imaging.jpl.nasa.gov/documentation/Isaacson_M3_Workshop_Final.pdf [8] Bandfield, J. L. et al. (2016) *LPSC XXXXVII*, abstract #1594. [9] Shkuratov, Y. G. et al. (2011) *PSS 59*, 1326-1371. [10] Davidsson, B. J. R. et al. (2015) *Icarus 252*, 1-21. [11] Mitchell, E. H. et al. (2013) *PSS 89*, 42-46.

NEW VIEWS OF THE MOON 2: LUNAR VOLCANISM (VOLCANIC FEATURES AND PROCESSES)

James Head[1], Brown University; Harald Hiesinger[1], Westfälische Wilhelms-Universität Münster (co-leads)
Carloyn van der Bogert[2], Westfälische Wilhelms-Universität Münster; Lisa Gaddis[3], USGS Astrogeology Science Center; Junichi Haruyama[4], Institute of Space and Astronautical Science; Debra Hurwitz Needham[5], NASA Marshall Space Flight Center; Lauren Jozwiak[6], John Hopkins Applied Physics Laboratory; T. Morota[7], Nagoya University; Carle Pieters[8], Brown University; Tabb Prissel[9], Rutgers University; Lionel Wilson[10], Lancaster University; Jennifer Whitten[11], Smithsonian National Air and Space Museum

Lunar volcanism is a fundamental process in the geological and thermal evolution of the Moon. Early studies have used geological, petrological, and remote sensing data to define and characterize deposits and features associated with lunar volcanism, and to model the generation, ascent and eruption of lunar magma. Remote sensing data have been used to define and characterize geological units of volcanic origin, to link these units to samples returned from Apollo and Luna missions, and to assess the role of volcanism in lunar thermal history. The advent of Galileo and Clementine remote sensing data permitted more extensive definition and characterization of units, and impact crater size-frequency distribution (CSFD) analyses provided an important assessment of the chronology of emplacement. Improved data (e.g., spatial and spectral resolution and coverage) permitted further documentation of the characteristics of lunar volcanic features and deposits and the implications for the generation, ascent and eruption of magma. A plateau was reached in 2006 with the synthesis and publication of New Views of the Moon, a compendium of the geology, remote sensing, petrology, chronology and thermal evolution of the Moon and, implicitly and explicitly, the role of volcanism.

In the decade since this time, a flood of new data has been acquired and continues to be acquired for the Moon. Missions such as Lunar Reconnaissance Orbiter, Chandrayaan-1, SELENE-Kaguya, Chang'e 1-3, LADEE, LCROSS, and GRAIL have provided views of the Moon and its environment in unprecedented detail. Much of this new information has significant implications for the characterization and understanding of lunar volcanism. From these missions, extremely high-resolution image data have revealed the characteristics and distribution of volcanic features and structures (sinuous rilles, cones, domes, flow fronts, vents, pits, etc.) and permitted improved and more extensive chronology from CSFD analyses. Spectral data have revealed the mineralogy of volcanic features, and gravity data have provided new insight into the thickness and physical properties of the lunar anorthositic crust that mantle-derived melts must transect. These new data have permitted a host of analyses in the last decade that have changed our view of lunar volcanism and the processes of magma generation, ascent and eruption. We now have an improved understanding of the array of volcanic features and provinces: irregular mare patches, IMPs, interpreted as very recent volcanism; floor-fractured craters and evidence for shallow intrusions and eruptions; the global distribution and characteristics of sinuous rilles; new definitions of shield volcanoes; improved understanding of pyroclastic deposits; improved definition and documentation of cryptomaria; documentation of silicic domes and pyroclastic deposits; improved understanding of the cones, domes and flows in volcanic complexes; and many other features. New data have permitted improved chronology for lunar volcanic deposits on the lunar nearside and farside adding constraints on the geological and thermal evolution of the Moon. Finally, these new data have permitted the reassessment of the generation, ascent and eruption of magma on the Moon [1-2].

Progress Since the Last Workshop: New Views of the Moon 2 provides a unique opportunity to synthesize the important developments of the last decade in our understanding of lunar volcanism and its implications for lunar petrology and the thermal evolution. Equally importantly, we are working to identify the set of outstanding questions that will help us improve our current understanding in the coming decades. In the future exploration of the Moon, where do we need to go and what do we need to do to address these most critical questions? How can this information inform the design of new instruments and spacecraft and the architecture of new lunar exploration strategies? What are the roles for robotic orbiters, landers, rovers, and sample return missions? What are the roles for human exploration and human-robotic partnerships? How can humans contribute from lunar orbit or cislunar space?

[1] L. Wilson and J. Head (2017) Generation, ascent and eruption of magma on the Moon: New insights into source depths, magma supply, intrusions and effusive/explosive eruptions (Part 1: Theory), Icarus, 283, 146-175, doi: 10.1016/j.icarus.2015.12.039.. [2] J. Head and L. Wilson (2017) Generation, ascent and eruption of magma on the Moon: New insights into source depths, magma supply, intrusions and effusive/explosive eruptions (part 2: observations), Icarus, 283, 176-223, doi: 10.1016/j.icarus.2016.05.031.

LUNAR IMPACT CHRONOLOGY: STATUS, ADVANCEMENTS, IMPLICATIONS, AND THINGS TO CONSIDER. H. Hiesinger[1], C. H. van der Bogert[1], J. B. Plescia[2], M. S. Robinson[3], S. Robbins[4]. G. Michael[5], N. Schmedemann[5], B. Ivanov[6], W. Hartmann[7], L. Ostrach[8], J.-P. Williams[9], M. Zanetti[10], E. Speyerer[3], S. Werner[11], [1]Institut für Planetologie, Westfälische Wilhelms-Universität, Münster, Germany, Hiesinger@uni-muenster.de; [2]Johns Hopkins University; [3]Arizona State University; [4]Southwest Research Institute; [5]Freie Universität Berlin,; [6]Russian Academy of Sciences; [7]Planetary Science Institute; [8]USGS; [9]UCLA; [10]Western University Ontario; [11]University of Oslo.

Motivation: In 2006, the New Views of the Moon initiative published a seminal book that summarized our understanding of the Moon [*1*]. Since then, numerous innovative and highly capable space missions visited or are visiting the Moon, acquiring data at unprecedented quality and quantity. These data allow us to see the Moon in completely new ways. One area of research that has experienced significant progress since the first book is cratering chronology. Because an accurate understanding of the lunar chronology is not only important to derive absolute model ages (AMAs) of any lunar surface but is also extrapolated to date surfaces on other planetary bodies, it is well justified to reflect the current status, progress, and implications in a dedicated chapter.

In particular, the new global mosaics generated by the Kaguya SELENE (10 m/pixel) and Lunar Reconnaissance Orbiter Camera (LROC) Wide-Angle Camera (WAC; 100 m/pixel) have provided data that have allowed numerous new studies of lunar stratigraphy and crater size-frequency distribution (CSFD) measurements. The LRO Narrow-Angle Camera (NAC) provides higher resolution images with pixel scales of 0.5 m. These data have allowed comprehensive studies of previously uninvestigated mare on the near and farsides [*2-4*], and more detailed studies of regions such as Orientale [*5*] and Australe [*6*]. The new data also allow a renewed investigation of the origins of light plains (e.g., [*7-9*]) and other plains deposits [*10*].

In addition to the many new geological investigations, LROC NAC resolutions have driven new investigations of the limitations of the CSFD technique in relation to, for example, the minimum tenable count area size [*11*], appropriate illumination conditions for measurements [*12*], count area definition – including slope constraints [*13*]; effects of target properties on crater diameters [*14*]; and significance of the population of secondary and self-secondary craters [*15-17*]. Finally, the new data are used to reinvestigate the locations used to calibrate the lunar chronology to improve the robustness/precision of the method [e.g., *18-21*]. The current extension of the lunar crater production SFD shape down to ~2 m craters allows valuable interplanetary comparisons, for example with Mars [*22*].

Chapter Outline: We summarize the current outline for the lunar impact chronology chapter to provide a framework for its ongoing construction. We will heavily crossreference other chapters, including those on magmatic evolution, volcanism, tectonism, impact history, regolith and surface processes, the evolution of the lunar crust, and the interior of the Moon.

This chapter describes our general understanding of the lunar chronology and progress that has been made since the publication of [1]. We provide a historic perspective on CSFD measurements and the development of the lunar chronology. We then discuss the production function (PF) (e.g., origin, shapes, link to chronology) and the chronology function (CF) (e.g., CSFD of landing sites, sample information). Next, we describe method-specific factors that affect CSFDs (e.g., count area size/selection, illumination geometry, image resolution), followed by geology-specific factors (e.g., resurfacing, target properties, secondary craters, self-secondary craters). There will also be a short section on the graphical presentation of CSFDs and the fitting of the data to derive AMAs (e.g., cumulative, differential, Poisson timing analysis, randomness test, and error discussion). After a section on the application of the lunar chronology to date surfaces of other planetary bodies, the main focus of the chapter is to summarize the AMAs of various lunar surface features, including highlands, basins and craters, mare basalts, domes, pyroclastic deposits, Ina and other young volcanic features, light plains, and lunar scarps. This section provides the reader with a comprehensive compilation of AMAs to date as a reference. The final section elaborates on the implications of AMAs for lunar history and evolution, including volcanism, tectonism, the cataclysm, the recent impact rate and the thermal evolution of the interior, crossreferencing other chapters as necessary. The goal of this comprehensive chapter is to offer a valuable resource for people new to the field of dating planetary surfaces, people who are interested in AMAs for a specific region of interest, as well as space agencies, private enterprises, and decision makers.

References: [1] New Views of the Moon, 2006, Rev. Min. Geochem., 60 [2] Morota et al. 2009, Geophys Res. Lett., 36; [3] Paskert et al., 2015, Icarus, 257; [4] Hiesinger et al., 2011, LPSC, 42, 2179; [5] Whitten et al., 2011 JGR, 116; [6] Lawrence et al., 2015, LPSC, 46, 2739; [7] Meyer et al., 2016, Icarus, 273; [8] Thiessen et al., 2012, LPSC, 43, 2060; [9] Hiesinger et al. 2013, LPSC, 44, 2827; [10] Robinson et al., 2016, Icarus, 273; [11] van der Bogert et al., 2015, LPSC, 46, 1742; [12] Ostrach et al., 2011, LPSC, 42, 1202; [13] Meyer et al., 2016, LPSC, 47, 2740; [14] van der Bogert et al., 2017, Icarus, in press; [15] Williams et al., 2014, Icarus, 235; [16] Xiao and Strom, 2012, Icarus, 220; [17] Zanetti et al., 2017, Icarus, in press; [18] Hiesinger et al., 2012, JGR, 117; [19] Robbins, 2014, EPSL, 403; [20] Hiesinger et al., 2015, LPSC, 46, 1834; [21] Iqbal et al., 2017, LPSC, 48, 1258; [22] Hartmann and Daubar, 2017, MAPS, in press.

HETEROGENEOUS IMPACT TRANSPORT ON THE MOON. Y.-H. Huang[1], D. A. Minton[1], M. Hirabayashi[1], J. R. Elliott[1], J. E. Richardson[2], C. I. Fassett[3], and Nicolle E. B. Zellner[4] [1]Department of Earth, Atmopsheric, and Planetary Sciences, Purdue University, West Lafayette, Indiana USA 47907 (huang474@purdue.edu), [2]Planetary Science Institute, Tucson, Arizona USA 85719, [3]NASA Marshall Space Flight Center, Huntsville, Alabama, USA, [4]Department of Physics, Albion College, Albion, Michigan USA 49224.

Introduction: Impactors not only bombard the Moon but also induce the transport of materials on the lunar surface. Excavated materials are deposited in the form of either continuous ejecta surrounding craters or discontinuous crater rays further away from them, and the relative abundances of proximal ejecta vs distal ejecta on the Moon have been debated.

An unexpected highland component in a mare soil sample must be transported from large distances, because the majority of mare plains are thick enough that small craters cannot excavate the underlying highland materials [1]. Especially for mare soil sample collected >20 km away from their nearest mare and highland contact (the source of non-mare material), the contribution of distal ejecta is important to explain the observation of an elevated abundance of a non-mare component seen in most of mare soil samples (20-70%). Yet, the importance of distal ejecta was brought into question when researchers examined samples collected within 4 km of the mare/highland boundary and found that the non-mare abundance dropped rapidly from 80-50% to about 20% at the edge of the mixing zone. The narrow mixing zone, ~4 km, had been interpreted as consistent with the limited transport distances of local materials.

It was then understood that the width of 4-5 km of the mixing zone across mare/highland contacts resulted from the contribution of distal ejecta [2]. However, the relative importance of proximal ejecta vs distal ejecta and how these affect the the transport of materials across contacts are still unclear, and at odds with an exceptionally high non-mare abundance seen in some Apollo 12 mare soil samples [3]. Here we propose a new 3D regolith tracking model that accounts for the spatially heterogeneous nature of ejecta. Using our model, we are able to demonstrate that both proximal and distal ejecta are important to regolith transport, and the nature of ejecta can result in a significant heterogeneity of surface materials seen in a sample.

Method and simulation setup: We developed a 3D regolith tracking code based on the Cratered Terrain Evolution Model (CTEM) that studies the evolution of an impact-dominated surface [4,5]. Our new model includes an ejecta layer tracking system described by (1) a first-in last-out linked list data structure to deal with the generation of a distinct ejecta layer each time, (2) sub-pixel crater mixing that accounts for craters under the resolution limit [6], (3) the crater-ray-like ejecta distribution described by the Superformula [7], and (4) the mixing of crater ray deposits [8]. We have chosen Grimaldi Crater (D =175 km), a pre-Nectarian crater that was flooded by mare basalt ~3.2 Ga ago [9]. The simulation grid space is 175 km by 175 km with the resolution of 120 meter. We split the grid space into an equal area of mare on one side and highland on the other. Our simulated mare side has a 4 km-thick mare layer sitting on the top of an infinitely thick highland layer, and the simulated highland side possesses an infinitely thick layer. We performed five simulations with key components turned on one by one. These simulations are: proximal ejecta only with no sub-crater mixing (Case A); proximal ejecta only with sub-crater mixing (Case B); distal ejecta with no sub-crater mixing (Case C); distal ejecta with sub-crater mixing (Case D); and distal ejecta with sub-crater and ray/ejecta mixing (Case E).

Results: The Case A/B result yields <1 km of the mixing zone in which materials from both sides barely cross the contact. The Case C result has the largest mixing zone, >10 km. The Case D/E results show ~4-5 km of the mixing zone. This suggests that all sizes of craters are essentially important to the transport of materials across the lunar surface. While distal ejecta is capable of carrying a significant amount of exotic material from large distances, the local small craters constantly rework/dilute them with local materials. Besides our 175 km by 175 km mare/highland contact simulation, we also have a global scale simulation that takes into accout the large craters from large distances [8]. As a highly elevated non-mare abundance of 70% is seen in some Apollo 12 mare soil samples, the easiest explanation is the contribution of a Copernicus Crater ray. Our result shows a bimodal distribution between a rayed region (20-40%) and non-rayed region (50-70%). We infer that the patchy nature of crater rays may have resulted in a high heterogeneity of exotic materials among Apollo 12 mare soil samples. Our results strengthen the idea for the presence of Copernicus crater material at the Apollo 12 landing site.

References: [1] De Hon, R. A. (1974) *Proc. 5th LPSC*, 53-59. [2] Li, L and Mustard, J. F. (2000) *JGR, 105,* 20431-20450. [3] Hubbard, N. J., et al. (1971) *Earth Planet. Sci. Lett*, 10(3), 341-350. [4] Richardson, J. E. (2009) *Icarus*, 204, 697-715. [5] Minton, D. A. et al. (2015) *Icarus*, 247, 172-190. [6] Hirabayashi, M. et al. (2017) *Icarus*, in press. [7] Gielis, J. (2003) *Am. J. Bot.* 90, 333-338. [8] Elliott, J. R. et al. (2016) 47th *LPSC*. [9] Greeley, R. (1993) *J. Geophys. Res*. 98(E9), 17182-17205. [10] Li, L. and Mustard, J. F. (2005) *JGR*, 110, 1-16.

SURFACE VOLATILES CHAPTER UPDATE. D. M. Hurley[1] and M. A. Siegler[2], [1]Johns Hopkins University Applied Physics Laboratory (11100 Johns Hopkins Rd., Laurel, MD, 20723 USA; dana.hurley@jhuapl.edu), [2]Planetary Science Institute and Southern Methodist University.

Introduction: The New Views on the Moon 2 "Surface Volatiles" chapter will cover volatile abundance, composition, distribution, and their physical form within the upper ~10m of the lunar surface. This chapter will describe our present state of knowledge about lunar surface volatiles (focusing namely on water and hydrogen), looking at global and polar volatile stability, loss processes, migration (surface and subsurface), and origin. We will briefly discuss evidence from recent missions, outstanding questions and comparisons with other volatile-rich airless bodies (e.g. Mercury, Ceres). The greater community is actively involved in contributing content to the chapter. Content from this chapter overlaps in part with many other chapters including "Summaries of Recent Missions," "Endogenous Volatiles," "Lunar Exosphere," "Space Weathering and Exosphere-Surface Interactions," "Surface Processes (Regolith)," "Lunar Resources," and "The Role of Human Exploration."

Chapter Outline: The chapter is divided into 4 sections.

Introduction. The introduction defines volatiles, provides the old view of volatiles, discusses the significance of volatiles, introduces the reservoirs of volatiles, and summarizes the data sources since the first book.

Quantifying present day volatiles. This section steps through the measureable quantities of the current volatile inventory on the surface of the Moon, both for global volatiles and those concentrated in polar cold traps. We assess the abundance, composition, distribution laterally, with depth, and temporal variability, and the physical/chemical form.

Processes relevant to surface volatiles as a system. This section approaches lunar surface volatiles as a system (or set of systems) beginning with sources. Next it includes redistribution processes and stability of volatiles. Finally it examines loss processes

Outstanding questions and data needed. The final section of the chapter looks to the future and poses the outstanding issues to be addressed, including the complete quantification of the current volatile contents, the age of the deposits, the replenishing rate, the relative importance of source and loss mechanisms, accessibility as a resource, and the integration of knowledge from other related bodies. Volatiles at Mercury, Vesta, Ceres, and in meteorites provide important insight into the understanding of lunar surface volatiles, and vice versa. Future missions to lunar volatiles will enlighten many processes important throughout the solar system.

Contributing Authors: Community involvement in the chapter has been outstanding. The following people are contributing to the chapter at present: Oded Aharonson; Megan Bruck Syal; Joshua Cahill; Anthony Colaprete; Emily Costello; Mona Delitsky; Ariel Deutsch; Richard Elphic; Wenzhe Fa; David Goldstein; Cesare Grava; Ben Greenhagen; Junishi Haruyama; Paul Hayne; Jennifer Heldmann; Amanda Hendrix; Charles Hibbitts; Dana Hurley; Andrew Jordan; Rosemary Killen; Georgiana Kramer; David Lawrence; Shuai Li; Yang (Steve) Liu; Yang Liu; Paul Lucey; Erwan Mazarico; Wes Patterson; Michael Poston; Parvathy Prem; Kurt Retherford; Micah Schaible; Nobert Schorghofer; Matthew Siegler; Paul Spudis; Julie Stopar; Stephen West; Kris Zacny.

Changes Since Last Meeting: No real content changes have occurred since the first workshop.

Potential Overlaps: We are assuming that the "Recent Mission Summary" chapter will provide brief descriptions of the missions, instrumentation, objectives, and relevant references for the recent missions. Therefore we are not providing descriptions of missions or instrumentation in this chapter. We will start with the observations relevant to surface volatiles and their interpretation.

The systems of surface volatiles and endogenous volatiles may overlap. We consider the "surface" to be within 10 m of the surface of the Moon. The primary focus of this chapter is exogenous sources because we assume that endogenic sources will be included in the "Endogenous Volatiles" chapter.

Each of the chapters "Exosphere," "Space Weathering" and "Regolith" contain some overlap with this chapter in that the interaction between volatiles and regolith are a key component. Repeated coverage of this topic is appropriate given the critical importance of this to understanding the stability of volatiles, the modulation of the exosphere, the interpretation of spectroscopic observations, and the thermal properties of the regolith.

Volatiles are one of several potential resources that can be used to facilitate exploration and human operations in deep space. Therefore there is overlap with both the "Lunar Resources" and "Human Role" chapters. We assume that the "Resources" chapter will handle the uses, extraction methods, and economic considerations. This chapter will provide the current state of knowledge regarding current contents that can be referred to by the "Resources" chapter.

ISOTOPIC CONSTRAINTS ON THE ORIGIN OF THE MOON. T. Kleine[1], T. S. Kruijer[1] and C. Burkhardt[1], [1]Institut für Planetologie, University of Münster, 48149 Münster, Germany (thorsten.kleine@wwu.de).

Introduction: The Earth and Moon exhibit a surprising isotopic similarity for several elements that otherwise show large variations among solar system objects [1]. This isotopic similarity is surprising, because the giant impact model typically predicts a significant fraction of impactor material in the Moon. Thus, if the isotopic heterogeneity seen among meteorites extends to the Moon-forming impactor, then the Moon should *not* be isotopically identical to the Earth. Several solutions to this problem have been proposed: (*i*) post-giant impact Earth-Moon equilibration [2]; (*ii*) 'new' giant impact models in which the Moon largely consists of proto-Earth material [3, 4]; (*iii*) formation of Earth and impactor from the same homogeneous inner disk reservoir [1]. In this case no isotopic anomaly is expected for the Moon, regardless of how much impactor material was incorporated into the Moon.

While all these models provide potential solutions for the isotopic similarity of the Earth and Moon for most elements, they cannot easily account for the similar ^{182}W compositions of the Earth and Moon [5, 6]. This is because, unlike genetically relevant isotope variations in elements like O or Ti, ^{182}W compositions reflect the distinct accretion and core formation histories of the Earth and the impactor. As such, the proto-Earth's mantle as well as the impactor mantle and core must have had different ^{182}W compositions. Because during the giant impact, these components were mixed, the Moon should exhibit a ^{182}W anomaly compared to Earth's mantle.

***Expected* ε^{182}W of the Moon:** We calculated the *expected* ^{182}W composition of the Moon in various giant impact scenarios. The main purpose of these calculations is to assess the *likelihood* of producing nearly identical ^{182}W compositions for the Earth's mantle and the Moon. The results of these calculations show that the probability to obtain nearly identical ^{182}W compositions of the Earth and Moon is only ~5% if the Moon predominantly consists of proto-Earth material, and is reduced to ~1% if the Moon largely derives from the impactor (Fig. 1).

Implications for the origin of the Moon: Altbough the nearly identical ^{182}W compositions of the Moon and the Earth's mantle could be coincidence, the probability of this is uncomfortably low. Thus, additional processes might have been important. It has recently been proposed that the Procellarum basin on the Moon formed by a giant impact [7]. Mass balance calculations show that this impact might have lowered the ^{182}W composition of a significant portion of the lunar mantle by up to ~1 ε^{182}W. If the lunar samples analyzed to date would all derive from this modified area, then the Moon might initially have had a larger ^{182}W anomaly, as predicted by our calculations.

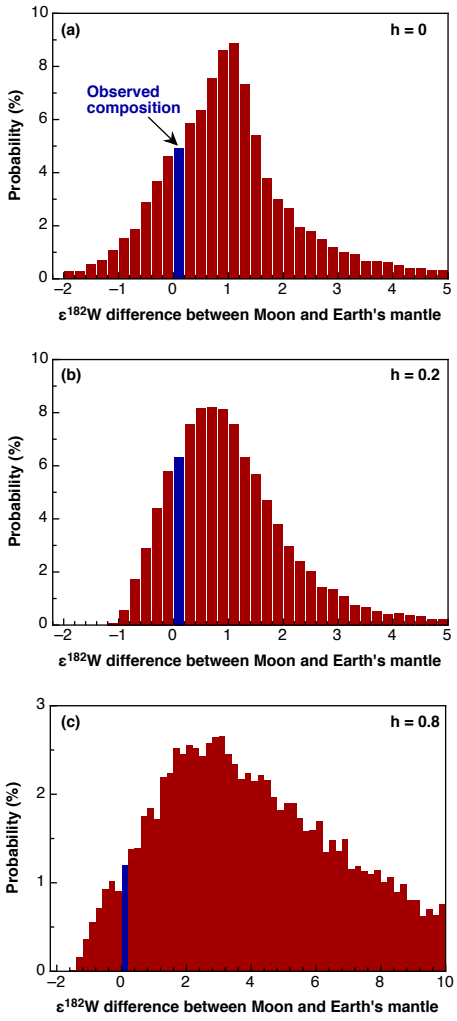

Fig. 1: Histogram showing the expected ε^{182}W difference between the Moon and Earth's mantle. h = mass fraction of impactor material in the Moon.

References: [1] Dauphas, N. et al. (2014) *PTRS A*, *372, 20130244*. [2] Pahlevan, K. and D.J. Stevenson (2007) *EPSL*, *262, 438-449*. [3] Canup, R.M. (2012) *Science*, *338, 1052-1055*. [4] Cuk, M. and S.T. Stewart (2012) *Science*, *338, 1047-1052*. [5] Kruijer, T.S. et al. (2015) *Nature*, *520, 534-537*. [6] Touboul, M. et al. (2015) *Nature*, *520, 530-533*. [7] Zhu, M.H. et al. (2017) *LPSC*, #1851.

USING LUNAR REGOLITH FOR ORGANICS: PLANT GROWTH TESTS USING SOIL ANALOGUES

Kołodziejczyk A. [1] , Vos H. C. [1,2,3] , Harasymczuk M. [1,4], Kraiński M. [1], Foing B. H. [1,2,3], Eifel ILEWG Euro MoonMars 2016 & 2017 support team, [1]ESA/ESTEC, Postbus 299, 2200 AG Noordwijk, NL, [2]ILEWG - International Lunar Exploration Working Group, [3]Vrije Universiteit Amsterdam, [4]University of Warsaw

Introduction: Plant development depends on environmental factors such light, humidity and temperature, seed quality, contaminations and soil type. We study the use of lunar regolith simulants from Eifel volcanic region on the growth of plants.

Methods: In order to analyze growth rate in plants on regolith soil, 10 seeds of cress *Lepidium sativum* (Superseeds, NL) per pot were planted in 4 copies of subsequent soil types: 20 g of autoclaved (2h in 120°C) Eifel regolith simulant soil (RA), 20 g of autoclaved Eifel regolith simulant soil with 2 ml of nutrients (KNOP medium [17]), (RAN), 20 g not autoclaved Eifel regolith simulant soil (R), 10g of peat (S), 10 g of autoclaved peat (SA). Lowered mass of peat (Potgrond universel, BVB Gardening, NL), was used to obtain the same volume of soil in experimental pots. 35 transparent pots were used in the experiment. 20 pots containing seeds, 4 pots per one soil type, and 15 blank pots only with various types of used soils to control contamination processes, 3 pots per one soil type (Figure 1).

Figure 1: Experimental setup for plant growth analysis on regolith simulant Eifel soil. Left side with rows of cress: RA - autoclaved regolith, RAN - autoclaved regolith with nutrients, R - regolith, SA - autoclaved peat, S - peat. On the right side soil samples without plants to analyze contamination effects during watering and cultivation period. Regolith soil differs in color comparing to the dark peat

Two week long experiment was performed in a microharvester (MicroHarvester V3, Germany), in 32°C with 12:12 L:D light/dark conditions (12 hours lights on, 12 hours darkness). Every second day plants were watered with 5 ml of distilled water. Growth rate analysis was performed based on data collected in four subsequent days of the fastest morphological plant transformation (5th, 6th, 7th and 8th day of the experiment), by using imaging method. Images were processed and measured in ImageJ Software. Obtained data was analyzed in Excel.

Results: Morphological changes and diverse plant growth on the regolith simulant soils. In laboratory conditions we could control all parameters, so observed differences were only the effect of soil type and added nutrients. In the 4th day of the experiment plants already emerged from seeds in subsequent values: 60% of plants in RA, 85% in RAN, 95% in R, 90% in SA, and 67% in S. This results suggest that emerging cress from seeds was not affected by the quality of soil, however influence of nutrients could be seen. On the next 4 following days the lengths of stems were measured and visualized in Figure 2.

Figure 2 : Imaging method used in the plant growth analysis. For each testing sample lengths of plant stems were measured and standardized to the imaged scale. Significant morphological changes were observed between compared soil types. This images visualize 12 days old cress.

In general, we observed that plant development was different in different types of soil. In particular, plants grown on the regolith simulant have had thinner leaves and were shorter than the plants grown on peak or regolith with nutrients. Interestingly, autoclaved peak (SA) was better for the plant development than not autoclaved one (S). This suggests, that microorganisms living in not autoclaved soil suppress plant development by evoking stress responses. The growth process reached maximal value in the 6th day of the experiment on regolith soil. The highest averaged growth rate 0.96 cm/day was observed for plants growing on the nutrient-enhanced regolith simulant (RAN).

Acknowledgements. We thank participants to Eifel ILEWG Euro MoonMars 2016 & 2017 support team.

RADIOACTIVE HEAT SOURCES DISTRIBUTION AND MAGNETIC FIELD. M. Laneuville[1], J. Taylor[2], and M. Wieczorek[3]. [1]Earth-Life Science Institute, Tokyo Institute of Technology, Tokyo, Japan, [2]Hawai'i Institute of Geophysics and Planetology, University of Hawai'i, Honolulu, HI 96822, USA, [3]Laboratoire Lagrange, Observatoire de la Côte d'Azur, Nice, France.

Introduction: The Moon possesses a notable enrichment in thorium and other incompatible elements (KREEP) on the nearside in a region called the Procellarum KREEP Terrane (PKT). The exact nature of the relationship between this enrichment and the highly correlated volcanic activity is debated, but it has been shown that different distributions of heat sources will lead to drastically different long term evolution, with influence on magnetic field generation [1,2], crater morphology [3], true polar wander [4], and magmatism [e.g. 5-7].

Here we use updated radioactive heat sources budget estimates as well as insights from remanent magnetization of the crust to test different scenarios of heat sources distribution. In particular, we start by focusing our attention on the implications for magnetic field generation (as dictated by core cooling), and the ability of the crust to record that field (by comparing its temperature to the Curie temperature of iron).

Modeling approach. We use the 3D thermo-chemical convection code Gaia already used in [5], changing only the initial distributions of radioactive heat sources. As an initial set of parameters, the core is 330 km and possesses 4 wt.% S as an alloying element, the melting curve and reference viscosity correspond to that of a dry peridotite, and there is no density contrast in the mantle other than that generated by melting (Boussinesq approximation).

New estimates of the thickness of the lunar highlands from the GRAIL mission allow us to update refractory elements budget. We use the model definitions from [8] in addition to a model 5, where the inner most region of the PKT (about 1700 km in diameter) is richer in radiogenic elements. See the Table below for a description of the models.

	M1	M2	M3	M4	M5
Highlds.	0.2	1	0.2	0.2	0.2
PKT	5.7	5.7	8.2	5.7	4
In. PKT					8.2
Highlds.	0.04	0.0074	0.025	0.038	0.04
PKT	0.04	0.0074	0.025	0.055	0.055

Table 1. Thorium content of the different regions in ppm (Th/U = 3.68, K/U = 1250). "Highlds." stands for highlands crust and "In. PKT" is the innermost PKT region. Gray areas are crust and white are mantle concentrations.

Preliminary results. The first result is that the evolution of the Curie isotherm depth within the PKT is, not unexpectedly, directly related to the heat sources content of that region. Interestingly, the underlying mantle's concentration plays a role only after the Curie isotherm reaches the upper mantle. Figure 1 shows that a delay of about 500 Ma exists between the time required by the C-isotherm to reach the bottom of the crust in models 1, 2 and 4 versus model 3, and finally model 5. This may help explain the lower remanent magnetization observed in the innermost PKT: the crust was simply too hot to record the ambient magnetic field at the time where it was the strongest.

It is interesting to note that these different models will also have implications for the mantle melting rate and core cooling rate, which will in turn influence the timing of the dynamo. For instance, model 4-5 have an earlier peak in volcanic activity and a larger production in general than the other models.

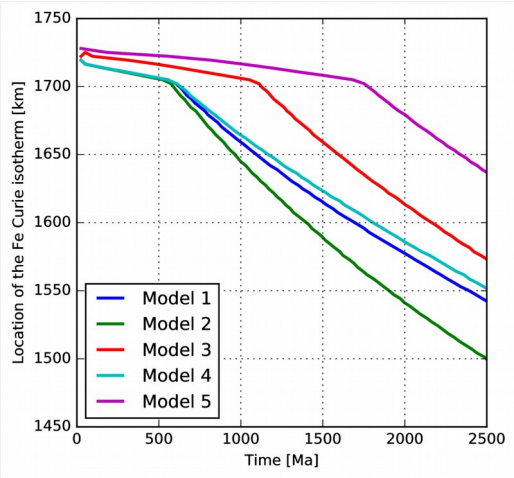

Figure 1. Evolution of the Curie isotherm for iron (1043 K) for the different models presented here.

Concluding remarks. Understanding the distribution of KREEP material in the lunar crust is key to unravelling its early history. Here we propose a new constraint and test the implications of those distributions on both mantle and core evolution of the Moon.

References. [1] Laneuville et al. (2014) *EPSL*, [2] Scheinberg et al. (2015) *Icarus*, [3] Miljkovic et al. (2013) *Science*, [4] Siegler et al. (2016) *Nature*, [5] Laneuville et al. (2013) *JGR*, [6] Zhang et al. (2013) *JGR*, [7] Evans and Zuber (2014) *JGR*, [8] Taylor & Wieczorek (2014), *Phil. Trans. R. Soc. A.*.

LUNAR EXPLORATION MISSIONS SINCE 2006. S. J. Lawrence[1], L. R. Gaddis[2], K. H. Joy[3], N. E. Petro[4]
[1]Astromaterials Research and Exploration Science, NASA Lyndon B. Johnson Space Center, Houston, TX, USA (samuel.j.lawrence@nasa.gov) [2]Astrogeology Science Center, United States Geological Survey, Flagstaff, AZ, USA [3]School of Earth and Environmental Sciences, University of Manchester, Manchester, UK [4]NASA Goddard Space Flight Center, Greenbelt, MD, USA

Introduction: The announcement of the Vision for Space Exploration in 2004 [1] sparked a resurgence in lunar missions worldwide. Since the publication of the first "New Views of the Moon" volume [2], as of 2017 there have been 11 science-focused missions to the Moon. Each of these missions explored different aspects of the Moon's geology, environment, and resource potential. The results from this flotilla of missions have revolutionized lunar science, and resulted in a profoundly new emerging understanding of the Moon.

The New Views of the Moon II initiative itself, which is designed to engage the large and vibrant lunar science community to integrate the results of these missions into new consensus viewpoints, is a direct outcome of this impressive array of missions. The "Lunar Exploration Missions Since 2006" chapter will "set the stage" for the rest of the volume, introducing the planetary community at large to the diverse array of missions that have explored the Moon in the last decade.

Content: This chapter will encompass the following missions:

- Kaguya
- ARTEMIS
- Chang'e-1
- Chandrayaan-1
- Moon Impact Probe
- Lunar Reconnaissance Orbiter (LRO)
- Lunar Crater Observation Sensing Satellite (LCROSS)
- Chang'e-2
- Gravity Recovery and Interior Laboratory (GRAIL)
- Lunar Atmosphere and Dust Environment Explorer (LADEE)
- Chang'e-3

At the present time, we envision the content presented in this chapter as a succinct description of each mission, with only a limited discussion of mission discoveries and outcomes. For each of these missions, we will discuss in general terms the mission parameters and the capabilities of each spacecraft, with an emphasis on the instrument suites. The goal of this chapter is to serve as a reference so that subsequent chapters can simply cite this chapter for details about aspects of the mission, such as instrument performance and characteristics, and help avoid repetition in subsequent chapters of the NVMII volume.

The reason for this approach is that ideally, the discoveries and implications arising from each of these missions will be infused throughout the NVMII volume. By necessity, this means that the content presented in this chapter will be dependent to some degree upon the content presented in other chapters. Any discussion of discoveries and outcomes in this chapter will accordingly emphasize discoveries and outcomes not discussed in other chapters.

Future Work: In order to ensure that the perspective of each mission is adequately expressed in this chapter, we will contact members of each mission team to solicit input for specific subsections, and when necessary, define needed additional limited-scope prospective writing contributions. The lead author will work to integrate these specific contributions when needed into the chapter.

Expected Outcome: The goal of the NVMII initiative is to synthesize the emerging results of these missions into new consensus understandings of the Moon. This is a key aspect of understanding our Solar System and vital for defining the next decade of activity on and around the Moon with humans and their robotic precursors. By serving as a concise summary of recent lunar activity, we expect that this chapter will play an important role in the structure of the NVMII volume itself and serve as a useful reference for subsequent chapters and the larger planetary science community.

References: [1] NASA, "The Vision for Space Exploration [NP-2004-01-334-HQ]," NASA, Washington, D. C., NP-2004-01-334-HQ, 2004. [2] B. L. Jolliff, M. A. Wieczorek, C. Shearer, C. R. Neal (eds.), *Rev. Mineral. Geochem.*, vol. 60, no. 1, Jan. 2006.

MINERALOGY AND IRON CONTENT OF THE LUNAR POLAR REGIONS USING THE KAGUYA SPECTRAL PROFILER AND THE LUNAR ORBITER LASER ALTIMETER.

M. Lemelin[1], P. G. Lucey[2], S.T. Crites[3], K. Jha[4], [1]Department of Earth & Space Science & Engineering, York University, 4700 Keele St, Toronto, ON, Canada M3J 1P3, lemelin@yorku.ca, [2]Hawaii Institute of Geophysics and Planetology, Department of Geology and Geophysics, University of Hawaii at Manoa, 1680 East-West Rd, POST 602, Honolulu, HI 96822, USA, [3] Institute of Space and Astronautical Science (JAXA/ISAS), 3-1-1 Yoshino-dai, Chuo-ku, Sagamihara, Kanagawa 252-5210, Japan, [4]NASA Goddard/Sigma Space Corporation, 4600 Forbes Boulevard, Lanham, MD 20706, USA.

Introduction: Quantitative assessment of the mineralogical composition of the lunar surface using visible (VIS) and near-infrared (NIR) wavelengths can be obtained by comparing calibrated reflectance spectra to modeled spectra of known composition, and assigning the composition to the best spectral match using FeO as a constraint to ensure that the best spectral match is compositionally and physically plausible. However, in the polar regions, calibrated reflectance data had not been derived until recently, and the FeO abundances currently available have a coarse spatial resolution (~15 km per pixel). As a result, beside a few local studies [e.g., 1-4], most mineral analyses have been constrained to within 50° in latitude. The mineralogy of the polar regions, or ~44% of the lunar surface, is mostly unknown. Here we took a novel approach to derive the first mineral and FeO maps of the polar regions (50-90° in latitude) at 1 km per pixel.

Methods: We used of the newly available calibrated reflectance data from the Lunar Orbiter Laser Altimeter (LOLA) [5,6] along with reflectance ratio from the Kaguya Spectral Profiler (SP) [7,8] to derive the first high resolution FeO maps of the polar regions. These maps are in excellent agreement with the FeO abundances measured by the Lunar Propector Gamma-Ray Spectrometer [9] (r = 0.96, σ = 5 wt.%).

We used continuum-removed reflectance from SP (level 2B1) acquired during the North and South polar summers (orbits 2000-2999 and 4000-4999) and radiative transfer equations to model the mineral abundances of each spectrum, constrained by its FeO abundance. We used Hapke's radiative transfer equations and the optical constants of Lucey et al. [10] to model 118,818 spectra. This includes: 6601 mixtures of olivine, low-calcium pyroxene, high-calcium pyroxene and plagioclase, nine different amount of nanophase iron (0-0.7 wt.% [11]) and Britt-Pieters particles [12], two different grain sizes (17 and 200 μm), and a Mg-Number of 65. For each SP spectrum, we then identified the most similar modeled spectra that contains within ±5 wt.% FeO of the local FeO.

Results: Our preliminary results indicate that the FeO and mineral mapping methods are promising. The new FeO abundance maps allows to resolve details such as pyroclastic deposits and small geological units with high FeO content. The mineral maps reveal that low-calcium pyroxene is widely abundant (especially in the South Pole-Aitken with up to ~40 wt.%). High-calcium pyroxene is much less abundant (up to ~10 wt.%) and especially concentrated in the center of the South Pole-Aitken basin, as found by [3]. We find exposures with ≥98 wt.% plagioclase on the rim of Shackleton crater consistent with the observations of Yamamoto et al. [2]. Next, in an effort to reduce the orbit-to-orbit noise resulting from the interpolation of the SP points into mineral maps, we will derive new versions of the mineral maps using data points from the nearly 7000 available SP orbits.

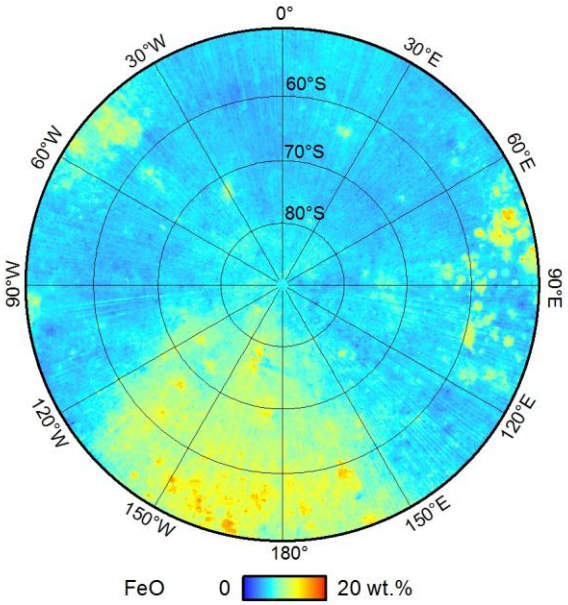

Figure 1. South polar map of FeO derived using Kaguya Spectral Profiler 955.5/752.8 nm reflectance ratio, and Lunar Orbiter Laser Altimeter 1064 nm reflectance data at 1km/pixel.

References: [1] Ohtake M. et al. (2009) *Nature*, *461*, 236-241. [2] Yamamoto S. et al. (2012) *GRL*, *39(L13201)*. [3] Ohtake M. (2014) *GRL*, *41*, 2738-2745. [4] Kramer et al. (2013) *Icarus*, *223*, 131-148. [5] Smith D.E. et al. (2010) *Space Sci. Rev*. *150*, 209-241. [6] Lemelin M. et al. (2016) *Icarus*, *273*, 315-328. [7] *Matsunaga* T. *et al.* (*2001*) *Proc. SPIE*, *4151*, *32-39*. [8] Haruyama J. et al. (2008) *EPS*, *60*, 243-255. [9] Lawrence D.J. et al. (2002) *JGR*, *107(E12)*, 5130. [10] Lucey P.G. (1998) *JGR*, *103(E1)*, 1703-1713. [11] Hapke B. (2001) *JGR*, *106(E5)*, 10,039-10,073. [12] Lucey P.G. and Riner M.A. (2011) *Icarus*, *212*, 451-462.

STABLE ISOTOPE CONSTRAINTS ON THE FORMATION OF MOON. T. Magna[1], N. Dauphas[2], K. Righter[3] and R. Canup[4]. [1]Czech Geological Survey, Prague, Czech Republic (tomas.magna@geology.cz), [2]Origins Lab, Department of the Geophysical Sciences and Enrico Fermi Institute, The University of Chicago, USA (dauphas@uchicago.edu), [3]Astromaterials Research & Exploration Science, NASA, Houston TX, USA (Kevin.righter-1@nasa.gov), [4]Space Science & Engineering Division, Southwest Research Institute, Boulder, Colorado, USA (robin@boulder.swri.edu).

Summary: The development of high-precision techniques to measure stable isotope compositions of a number of elements which, in the past, were considered homogeneous, implicated a new fresh look at the origin of Moon. Prior to 2004, only limited stable isotope information was available that mainly focused on oxygen isotopes in Apollo samples and lunar meteorites [1,2]. These studies have shown, to a high degree of confidence, that O isotope similarity (or identity) of Earth and Moon is a unique feature among bodies of the Solar System. More recent investigations [3,4] have re-assessed these earlier conclusions to an unprecedented precision of a few ppm. While the nature of this striking O isotope uniformity remains elusive, it either reflects effective homogenization of pre-collisional isotope disparity or indicates a broad isotope homogeneity of early Solar System planetesimals [5,6]. In general, the information and constraints on lunar origin derived from stable isotope systems are manifold as briefly outlined here.

It is notable that some other refractory elements show a similar degree of isotope identity between Earth and Moon. The highly refractory nature of W makes it an ideal candidate for tracing the earliest stage of Earth–Moon evolution. Advanced measurements of selected lunar materials have shown a slight excess of ^{182}W compared to Earth [7] but these authors were able to derive a pre-impact ε^{182}W which is identical for Earth and Moon [also 8]. Several models were discussed to account for W isotope homogeneity between Earth and Moon prior to the Giant impact. Given the refractory nature of W, a post-collisional exchange in hot atmosphere [5] may require substantial revisions.

Nucleosynthetic Ti anomalies were reported for a number of meteorite classes, including chondrites and achondrites, with the entire range of ε^{50}Ti values spanning nearly six ε units. Yet, lunar samples and their mineral constituents do not show any resolved departure from Bulk Silicate Earth value at ε^{50}Ti ~0 [9,10]. Zhang et al. [10] suggested that most lunar Ti should have a terrestrial origin, which appears to be in agreement with recent dynamic models [11]. Indeed, similar conclusions have been made for Cr [12] but given the still limited data set for stable Cr isotope compositions, further analyses are required because it could place constraints on the lunar core formation. In this respect, Si isotope analyses of lunar samples may provide further tests for core formation in the Moon. Silicon isotope homogeneity between Earth and Moon [13] requires that formation of a small metallic lunar core was incapable of sequestering a significant fraction of Si, a process thought to have occurred for Earth [14]. In this respect, [15] predicted isotopically heavy Si for Moon (~0.14‰ in δ^{30}Si) provided there had been a vapor-mediated exchange between Earth and Moon. The lack of any shift for current data set represents an argument against the equilibration model [5].

Stable isotope compositions of more volatile elements were rather rarely analyzed due to technical limitations. The early measurements of potassium isotope compositions in lunar rocks [16] have shown δ^{41}K values identical to those of Earth within contemporaneous analytical errors. The recent imporovements have allowed to distinguish between Earth and Moon at the δ^{41}K scale of ~0.2‰ [17]. Although the latter result is highly significant in itself as it requires high pressures and temperatures in the mantle atmosphere disc, the detailed implications for lunar origin are yet to be evaluated with the relevant experimental data.

References:

[1] Wiechert U. et al. (2001) *Science, 294*, 345–348. [2] Clayton R.N. & Mayeda T. (1996) *GCA, 60*, 1999–2017. [3] Herwartz D. et al. (2014) *Science, 344*, 1146–1150. [4] Young E.D. et al. (2016) *Science, 351*, 493–496. [5] Pahlevan K. & Stevenson D.J. (2007) *EPSL, 262*, 438–449. [6] Dauphas N. et al. (2014) *Phil. Trans. Roy. Soc. A, 372*, 20130244. [7] Kruijer T.S. et al.. (2015) *Nature, 520*, 534–537. [8] Touboul M. et al.. (2007) *Nature, 450*, 1206–1209. [9] Leya I. et al. (2008) *EPSL, 266*, 233–244. [10] Zhang J. et al.. (2012) *Nature Geosci., 5*, 251–255. [11] Canup R.M. et al. (2015) *Nature Geosci., 8*, 918–921. [12] Bonnand P. et al. (2016) *GCA, 175*, 208–221. [13] Armytage R.M.G. et al. (2012) *GCA, 77*, 504–514. [14] Georg R.B. et al. (2007) *Nature, 447*, 1102–1106. [15] Pahlevan K. et al. (2011) *EPSL, 301*, 433–443. [16] Humayun M. & Clayton R.N. (1995) *GCA, 59*, 2131–2148. [17] Wang K. & Jacobsen S.B. (2016) *Nature, 538*, 487–490.

TOWARDS AN UNDERSTANDING OF INITIAL CRATER ROCK POPULATIONS: COPERNICUS CRATER VS. AVERY CRATER. S. Mazrouei[1] and R. R. Ghent[2], [1]Department of Earth Sciences, University of Toronto, Toronto, ON, Canada. [2]Planetary Science Institute, Tucson, AZ, USA.

Introduction: A new method for determining the ages of lunar Copernican-aged craters younger than roughly a billion years old has recently been established. Ghent et al. [1] documented an inverse relationship between the rockiness of large craters' ejecta, derived from the Lunar Reconnaissance Orbiter's Diviner thermal radiometer data [2], and the craters' ages. In previous work [3, 4], we used this method to date all craters with d>10 km and younger than 1 Gyr. This method assumes that all impact craters with d>10 km produce statistically similar initial rock populations, independent of their size or location on the Moon.

To determine whether the survival time of rocks varies for different rock sizes, and to distinguish how much of this rock breakdown is due to micrometeorite impacts versus other factors, we need to have a better grasp on how initial rock population in an impact varies based on the two main following factors. a) Crater size: it has been shown that ejecta sizes from an impact are proportional to the crater diameter [5, 6]. However, it is not yet known whether survival times differ for rocks of different sizes. b) Target terrain (mare versus highlands): different target strengths in an impact result in different ejecta sizes [5]. However, whether similar sized impacts produce the same initial rock size or frequency population in different terrains is yet to be determined.

In this work, we compare the ejecta rock populations of craters of similar sizes but different ages, and vice versa, both in the highlands and the maria. We do this by mapping rock locations and sizes in the ejecta blanket of several craters.

Methodology: Here, we report on preliminary results of rock counts for Copernicus Crater with a model age of ~800 Ma [e.g., 7], and Avery Crater with a Diviner rock abundance derived age of ~150 Ma [4]. Both craters are in the maria but vary in age. Due to the large size of these craters (~93km and ~11km in diameter for Copernicus and Avery, respectively), we only map rocks in three 20° wedges in different radial directions (north, southeast, and southwest) to 1 radius from the crater rim. Further explanation of the methodology can be found in [8].

Preliminary Results and Discussion: We have mapped ~2000 resolvable rocks larger than 10m in the ejecta of Copernicus. Though 10m is larger than the smallest theoretically detectable rock based on the image resolutions (generally assumed to be 2-3 pixels), we are limited by the fact that only a few NAC images exist in some parts of our large mapping areas, and our image mosaics consist of NAC frames with different incident, emission, and phase angles. We observe a rollover in rock sizes < 20m in the preliminary size-frequency distribution (SFD) plot (Figure 1), which indicates an incomplete dataset. Similarly, we have mapped ~1350 rocks larger than 2m in the ejecta of Avery Crater, with an observed rollover in rock sizes < 4m.

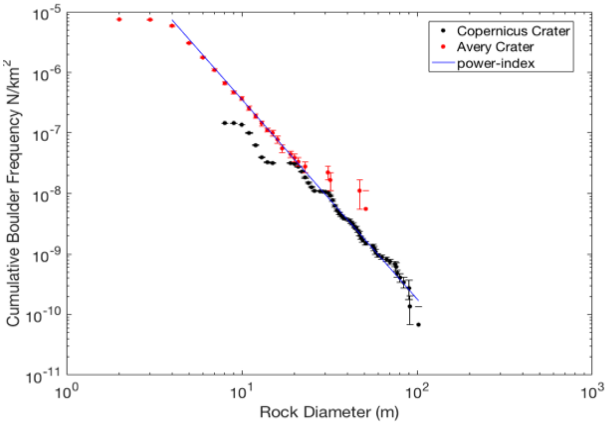

Figure 1: Rock size-frequency distribution in the ejecta of Copernicus and Avery craters.

The largest rock mapped at Copernicus is ~103m in diameter, versus ~52 m at Avery, consistent with the relationship between crater size and maximum ejected rock size. The preliminary slope derived from a linear fit to both rock populations, excluding a few outliers (rocks < 20 m at Copernicus, and 30m < rocks < 4m at Avery Crater), is ~-3.3. The similarity between these plots further shows the expected rock populations breakdown based on size. This slope is within the predicted range of -1.8 to -3.7 for lunar rocks [9]. The slope value lies within the steeper range of the previously mentioned power indices, indicating that smaller rocks are more numerous compared to larger ones.

To further determine the role of terrains, crater ages and sizes in the survival time of rocks, we will next map rocks on the ejecta blanket of similar size craters as Avery in the highlands and of an older age.

References: [1] Ghent, R.R., et al. (2014), *Geology 42,* 1059-1062. [2] Bandfield, J.L., et al. (2011), *Journal of Geophysical Research* 116: E12. [3] Mazrouei, S., et al. (2015) *LPSC XLVI*, Abstract # 2331. [4] Mazrouei, S., et al. (submitted) *Nature Astronomy*. [5] Vickery, A. M. (1986), *Icarus*, 67, 224-236. [6] Moore, H. J. (1971), *NASA Spec. Publ.* SP-232, 26-27. [7] Hiesinger, H., et al. (2012) *Journal of Geophysical Research* 117: E00H10. [8] Mazrouei, S. and Ghent R. R. (2017) *LPSC XLVIII*, Abstract #2507. [9] Cintala, M. J., and McBride, K. M. (1994), *LPSC XXV*, Abstract #261.

ENDOGENOUS LUNAR VOLATILES *Co-leads*: F. M. McCubbin[1] & Y. Liu[2]; *Contributors*: J. J. Barnes[1], J. W. Boyce[1], J. M. D. Day[3], S. M. Elardo[4], H. Hui[5], T. Magna[6], P. Ni[7], R. Tartèse[8], and K. E. Vander Kaaden[9], [1]NASA Johnson Space Center, Mailcode XI2, 2101 NASA Parkway, Houston, Texas 77058, USA [2]Jet Propulsion Laboratory, California Institute of Technology, Pasadena, California 91109, USA. [3]Geosciences Research Division, Scripps Institution of Oceanography, La Jolla, CA 92093-0244, USA [4]Geophysical Laboratory, Carnegie Institution of Washington, 5251 Broad Branch Rd. NW Washington DC 20015 [5]State Key Laboratory for Ore Deposit Research, School of Earth Sciences and Engineering, Nanjing University, Nanjing 210023, China [6]Czech Geological Survey, Kla´rov 3, CZ-118 21 Prague 1, Czech Republic [7]Department of Earth and Environmental Sciences, University of Michigan, Ann Arbor, MI 48109 [8]School of Earth and Environmental Sciences, University of Manchester, Manchester, UK [9]Jacobs, NASA Johnson Space Center, Mailcode XI, 2101 NASA Parkway, Houston TX 77058, USA (email: francis.m.mccubbin@nasa.gov).

Introduction: At the time of publication of New Views of the Moon [1], it was thought that the Moon was bone dry with less than about 1 ppb H_2O. However in 2007, initial reports at the 38th Lunar and Planetary Science Conference speculated that H-species were present in both apatites [2] and pyroclastic volcanic lunar glass beads [3]. These early reports were later confirmed through peer-review [4-8], which has motivated many subsequent studies on magmatic volatiles in and on the Moon within the last decade. Some of these studies have cast into question the post-Apollo view of lunar formation, the distribution and sources of volatiles in the Earth-Moon system, and the thermal and magmatic evolution of the Moon. Consequently, this chapter will synthesize and summarize all of the work on endogenous lunar volatiles that has occurred since 2007. Although we acknowledge that there have been a considerable number of studies on volatiles prior to 2007, these studies have been summarized previously in a recent review article in American Mineralogist [9] and in The Lunar Source Book prior to that [10].

Chapter Summary: The chapter will begin with an introduction that defines magmatic volatiles (e.g., H, F, Cl, S) versus geochemical volatiles (e.g., K, Rb, Zn). We will discuss our approach of understanding both types of volatiles in lunar samples and lay the ground work for how we will determine the overall volatile budget of the Moon. We will then discuss the importance of endogenous volatiles in shaping the "Newer Views of the Moon", specifically how endogenous volatiles feed forward into processes such as the origin of the Moon, magmatic differentiation, volcanism, and secondary processes during surface and crustal interactions.

After the introduction, we will include a review/synthesis on the current state of 1) apatite compositions (volatile abundances and isotopic compositions); 2) nominally anhydrous mineral phases (moderately to highly volatile); 3) volatile (moderately to highly volatile) abundances in and isotopic compositions of lunar pyroclastic glass beads; 4) volatile (moderately to highly volatile) abundances in and isotopic compositions of lunar basalts; 5) volatile (moderately to highly volatile) abundances in and isotopic compositions of melt inclusions; and finally 6) experimental constraints on mineral-melt partitioning of moderately to highly volatile elements under lunar conditions. We anticipate that each section will summarize results since 2007 and focus on new results published since the 2015 Am Min review paper on lunar volatiles [9].

The next section will discuss how to use sample abundances of volatiles to understand the source region and potential caveats in estimating source abundances of volatiles. The following section will include our best estimates of volatile abundances and isotopic compositions (where permitted by available data) for each volatile element of interest in a number of important lunar reservoirs, including the crust, mantle, KREEP, and bulk Moon. The final section of the chapter will focus upon future work, outstanding questions, and any insights on the types of samples or experimental studies that will be needed to answer these questions.

Chapter changes since the NVM II 2016 Workshop: In the months following the 2016 NVM II workshop, we were informed by the steering committee that the request to have a stand alone chapter on stable isotopes was denied. Consequently, we have decided to cover the topic of volatile stable isotopes in our chapter and include a synthesis/review of new stable isotope data where relevant. There were no additional major changes to report on the contents of this chapter.

References: [1] Jolliff et al (2006) *RiMG* 60 721 pp **[2]** McCubbin et al (2007) *37th LPSC* #1354 **[3]** Saal et al (2007) *37th LPSC* #2148 **[4]** Saal et al (2008) *Nature* 454, 192-195 **[5]** McCubbin et al (2010) *PNAS* 27, 11223-11228 **[6]** Boyce et al (2010) *Nature* 466, 466-469 **[7]** Greenwood et al (2011) *Nat. Geosci.* 4, 79-82 **[8]** Tartèse et al (2013) *GCA* 122, 58-74 **[9]** McCubbin et al (2015) *Am. Min.* 100, 1668-1707 **[10]** Taylor et al (1991) *The Lunar Source Book*, p. 183–284. Cambridge University Press, U.K.

AGES OF DIKE INTRUSIONS ON THE MOON. A. L. Nahm[1] and V. R. Chierici[1], [1]German Aerospace Center (DLR), Rutherfordstr. 2, 12489 Berlin, Germany. Amanda.Nahm@dlr.de; Valeria.Chierici@dlr.de.

Introduction: Recent work [1] has shown that several of the graben on the lunar nearside are dike-related, based on modeling of graben cross-sectional topography. In this study, we examine 3 regions containing 4 dikes identified by [1]: Rimae Daniell (37° N, 24° E), Rima Ariadaeus (7° N, 13° E), Rima Hyginus (7° N, 7°E), and Rima Hesodius (30° S, 22° W) to determine the age(s) of these graben and, therefore, the age(s) of the dike intrusions. Determination of the ages of these intrusions provides insight into the crustal and magmatic evolution of the lunar crust in both space and time.

Methodology: To determine the ages of the graben and the dike intrusions, we first created geologic maps of the 3 study regions and then determined the ages of the units crosscut by the graben by crater counting.

Geologic mapping was based on chemical composition of the lunar surface determined from spectral data from the Clementine spacecraft (http://www.lpi.usra.edu/lunar/tools/clementine/). To delineate the geologic units, three compositional maps were created: FeO and TiO_2 abundance (wt %) and the standard RGB color ratio map. For each study region, these 3 maps were overlain with varying transparencies in ArcGIS atop the portion of the 100 m/px Lunar Reconnaissance Orbiter (LRO) Wide Angle Camera (WAC) global morphologic map (http://wms.lroc.asu.edu/lroc/view_rdr/WAC_GLOBAL) to create an enhanced color ratio map, as described in [2].

Using the CraterTools extension [3] in ArcGIS, craters larger than 200 m within the units that are crosscut by the rimae were marked on the LROC WAC basemap. Model ages were derived from the crater size-frequency distribution using CraterStats [3]; the production and chronology functions used to determine the ages are from [4].

Results: *Rimae Daniell:* For the Rimae Daniell region, a total of 21 geologic units, ranging from fresh highland material to mature mare, were delineated. The ages derived for the 2 units crosscut by Rimae Daniell were found to be 3.4 Ga and 3.7 Ga [Fig. 1]; thus the maximum age of the dike intrusion here is 3.4 Ga.

Rimae Ariadaeus and Hyginus: For the Rimae Ariadaeus/Hyginus region, a total of 59 geologic units were mapped. The ages derived for the 13 units crosscut by the rimae can be grouped into three age groups: 3.3 Ga, 3.6 Ga, and 3.8 Ga; thus the maximum age of the dike intrusions here is 3.3 Ga.

Rima Hesodius: For the Rima Hesodius region, a total of 58 geologic units were mapped. The ages derived for the 11 units crosscut by the rima can be grouped into three age groups: 3.6 Ga, 3.7 Ga, and 3.8 Ga; thus the maximum age of the dike intrusion here is 3.6 Ga.

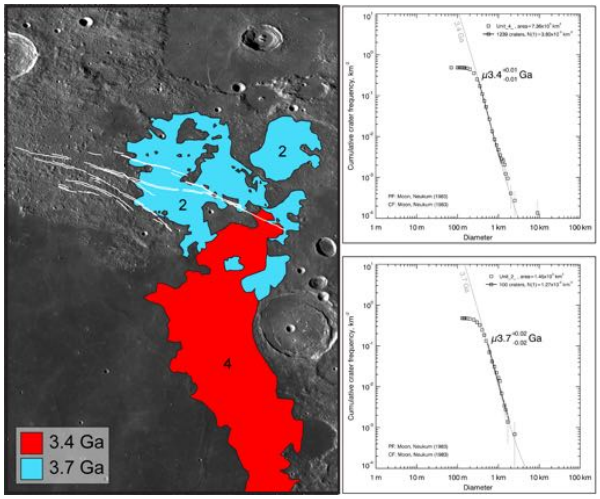

Figure 1. Map of Rimae Daniell (white lines) with numbered geologic units colored according to age. Right: Crater size-frequency distributions and isochrons for the 2 counted units. Basemap: LRO WAC mosaic.

Discussion: Model ages derived for the dike-induced graben in our study regions indicate that linear magmatism (i.e., dikes) and extensional tectonics on the lunar nearside was occurring as recently as 3.3 Gyr ago; this age is much younger than the widely cited age for the formation of the nearside graben of 3.6 ± 0.2 Ga [5]. Our results are consistent with both the ages determined for the Rupes Recta normal fault [6] and of mare basalt (3.93 to 1.2 Ga) [7].

References: [1] Klimczak, C. (2014), Geology, 963 – 966. [2] Kramer, G. Y. et al., (2015), JGR, 120, 1646-1670. [3] Kneissl T. et al. (2011), PSS, 59, 1243-1254. [4] Neukum G. (1983), Habilitation Thesis for Faculty Membership, Univ. of Munich, 186 pp. [5] Lucchitta and Watkins (1978), LPSC Proc., 9, 3459-3472. [6] Nahm and Schultz (2013), Geol. Soc. London Sp. Pub. 401, 377-394. [7] Hiesinger, H. et al (2003), JGR, 108, 5065.

Acknowledgements: The authors thank G. Y. Kramer and T. Öhman for help with delineating the geologic units and S. Adeli for help with the crater counting and interpretation. A. L. Nahm is funded by the Alexander von Humboldt Stiftung/Foundation and V. R. Chierici is funded by the Bundesausbildungsförderungsgesetz (BAföG).

LUNAR TECTONICS CHAPTER IN THE UPDATED NEW VIEWS OF THE MOON 2 VOLUME. A. L. Nahm[1] and C. L. Johnson[2], [1]German Aerospace Center (DLR), Rutherfordstr. 2, 12489 Berlin, Germany. Amanda.Nahm@dlr.de; [2]University of British Columbia, Vancouver, BC Canada V6T 1Z4, cjohnson@eos.ubc.ca.

Introduction: An updated version of the New Views of the Moon (NVM) volume from 2006 [1] is planned, in which our understanding of the Moon since the beginning of the 21st century will be synthesized. While the original NVM volume did not include a chapter on lunar tectonics, the best reference for the state of knowledge of lunar tectonics pre-Lunar Reconnaissance Orbiter (LRO) was published in the Planetary Tectonics book [2], authored by Watters and Johnson [3].

In our updated chapter regarding lunar tectonics, we will discuss tectonic features on the Moon and their implications for lunar tectonic evolution. The chapter will extend the work of [2], emphasizing new findings that resulted from the most recent lunar missions (since 2006), including the ongoing LRO mission, the Kaguya/SELENE mission, and the Gravity Recovery and Interior Laboratory (GRAIL) mission. The chapter will begin with descriptions of the tectonic structures on the Moon, i.e., graben, wrinkle ridges, lobate scarps, and the newly discovered small-scale normal faults. Each section on structure type will include maps of their global distribution (e.g., Figs. 1 and 2) as well as GIS-compatible files, morphological descriptions, and hypothesized formation mechanisms. Much recent work has focused on the timing of these tectonic structures, and a section of the chapter will focus on this aspect of lunar tectonics. Because the Moon is the only other planetary body to have had seismometers on its surface, any connections between lunar seismicity recorded by the Apollo-era seismometers and faults will be discussed. We will discuss the relationship of observed tectonic features to volcanic features and their implications for the stress fields during and postdating major magmatic periods in lunar history. Similarly, we will discuss any constraints that tectonic features place on regional and global thermal evolution models. We will conclude the chapter with outstanding questions, hopefully to be addressed in the next version of the chapter.

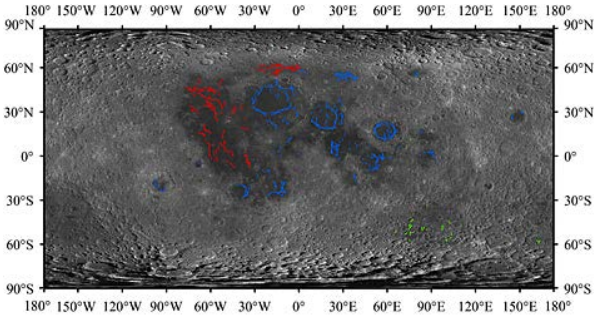

Figure 1. Global distribution of lunar wrinkle ridges, with different wrinkle ridge types color coded: concentric (blue), parallel (red), and isolated (green) ridges. From [4].

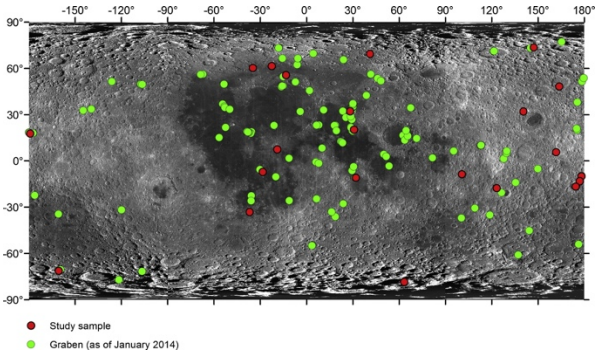

Figure 2. Distribution of small-scale graben discovered since January 2014 (green dots) and the sample analyzed in this study (red dots). From [5].

References: [1] Jolliff, B. L., et al. (editors) (2006), New Views of the Moon, Reviews in Mineralogy and Geochemistry, Vol. 60. Mineralogical Society of America, Chantilly, VA. [2] Watters, T. R. and R. A. Schultz (editors) (2010), *Planetary Tectonics*, Cambridge University Press. [3] Watters, T. R. and C. L. Johnson (2010), Lunar tectonics, in *Planetary Tectonics*, Watters and Schultz (editors), Cambridge University Press, pp. 121-182. [4] Yue, Z. et al. (2015), JGR-Planets, 120, 978–994. [5] French, R. A. et al. (2015), Icarus, 25, 95-106.

LUNAR IMPACT BASIN POPULATION AND ORIGINS REVEALED BY LOLA AND GRAIL G. A. Neumann[1], S. Goossens[2], J. W. Head[3], E. Mazarico[1], H. J. Melosh[4], D. E. Smith[5], M. A. Wieczorek[6] , M. T. Zuber[5], Lunar Orbiter Laser Altimeter and Gravity Recovery and Interior Laboratory Teams, [1]Solar System Exploration Division, NASA Goddard Space Flight Center, Greenbelt, MD 20771, USA (gregory.a.neumann@nasa.gov), Center for Research and Exploration in Space Science and Technology, University of Maryland, Baltimore County, Baltimore, MD 21250, USA, [3]Department of Earth, Environmental and Planetary Sciences, Brown University, Providence, RI 02912, USA, [4]Department of Earth, Atmospheric, and Planetary Sciences, Purdue University, West Lafayette, IN 47907, USA, [5]Department of Earth, Atmospheric and Planetary Sciences, Massachusetts Institute of Technology, Cambridge, MA 02139, USA, [6]Institut de Physique du Globe de Paris, Sorbonne Paris Cité, Université Paris Diderot, CNRS, Paris 75013, France.

Introduction: The Lunar Orbiter Laser Altimeter (LOLA) [1] and Gravity Recovery and Interior Laboratory (GRAIL) [2] missions created the basis for a global assessment of the crustal structure of the Moon [3] and the history of impact structures, in particular those of diameter exceeding ~200 km known as basins [4, 5]. The cumulative size-frequency distribution (CSD) of lunar basins has previously been estimated from imperfect data and was uncertain by factors of two or more, but no significant revisions to the numbers and sizes of basins since GRAIL are anticipated.

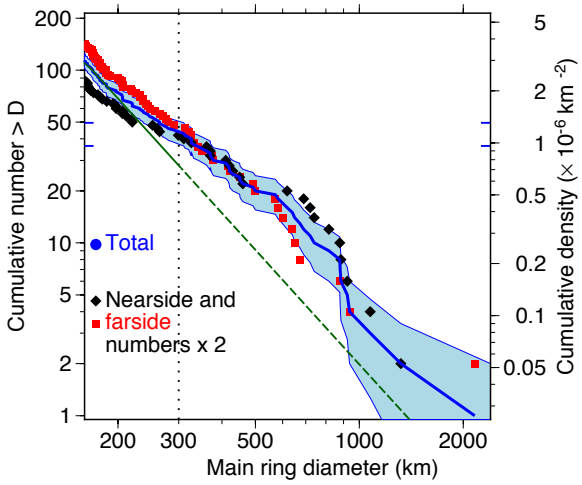

Figure 1: Cumulative size-frequency distribution for complex craters and basins [4]. The blue line shows data for all the craters and basins in Table 1. The shaded region spans the 1-SD error estimates. Black diamonds and red squares show the cumulative size-frequency distributions for nearside and farside craters, respectively, normalized by area; for these symbols, the cumulative number scale on the left reads two times the value. Blue horizontal ticks show confidence limits of N(300) for the overall population. The cumulative Hartmann production function [6] for craters larger than 64 km is shown by the green line with a slope of −2.2, extrapolated for diameters larger than 300 km (vertical dotted line). The main ring diameter was inferred from the diameter of the central Bouguer anomaly high for basins observed in GRAIL data that lack an outer topographic rim.

The CSD shown in Fig. 1 does not differ greatly from earlier Hartmann power-law production function [6], apart from uncertainties in the determination of the principal diameter of the basins, particularly those that possess multiple rings. GRAIL gravity data allow the exclusion of several incorrect identifications and confirm the existence of basins for which the topographic signature has been obscured by subsequent crater formation. The known relations among the diameters of a peak ring, the central Bouguer anomaly, and the main basin rim allow us to estimate the approximate size of basins that lack confidently measurable topographic rings. The precision of GRAIL is allowing the detection of one or more previously unknown craters using gravity gradiometry [7] for smaller sizes where the population is denser but less uniform [5].

The size of impactors in relation to the basin population is, however, a matter of current debate [8–10]. As well, the population and dynamics of the early solar system giving rise to a proposed cataclysmic bombardment continues to be discussed [11–13]. The integration of current lunar datasets will have strong bearing on the cratering flux and crater retention ages for the other terrestrial planets, because it is the lunar cratering rate that anchors the impact chronology for the entire inner solar system.

References: [1] Smith D. E. et al. (2010) *Geophys. Res. Lett. 37,* L18204. [2] Zuber M. T. et al. (2013) *Science 339*, 668–671. [3] Wieczorek M. A. (2013) *Science 339*, 668–675. [4] Hartmann W. K. and Kuiper G. P. (1962) *Commun. Lunar Planet. Lab. 1*, 51–66. [5] Neumann G. A. et al. (2015) *Sci. Advances 1*, doi: 10.1126/sciadv.1500852. [6] Stöffler D. et al. (2006). *Rev. Mineral. Geochem. 60*, 519–596. [7] Sood R. et al. (2015) *LPSC 46*, 1883. [8] Miljković K. et al. (2013) *Science 342,* 724–726). [9] Schultz P. H. and Crawford D. A. (2016) *Nature 535,* 391–394. [10] Bottke W. F. et al. (2012) *Nature 485*, 78–81. [11] Gomes R. et al. (2005) *Nature 435*, 466–469. [12] Strom R. G. et al. (2005) *Science 309,* 1847–1850. [13] Minton D. A. et al. (2015) *Icarus 247*, 172–190.

DISTRIBUTION AND COMPOSITION OF THE LUNAR MANTLE MATERIAL AND ITS IMPLICATION. M. Ohtake[1], S. Yamamoto[2], K. Uemoto[3], Y. Ishihara[1], [1]Japan Aerospace Exploration Agency (JAXA) (ohtake.makiko@jaxa.jp), [2]National Institute for Environmental Studies, [3]Tokyo Univ.

Introduction: No sample originating directly from the lunar mantle is known among currently available lunar samples and lunar meteorites. Therefore, it is critical to understand the composition of the lunar mantle based on remote-sensing data of the exposures of mantle materials.

Recent remote-sensing data obtained by the Kaguya Spectral Profiler (SP) found exposures with olivine-rich spectral features globally distributed on the lunar surface [1]. Based on their being on or near rings of large basins, it is suggested that these olivine-rich exposures may have originated from the mantle. Therefore, these locations can be the data source for mantle material analyses. Another data source is the South Pole-Aitken basin, which is the largest clearly recognized basin on the lunar surface and thought to be excavated mantle material deeper than other basins [2].

We conducted detailed mineralogical and morphological analyses of these locations to identify if the origin of material observed there is mantle and if so, to estimate the composition of the lunar mantle materials.

Origin and composition of olivine-rich materials: We evaluated reflectance, space weathering, geologic context, distribution and size of the exposures, composition (FeO abundance), surface texture (roughness and rock abundance), and local slopes of the each olivine site and estimated and classified their origins as likely mantle, volcanic, crustal, or unclear. About 60% of the sites are estimated to be mantle, 5% are volcanic, 30% are crustal, and 5% are of unclear origin. Mantle origin sites surround large basins whereas volcanic origin sites are within mare, and crustal origin sites either surround or are far from large basins. FeO abundance of the estimated mantle origin sites ranges from 6 to 13 wt.%. Though the percentage of each origin is not necessarily proportional to the volumes (surface area) of each category, there are many olivine sites of mantle origin around Crisium, Imbrium, and Nectaris. The estimated excavation depth of these basins indicates it is likely to reach the mantle, which is consistent with the estimation of mantle origin for these olivine sites. The identified volcanic and crustal olivine-rich sites, which have not been reported previously, are aslo important for understanding the formation mechanism of olivine-rich magma and crustal intrusion (troctorite). Note that some of the locations classified as crustal possibly result from spacial mixting of crustal rock (purest anorthosite: PAN) with more mafic silicate-rich rock such as Mg-suite rock because exposures of the olivine-rich material are sometimes very small and surrounded by PAN rocks.

Distribution and composition of mantle material of the SPA basin: Recent computer simulation of SPA basin formation suggests that SPA generated impact excavated mantle material and the mantle material was ejected and mounded on the basin interior except the central part, where impact melt was pooled [2]. Remote-sensing observation of the reflectance spectra of the SPA basin suggests that low-Ca pyroxene dominant rock appears to be the ejected and mounded mantle material [3]. Detailed analyses of the central part of the basin also indicates that the SPA impact melt underwent magmagic differentiation and made at least two differentiated layers (upper high-Ca pyroxene and lower low-Ca pyroxene layers) several kilometers thick. Furthermore, the composition of the two observed layers compared to the prediction by a petrologic magmatic differentiation model [4] suggests that the observation is consistent if the lunar magma ocean were solidified into two mantle layers (olivine dominant and low-Ca pyroxene dominant layers) and mantle overturn occurred before the SPA basin formed [5].

Implication of the distribution and composition of mantle material: These mineralogical analyses of the big basins including SPA basin indicate that vertical heterogeneity (possibly two layers of olivine dominant and low-Ca pyroxene dominant) of the lunar mantle, which apparently correspond to the original depth rather than the results of lateral variation. Furthermore, the lunar mantle possibly overturned after the magma ocean solidified.

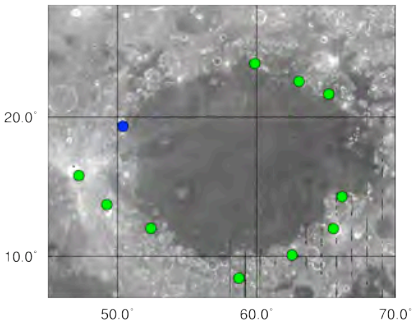

Fig. 1. Distribution of olivine-rich material at Mare Crisium. Green (blue) indicates the locations estimated to be mantle (crustal) origin.

References: [1] Yamamoto S. et al. (2012) *Geoph. Res. Lett.* 39, L13201. [2] Potter et al. (2012) *Icarus*, 220, 730-743. [3] Ohtake M. et al. (2014) *Geoph. Res. Lett.* 41, 2738-2745. [4] Hurwitz D. M. and Kring D. (2014) *J. Geophys. Res.*, 119, 1110-1133. [5] Uemoto K. et al. (2017) *submitted*.

IMPACT AMPLIFIED MAGNETIC FIELDS AS A POSSIBLE SOURCE OF CRUSTAL MAGNETIZATION

R. Oran, and B. P. Weiss, Department of Earth, Atmospheric and Planetary Sciences, Massachusetts Institute of Technology, Cambridge, Massachusetts, USA (roran@mit.edu)

Introduction: Although the Moon does not presently have a core dynamo magnetic field, spacecraft measurements have revealed the presence of remanent magnetization in the lunar crust. The formation of the crustal magnetic anomalies remains a mystery. Much of this magnetization is thought to have been produced by cooling in the presence of a core dynamo magnetic field [1]. However, the identification of lunar crustal magnetic anomalies at the antipodes of four of the five youngest large (>600 km diameter) impact basins [2-5] has motivated the alternative hypothesis that the lunar crust could have been magnetized by the impacts. The question whether the crustal magnetization is a record of ancient intrinsic fields or of external carries broad implications to our understanding of the Moon's history and internal structure. Furthermore, the lunar crustal field serves as a test case for understanding magnetization of other solar system bodies, such as Mars, Mercury, and asteroids.

Hypothesis: The theoreal picture that was suggested as an explanation of the antipodal anomalies can be described as follows. During the impact, lunar and impactor material are vaprorised and ionized. The resulting ionized vapor cloud interacts and compresses the surrounding solar wind towards the antipode, causeing the field there to amplify. Heated or shocked lunar rocks at the antipode would subsequently record these transient field amplifications [6-9]. Although this hypothesis has been studied for several decades using hydrodynamic and impact simulations, a conclusive answer can only be obtained by simulating the coupled interaction of the ionized vapor with the magnetized solar wind.

A natural framework for describing magnetized plasmas self-consistently is the system of magnetohydrodynamic (MHD) equations. The development of high performance MHD codes in the last decade allows us to revisit these previous important studies. We performed three-dimensional (3D) MHD simulations of a vapor cloud embedded within a background solar wind, and examined how these will effect the previous estimations of the strength and duration of the magnetic field enhancement at the antipodal points. The MHD simulations will also allow us to estimate the importance of removal of magnetic flux due to reconnection and expansion of the vapor cloud. This will help in assessing how likely it is for impacts to trigger remnant crustal magnetization.

Method: We use BATS-R-US [9], a highly parallelized, 3D MHD code, to simulate the coupled evolution of the vapor cloud and the magnetized solar wind plasma. BATS-R-US is capable of simulating ideal- and resistive-MHD regimes, as well as a single fluid or several fluids/species. Our effort currently focuses on the plasma phase of the cloud and does not aim to model the formation of the cloud from the impact itself. The initial cloud properties are taken from detailed impact simulations appearing in the literature.

We will consider different MHD processes, such as: 1) the finite resistivity of the lunar mantle and magnetic diffusion inside the body, 2) magnetic reconnection at the antipode, and 3) the transport of magnetic flux due to solar wind motion. This allows us to systematically examine whether impact-generated fields can indeed be responsible for the formation of crustal field enhancements on the Moon.

Results: We present a set of MHD simulations of this process. The strength of the amplified field depends on the rate of convergence of vapor in the antipode, as well as the time scale for diffusion of magnetic field, the strength of the solar wind field, and its direction. From scenarios explored thus far, impacts produce peak fields of ~0.2-1 μT, compared to the 30-100 μT required for shock remnant magnetization. We demonstrate that the level of field amplification is limited by the vapor expansion speed and magnetic field reconnection, which both act to remove magnetic flux from the system.

Discussion: Our simulation results suggest that the compression of the solar wind magnetic field at the antipodes of impacts is insufficient to explain the magnetization on the lunar crust. We propose that the source of magnetization is more likely to have been an internal core dynamo. This implies that the Moon formed an advecting metallic core in its early history.

References:

[1]Weiss, B. P. and Tikoo, S. M. (2014) [2] Anderson, K.A. and Wilhelms, D. G. (1979) [3] Hood et al. (1979) [4] Hood et al. (2001) [5] Halekas et al. (2001), [6] Hood, L. L. and Vickery, A. (1984) [7] Hood, L. L. (1987) [8] Hood, L. L. and Huang, Z. (1991), [9] Hood, L. L. and Artemieva, N. A. (2008) [10] Toth, G. et al. (2012)

DO THE OLIVINE-PLAGIOCLASE OBSERVATIONS AT BASINS IMPLY LUNAR MANTLE OVERTURN? C. M. Pieters[1] [1]DEEPS, Brown University, Providence, RI 02912 USA (Carle_Pieters@brown.edu)

Introduction: The role of olivine in lunar crustal evolution has been debated for decades. Remote characterization of olivine-dominated lithologies began with the first detection in the central peaks of Copernicus using earth-based telescopes [1] and continued to assessment of the global distribution of olivine exposures often associated with basins that are now possible using orbital sensors [2, 3]. Origin hypotheses for the olivine typically include excavation from a lunar mantle source or a layered pluton of Mg-suite crustal materials. However, different sources are likely for different geologic environments and perhaps even multiple source at a single location [4].

Existence of layered (Mg-suite) plutons is consistent with observation of material excavated by a few medium size craters that exhibit multiple lithologies (olivine-rich, pyroxene-rich, anorthositic) in close proximity along their rim or interior (e.g. Proclus [5]). Nevertheless, a large fraction of olivine detections obtained remotely (especially at basins) occur alone in association with extensive plagioclase or feldspathic terrain. This strongly suggests that the origin and evoluton of olivine from a deep-seated source must be intimately tied to association with extensive plagioclase.

Detectibility of olivine. As illustrated below, the diagnostic features of olivine can be readily detected when olivine is even 10% of a mixture with plagioclase. On the other hand, it is quite difficult to estimate the abundance of plagioclase in a mixture with olivine based on the shape of the multicomponent feature. For example, dunite and a 50/50 plag/olivine troctolite are almost indistinguishable.

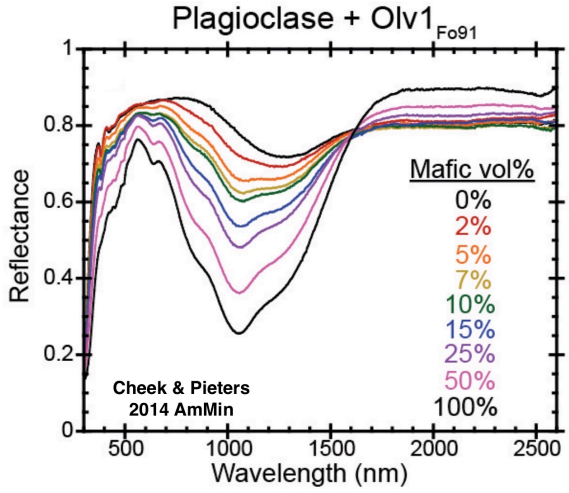

Laboratory spectra of crystalline plagioclase mixed with various amounts of volume % olivine [6]

Data constraints. The entire inner ring of Orientale (Inner Rook) has been shown to be dominated by massive amounts of plagioclase, including the pure crystalline anorthosite phase, PAN [7]. This not only supports the magma ocean prediction of extensive cumulate plagioclase forming the lunar crust, but (equally important) it also indicates that part of the basin-forming process can bring to the surface relatively coherent subsurface lithologies without extensive mixing, specifically for the inner ring [8, 9, 10].

The spatial context of olivine at basins evaluated with M3 data, such as at Crisium and Moscoviense [e.g. 11], indicates the olivine-rich areas are not found as a massive unit, but instead as a localized block of olivine-rich material (maximum a few km in size) embedded in a sea of plagioclase. Schrödinger may be an intermediate case [12] that also tapped a pluton. Although dunite cannot be ruled out for these areas, as discussed above the olivine occurs most likely as troctolite.

Inferences and questions. Clearly, a massive anorthositic crust formed early in lunar evolution. At basins, the observed olivine that is associated with this feldspathic crust (without other neighboring mafic minerals) argues against its origin as a Mg-suite layered pluton. The small localized occurrences of olivine also argue against it being derived directly from a olivine bearing mantle. Instead, the data suggest the olivine and plagioclase coexist in the lower crust, with olivine/troctolite being a common but not dominant component.

A question that merits discussion from multiple perspectives is the origin of this olivine/troctolite in the lower crust and whether this olivine-plagioclase association could be the result of mantle overturn early in crustal evolution.

References:

1] Pieters (1982) Science 215, 59-61.
2] Yamamoto et al. (2010) Nat. Geoscience 3, 533-536
3] Isaacson et al. (2011) JGR 116, E00G11
4] Dhingra et al. (2015) EPSL 420, 95-101
5] Donaldson Hanna et al. (2014) JGR 119, 1516-1545
6] Cheek and Pieters (2014) Am Min 99, 1871-1892
7] Cheek et al. (2013) JGR 118, 1-16
8] Johnson et al. (2015) LPSC #1362
9] Potter R (2015) Icarus 261, 91-99
10] Baker and Head (2015) Icarus 258, 164-180
11] Pieters et al., (2011) JGR 116, E00G08
12] Kramer et al. (2013) Icarus 223, 131-148

SURFACE PROCESSES. J. B. Plescia[1], M.S. Robinson[2], R. Clegg-Watkins[3], W. Fa[4], R. Ghent[5], J. Haryuma[6], H. Hiesinger[7], N. Hirata[6], G. Kramer[7], S. Lawrence[8], P. Mahanti[2], L. Ostrach[9], W. Patterson[1], P. Spudis[7], J. Stopar[7], M. Siegler[3], E. Spreyer[2], A. Stickle[1], J.-P. Williams[10], M. Zanetti[11], N. Zellner[12], [1]Johns Hopkins University, Applied Physics Laboratory, Laurel MD, [2]School of Earth and Space Exploration, Arizona State University, Tempe AZ, [3]Planetary Science Institute, Tucson AZ, [4]Peking University, Beijing China, [5]University of Toronto, Toronto Canada, [6]Japan Aerospace Exploration Agency, Sagamirhara, Japan, [7]Westfälische Wilhelms-Universitäte, Münster Germany, [7]Lunar and Planetary Institute, Houston TX, [8]NASA Johnson Space Center, Houston TX, [9]U.S. Geological Survey, Flagstaff AZ, [10]University of California, Los Angeles CA, [11]University of Western Ontario, London, Canada, [12]Albion College, Albion MI.

Introduction: Surfaces Processes chapter is one of the chapters in the *New View of the Moon 2* volume (www3.nd.edu/~cneal/NVM-2/). The chapter focuses on the primary processes of surface formation and evolution: cratering, volcanism, tectonism, and mass wasting and how those processes shape the physical properties of the regolith. The chapter will also address how the regolith interacts with the space environment and lunar volatiles.

Chapter Outline: The chapter will review the present stage of our understanding of the properties of the lunar regolith and active surface processes [1, 2]. It will then explore in detail the major advances that have occurred since the Apollo era. A particular point of focus will be the change of the view of the regolith as a layer composed of a range of particles that idly lay on the surface, bounced about by the occasional impact, and generally just keeping the interior warm, to a view of a dynamic regolith that is source for and a medium of transport for lunar volatiles, a storage place for volatiles, a surface that is dynamic and changing on timescale must faster than previously thought and one that may breathe on diurnal timescales.

The chapter will examine the questions that were posed in the New Views of the Moon 1 volume and the extent to which those questions have been answered. It will also discuss the new questions that have been posed and what might be required to answer them (e.g., data analysis, new measurements, samples).

What's New? As a result of new data our view has significantly changed since the Apollo.

The turnover rate and the lifetime of blocks on the surface may be, respectively, faster and shorter than previously recognized [3-6]. Locating and measuring craters that have formed over the life of the LRO mission has lead to estimates that regolith gardening occurs on a timescale about 100x previous estimates [7]. The concept of the destruction of boulders by thermal fatigue, in addition to bombardment, suggests that thermal fatigue may be more a efficient mechanism, shortening the expected lifetime.

Thermal data allows a more detailed analysis of the density / thermal conductivity profile with depth [8, 9]. Using diurnal and eclipse data, the structure of the regolith at various depths has been determined. An intriguing observation is that the ejecta of many fresh craters is colder than the surrounding terrain at night [10].

Volatiles are of interest not only for the scientific aspect of their origin and evolution, but also from the perspective of resources. We have begun to recognize that H distribution is not simply a function of latitude and permanent shadow. Regolith H appears to be spatially variable at the poles [10, 11]. Surface volatiles, OH and H_2O, appear to vary as a function of latitude and time of day [12, 13]. Existing data are, however, insufficient to define the mobility. It is also unclear exactly what is moving across the surface. Perhaps only H is moving, ephemerally attaching to the surface to form OH or H_2O and then moving on. There is also the suggestion that H moves into and out of the regolith on a diurnal timescale [14, 15]. This has implications for the permeability and porosity of the regolith to 10s cm but also the nature of the driving force.

Various processes shape the large-scale lunar surface including cratering, volcanism, tectonism and mass wasting. We will examine each of these processes, as it relates to the formation and evolution of the regolith. Detailed examination of these processes will be found in other chapters of the volume.

Finally, we will examine the list of outstanding questions and how those questions might be addressed.

References: [1] Jolliff, B. et al. (2006) New Views of the Moon 1, Rev. Min. Geochem., 60, 721 pp. [2] Heiken, G. et al. (1991) Lunar Source Book, 736 pp. [3] Delbo M. et al. (2014) *Nature*, 508, 233-236. [4] Molaro J. et al. (2015) *JGR*, 120, 255-277. [5] El Mir C. et al. (2016) *LEAG*, #2073. [6] Speyerer E. et al. (2016) *Nature*, 538, 213-218. [7] Gault, D. et al. (1974) Proc. 5th Lunar Sci. Conf., 2365-2386. [8] Hayne P. et al. (2016) *NVM 2*, #6065. [9] Greenhagen, B. et al. (2015) *LPSC XLVI* #2949. [10] Bandfield, J. (2014) Icarus, 221-231. [11] Mitrofanov, I. (2011) Science, 330, 334- [12] Feldman W. et al. (2000) JGR, 105, 4175-4195. [13] Pieters, C.M., et al. (2009) Science, 326, 568-582, [14] Sunshine J. et al. (2009) *Science*, 326, 565-568. [15] Livengood T.A. (2015) I*carus*, 255, 100-115. [16] Schwadron, N. et al. (2016) *Icarus*, 273, 25-35.

LUNAR REGOLITH - NEW VIEWS. J. B. Plescia[1], M.S. Robinson[2] and G. Kramer[3] [1]The Johns Hopkins University, Applied Physics Laboratory, Laurel, MD USA 20723, [2]School of Earth and Space Exploration, Arizona State University, Tempe, AZ 85287, [3]Lunar and Planetary Institute, Houston, TX 77058.

Introduction: The lunar regolith, that grainy, texturally complex, deposit that covers the Moon's surface has been revealed to be a more complicated system than previously recognized. Pre-Apollo, the regolith was viewed as a static layer that kept the Moon warm in the coldness of space. More recently, data from many robotic missions indicate that the regolith hosts and possibly drives a complex volatile cycle. We now have a better view of how density and thermal properties of the regolith vary with depth and across the surface, the current cratering rate and the timescale of overturn and gardening, latitudinal variations in regolith properties and temporal variability of volatiles (H, OH, H_2O) on and within the surface. An intriguing aspect is that many fresh craters have ejecta blankets that are thermally anomalous (unusually cold at night).

Density: The regolith density profile, based on Apollo and Luna cores, is not a simple function of depth, but varies among layers and between cores [1]. Individual core layers can not be traced laterally and so at any given point, details vary. However, the sum of these individual layers results in a density stratigraphy that smoothly increase with depth and can be modeled using the Diviner thermal data [2, 3, 4].

Regolith Gardening: The process of crater formation causes overturn of the regolith; the depth of turnover and amount of material displaced correlate with the energy of the event. The rate of overturn is an important control on the maturity of the regolith, and the rate at which rocks and boulders are excavated from depth. Originally, a gardening rate (99% of the material would be overturned) for 20 cm was estimated at >5 x 10^9 yr. [4, 5]. Using the number of contemporary impact events, revealed through LROC temporal imaging, the overturn rate for the top 20 cm was estimated to be 10^7 yr. [6].

Siegler et al. [7] observed a mirror image offset from the north and south poles of large-scale H deposits and proposed that the offset was due to true polar wander. If H enriched regions indeed indicate polar wander, the retention of anomalously high H over billions of years demands that the gardening rate is significantly lower than current estimates or gardening does not effect adsorbed H.

Rock Survival: Rocks on the lunar surface have been assumed to be obliterated by catastrophic rupture (largest fragment <50% of the original). Such models [8] predict the median lifetime for a population of 10 cm rocks of the order 10^7 years. Catastrophic breakup dominates over micro-meteorite abrasion. More recently, thermal fatigue has been suggested to contribute to rock breakdown. Interior temperature gradients cause stresses that propagate fractures and break apart the rock [9-11]. This process is estimated to considerably reduce surface rock lifetime.

Latitude Variability: The H parameter [3], an estimate of the density profile (and thus thermal inertia) of the top 10s cm of the regolith, may vary with latitude suggesting a change in the regolith properties with latitude. Polarimetry [12] indicates the grain size of the uppermost surface increases from ~ 60 μm at the equator to 115 μm at high latitude. Radar CPR decreases with latitude [13] suggesting that the polar regolith (top 10s cm) is less dense than equatorial regolith. Far-UV and thermal data also suggest a decrease in regolith density profile [3, 14].

Volatile Variability: Absorptions near 3 μm in reflectance spectra indicate that the amount of OH and/or H_2O on the surface (to mm depth) varies as a function of latitude and time of day [15-16]. Neutron absorption [LRO LEND; 17] and proton reflectivity [CRaTER; 18] also both suggest that the amount of H in the shallow subsurface (10s cm) varies diurnally. The implication is that significant quantities of H must be moved into and out of the regolith (10s of cm) over diurnal timescales.

Conclusions: New measurements are providing insight into processes occurring on and in the regolith, answering some questions and raising many new questions about regolith formation and evolution and how the regolith forms, stores and transports volatiles.

References: [1] Carrier W. et al. (1991) *Lunar Sourcebook*, pp. 475-567. [2] Vasavada A. et al. (2012) *JGR*, 117, doi:10.1029 / 2011JE003987. [3] Hayne P. et al. (2016) *NVM 2*, #6065. [4] Greenhagen, B. et al. (2015) *LPSC XLVI* #2949. [4] Gault D. et al. (1974) *5th LSC*, 2365-2386. [5] Ghent R. et al. (2014) *Geology*, 42, 1059-1062. [6] Speyerer E. et al. (2016) *Nature*, 538, 213-218. [7] Siegler M. et al. (2016) *Nature*, 531, 480-484. [8] Hörz F. et al. (1975) *The Moon*, 13, 235-238. [9] Delbo M. et al. (2014) *Nature*, 508, 233-236. [10] Molaro J. et al. (2015) *JGR*, 120, 255-277. [11] El Mir C. et al. (2016) *LEAG*, #5073. [12] Jeong M. et al. (2015) *Astrophys. J.*, 221:16, 18 pp. [13] Thomson B. et al. (2016) *LPSC XLVII*, #2426. [14] Gladstone G. et al. (2012) *JGR*, 117, E00H04, doi:10.1029 /2011JE003913. [15] Pieters, C.M., et al. (2009) Science, 326, 568-582, [16] Sunshine J. et al. (2009) *Science*, 326, 565-568. [17] Livengood T.A. (2015) I*carus*, 255, 100-115. [18] Schwadron, N. et al. (2016) *Icarus*, 273, 25-35.

IMPACT ORIGIN OF THE MOON: NEW DATA, NEW MODELS, AND NEW CHALLENGES. K. Righter[1], R. M. Canup[2], N. Dauphas[3], T. Magna[4], [1]NASA JSC, Mailcode XI2, NASA Parkway, Houston TX 77058; kevin.righter-1@nasa.gov, [2]Southwest Research Institute, 1050 Walnut Street - Suite 300, Boulder, CO, USA, [3]Department of Geophysical Sciences, The University of Chicago, 5734 South Ellis Avenue Chicago, IL 60637, [4]Czech Geological Survey, Klarov 3, CZ-118 21 Prague 1, Czech Republic.

Chapter summary. The leading hypothesis for the origin of the Moon is the giant impact model, which can explain the high Earth-Moon system angular momentum and the small lunar core, and is consistent with an early lunar magma ocean [1-2]. In this chapter, we will discuss 1) key geochemical measurements that have prompted a healthy re-evaluation of the giant impact model, 2) varied impact scenarios that are either newly proposed or somewhat modified relative to prior ideas, 3) assessments of the likelihood that current models can explain the physical and dynamical constraints derived from the Earth-Moon system, and 4) key areas requiring additional research to enable further progress.

Background. The standard giant impact hypothesis implies that the Moon is made predominantly from material originating from the impactor. At face value, this seems at odds with the nearly identical oxygen isotopic composition of the Earth and Moon, which might be expected to be different if Moon came from a distinct impactor, given the quite different O compositions of Earth and Mars. Recent work has highlighted the similarity of both geochemical and isotopic compositions of the Earth and Moon across multiple elements [3], and measured small but significant amounts of volatiles in lunar glassy materials [4], both of which are seemingly at odds with the standard giant impact model. As such, much recent work has focused on attempts to reconcile an impact origin with the physical and chemical aspects of the Earth-Moon system.

New Datasets

Isotopic measurements: Many isotopic measurements of lunar and terrestrial materials have revealed nearly identical values. Although for some isotopic systems the inner solar system is quite uniform, there are some differences. For example a small difference between lunar and terrestrial W and O [5,6,22] isotopic composition has been measured, although for O other analyses find no difference [21]. The significance of the similarities/differences is actively debated.

Volatiles: Lunar glasses contain measurable amounts of H, C, and S, which was surprising since many previous studies had concluded that lunar materials are dry or even "bone dry" [4,7]. Terrestrial zircons have O isotopic compositions indicating influence of water at the surface of the Earth [8], suggesting that the early Earth-Moon system may have contained more volatiles than previously thought [9]. Newly measured isotopic fractionation of volatiles (Zn and K) in lunar samples has been interpreted as evidence of volatile escape [10-11].

New Models. A variety of impact scenarios have been proposed to attempt to explain the Earth-Moon system characteristics. These include 1) a canonical impact by a Mars-sized projectile [12], with either post-impact equilibration [13] or an Earth-like composition impactor [3,14-15]; 2) a smaller, high-velocity impact into a rapidly rotating Earth, followed by a mechanism to remove excess angular momentum produced by such an event [16-17]; 3) a half-Earth impact, followed by a mechanism to remove excess angular momentum produced by this event [18]; 4) a hit-and-run impact by a relatively Earth-like composition impactor [19]; and 5) formation through a series of ~20 sub-Mars sized impactors [20].

In addition there have been a number of new works that have explored the protolunar disk conditions and evolution, the accumulation of the Moon and its expected composition, new dynamical evolutions of the early Earth-Moon system, the role of the evection resonance with the Sun, and the statistics of impactor properties based on terrestrial accretion models.

Changes since NVM-2 Houston. NVM-2 highlighted the need to cover stable and radiogenic isotope constraints on the origin of the Earth-Moon system because these would not be covered in any other chapter. In addition, there are multiple new relevant works as on topics discussed above.

References: [1] Origin of the Moon book (1984). [2] Canup, R.M. (2004) Ann. Rev. Astron. Astrophys. 42, 441. [3] Dauphas, N. et al. (2014) PTRSL A372, 201302444. [4] Saal, A. et al. (2008) Nature 454, 192. [5] Kruijer, T. et al. (2015) Nature 520, 534. [6] Herwartz, D. et al. (2014) Science 344, 1146. [7] Wetzel, D. et al. (2015) Nature Geosc. 8, 755. [8] Valley, J.W. et al. (2005) CMP 150, 561. [9] Canup, et al. (2015) Nature Geosc. 8, 918. [10] Paniello, R.C. et al. (2012) Nature 490, 376. [11] Wang, K., Jacobsen, S. B. (2016) Nature 538, 487. [12] Canup, R.M., Asphaug, E. (2001) Nature 412, 708. [13] Pahlevan, K., Stevenson, D. (2007) EPSL 262, 438. [14] Mastrobuono-Battisti et al. (2015) Nature 520, 212. [15] Belbruno, E., Gott, J.R. (2005) Astron. J. 129, 1724. [16] Cuk, M., Stewart, S.T. (2012) Science 338, 1047. [17] Cuk, M. et al. (2016) Nature 539, 402. [18] Canup, R. (2012) Science 338, 1052. [19] Reufer, A. et al. (2012) Icarus 221, 296. [20] Rufu, R. et al. (2017) Nature Geosci. 10, 89. [21] Young et al. (2016) Science 351, 493. [22] Touboul et al. (2015) Nature 520, 530.

Compositional convection in a Fe-FeS core of the Moon T. Rückriemen, D. Breuer, and T. Spohn Deutsches Zentrum f. Luft und Raumfahrt (DLR), Berlin, Germany (tina.rueckriemen@dlr.de)

Introduction: Since the Apollo era it is well known that the Moon's crust is remanently magnetized [1]. Paleomagnetic studies suggest that a dynamo operated in the Moon's core for a substantial amount of time from at least 4.25 Ga to potentially 1.3 Ga ago [e.g. 2,3,4,5]. One possible mechanism for magnetic field generation is thermo-chemical convection driven by core crystallization [6,7]. Most thermo-chemical core evolution models concentrate on bottom-up core crystallization in iron-rich Fe-FeS cores ($x_S \leq 20$ wt.%). However, given that the Moon's core features low pressures the core might start to crystallize iron at the top for a considerable range of iron-rich core sulfur concentrations [8]. A consequence is the emergence of a snow zone with settling iron crystals on top of a deeper liquid core that convects due to the remelting of those iron crystals [9,10]. In this so-called iron snow regime the lifetime of the thermo-chemical dynamo in the deeper core is determined by the time it takes for the snow zone to grow across the entire core. Those lifetimes can vary depending on several parameters, e.g., the core sulfur concentration, but are generally found to be short and may not be substantially longer than 1 Gyr [10].

Furthermore, it has been suggested that the bottom-up core freezing shifts to top-down crystallization with increased sulfur concentration in the outer core [6]. As soon as this shift has occurred, dynamo activity probably shuts down rapidly since the dynamo region vanishes quickly for a growing snow zone.

We want to build upon existing thermo-chemical studies and further explore which core crystallization scenario we find for a given core sulfur concentration. Moreover, we investigate the lifetimes of an iron snow dynamo in the Moon's core as well as the timing of the shift from bottom-up to top-down crystallization.

Model: We employ a 1D thermo-chemical evolution model of the Moon that includes the evolution of the mantle and the core. Mantle evolution is modeled according to the approach by [11] and [12], where the energy transport in the mantle is treated by parametrized stagnant lid convection. The evolution of the core in the bottom-up mode is handeled as in [13]. The top-down core crystallization follows the approach by [10]. In the case of bottom-up crystallization, the temperature follows an adiabat in the well-mixed outer core and is set to the liquidus at the inner core boundary. For the iron snow scenario the temperature in the snow zone follows a conductive profile, whereas the temperature in the deep convecting core is adiabatic. The temperature at the interface between snow zone and deeper core is at the liquidus. Both crystallization models include the energy contributions from latent heat, gravitational heating, and secular cooling. The liquidus for the iron-rich Fe-FeS alloy is taken from [14].

Results: We find that the iron snow regime occurs for a broad range of core sulfur concentrations from 7 wt.% to 20 wt.%. Bottom-up freezing occurs only for sulfur concentrations less than 3 wt.% while between 3 wt.% and 7 wt.% the core freezes neither at the bottom nor at the top but somewhere in between.

It can be shown that for a lunar core starting to crystallize in the iron snow regime (top down) the resulting dynamo lifetimes are strikingly short (< 19 Myr) and may not explain the oberserved magnetitzation. Also slower core cooling for instance due to an increased reference mantle viscosity (i.e., assuming stiffer mantle material) cannot prolong the dynamo lifetime. For these cases, only the onset of core freezing is retarded.

Alternatively, assuming a low sulfur content, the lunar core can start with bottom-up core freezing that later transitions to top-down freezing. For example, this transition occurs 726 Myr after the onset of inner core freezing if the core has an initial core sulfur concentration of 1 wt.%. Those roughly 700 Myr can explain the lifetime of the lunar dynamo up to 3.56 Ga ago and possibly a few hundred million years longer assuming an early thermal dynamo before the start of crystallization. However, this scenario cannot explain the recently extended lifetime up to 1.3 Ga.

References: [1] Wieczorek et al. (2006) Reviews in Mineralogy and Geochemistry, Mineralogical Society of America, 60, pp. 221-364, [2] Garrick-Bethell et al. (2009), Science, 323, pp. 356-359, [3] Tikoo et al. (2014), EPSL, 404, pp. 89-97, [4] Suavet et al. (2013), Proceedings of the National Academy of Science, 110 ,pp. 8453-8458 , [5] Shea et al. (2012), Science, 335, pp. 453-456, [6] Laneuville et al. (2014), EPSL, 401, pp. 251–260, [7] Scheinberg et al., Icarus, 254, pp. 62-71, [8] Williams (2009), EPSL, 284, pp. 564-569, [9] Hauck et al. (2006), JGR, 111, [10] Rückriemen et al. (2015), 120 , pp. 1095-1118, [11] Grott et al. (2008), Icarus, 193, pp. 503-515, [12] Morschhauser et al. (2011), Icarus, 212, pp. 541-558, [13] Stevenson et al. (1983), Icarus, 54, pp. 466-489, [14] Buono et al. (2011), Geochimica et Cosmochimica Acta, 75, pp. 2072-2087

MAGMATIC EVOLUTION 2: A NEW VIEW OF POST-DIFFERENTIATION MAGMATISM.

C.K. Shearer[1], C.R. Neal[2], L. Gaddis[3], B.L. Jolliff[4], J.Head[5], H. Hiesinger[6], A.S. Bell[1], G.J. Taylor[7], T.D. Glotch[8], J.I. Simon[9], T.C. Prissel[10], and T. Magna[11]. [1]Institute of Meteortics, Department of Earth and Planetary Sciences, University of New Mexico, Albuquerque, NM 87131, [2]Department of Civil and Env. Eng. and Earth Sci, University of Notre Dame, IN 46556, [3]Astrogeology Science Center, USGS, Flagstaff, AZ 86001, [4]Washington University in St Louis, MO 63130, [5]Brown University, Providence, RI 02912, [6]Westfälische Wilhelms-Universität Münster, Germany, [7]HIGP, U. Hawaii, 1680 East-West Rd., Honolulu, HI 96822, [8]Department of Geosciences, Stony Brook University, StonyBrook, NY 11790 [9]NASA Johnson Space Center, Houston, TX 77058, [10] Department of Earth and Planetary Sciences, Rutgers University, Piscataway, NJ 98854, [11]Czech Geological Survey, Prague, Czech Republic.

Introduction: This chapter focuses on the post-differentiation magmatism on the Moon. It includes a summary of our knowledge of this stage of lunar magmatism up to 2006. It then focuses on advances in understanding the following stages of magmatism: (1) the earliest stages of post-differentiation magmatism such as the Mg-suite, alkali suite, and associated volcanism, (2) mare basaltic magmatism and pyroclastic deposits, (3) KREEP basaltic magmatism, and (4) silicic-felsic magmatism. The list of co-authors for this abstract has thus far been identified as participants that will be involved in contributing to this chapter. Other co-authors will be added based on their unique contributions and insights. Please contact C. Shearer during or following this workshop with additional potential contributions (cshearer@unm.edu).

Overlap with other chapters: There are numerous topical chapters that overlap with Lunar Magmatism 2. These chapters include (1) ***Origin of the Earth-Moon System, (2) Magmatic Evolution 1: Initial differentiation and late-accretion, (3) Evolution of the Lunar Crust, (4) The Structure of the Lunar Interior, (5) Lunar volcanism, (6) The Contributions of Lunar Meteorites, (7) Lunar Tectonics, and (8) Endogenous Volatiles***. Our intent for this chapter is not to duplicate or compete with these chapters but to integrate recent observations to establish an updated foundation for reconstructing the petrogenesis and chronology of lunar magmatism. Further, this chapter will feed into the chapters on ***Lessons Learned and Future Goals of Exploration*** and the ***Development of the Moon and cis-Lunar Space*****.**

Important Questions Tied to Lunar Magmatism 2: Through the integration of a variety of data sets (e.g., distribution of rock types, volatiles in various magmatic lithologies, chronology of emplacement and eruption, styles, compositions, and duration of volcanism, models for primordial differentiation, models for the structure of the lunar interior), a new understanding about the magmatic evolution of the Moon will be produced. Numerous important questions will be explored that are relevant to all stages of lunar magmatism. These questions include: (1) How do endogenous mantle volatiles influence mantle melting? (2) What are the source regions for the various stages of lunar magmatism? (3) How does duration and volume of lunar magmatism reflect mantle sources, melting-transport processes, and thermal history of the Moon? (4) What is the petrogenesis of the various stages of lunar magmatism? (5) What are the "petrogenetic linkages" among all stages of lunar magmatism? (6) What processes are important in driving lunar magmatism? (7) What are the implications of potentially very young volcanics, i.e., 1 Byr or younger?

Schedule for Chapter and Initiative: Based on the schedule for NVM2, chapters should be submitted near the end of 2018. It is the intent for this chapter to be submitted by this deadline. We intend to have a chapter meeting at the 2017 Lunar and Planetary Science Conference and the NVM2 meeting in Europe 2018 to review and expand on chapter content. During the summer of 2017, we will allocate writing assignments based on this outline. During the Fall 2017 and Spring 2018, we will discuss directions of the text and potential solutions to chapter overlaps. Finally, in mid-2018 we will provide additional input to the chapter on ***Lessons Learned and Future Goals of Exploration***.

NEW VIEWS OF LUNAR SURFACE MATURITY USING LRO DATA FROM UV TO RADAR. A. M. Stickle[1], J. T. S. Cahill[1], J. A. Grier[2], B. Greenhagen[1], G. W. Patterson[1], [1]Johns Hopkins University Applied Physics Laboratory, Laurel, MD, 20723, USA (angela.stickle@jhuapl.edu),[2]Planetary Science Institute, Tuscon AZ USA.

Background: The physical evolution of the lunar surface with exposure to the space environment (particularly impacts) is termed "maturation", can take place over relatively short timescales, and has been attributed to the amount of glass and agglutinate content within the lunar soil [e.g., 1-8], the amount of trapped solar wind nitrogen [9], solar wind sputtering and vapor deposition [10-11], and/or the amount of sub-microscopic iron (SMFe) in the material. Studies show that the abundance of these glasses and agglutinates increases with age of the soil and can account for large portions of a given mature soil [e.g., 2,4,9]. Changes in physical properties of the lunar soil are quantified in terms of specific maturity indices (e.g., Optical maturity (OMAT) [13]), and thus soils are generally classified on the basis of one or more of these specific indices [3]. Though sampling maturity effects from different processes and on different time- and depth-scales, comparisons indicate that maturity of the soil can be tracked across wavelengths, which is a powerful tool when examining the surface evolution of the Moon. New data from the LRO and Kaguya missions (coupled with Clemetine OMAT) provide important new ways to examine lunar surface maturity.

Observations of Crater Age Across Wavelengths: There are a number of methods for representing maturity: e.g., OMAT, LROC, Diviner, Mini-RF. Using OMAT, [13] classify Byrgius A as "young", Dufay B as "intermediate" and Golitsyn J as "old". Here, we survey how these ages are manifested across wavelengths to examine if correlations exist for maturity indices as a function of wavelength.

Comparisons of observations from UV to radar for these three craters (e.g., Fig. 1) indicate that maturity of the soil can be tracked across wavelengths. These comparisons suggest that specific "maturity parameters" manifest differently at different wavelengths. Further, more detailed comparisons are underway, and they are necessary to more fully understand when these maturity trends can be correlated and how to quantify the correlation. If trends can be correlated, this will provide a powerful tool when examining the surface evolution of the Moon and determining relative ages between features.

References: [1] Adams, J.B. and T.B. McCord (1971) *Science*, 171, 567-571; [2]McKay, D.S., et al. (1974) *Proc. Lunar. Sci Conf 5th,* p. 887-906; [3]Adams, J.B., and M.P. Charette (1975) *The Moon, 13*, 293-299; [4]Charette, M.P., et al. (1976) *Proc. Lunar Sci. Conf. 7th*, p. 2579-2592; [5]Wells, E., and B. Hapke (1977) *Science*, 195*,* 977-979*;* [6] Pieters, C. M. et al (1993) *J. Geophys. Res. Planet. 98*(E11), 20817-20824; [7] Britt, D.T., and C.M. Pieters (1994) *Geochim. Cosmochim. Acta 58*, 3905-3919; [8] Lucey, P. G., & Riner, M. A. (2011) *Icarus*, *212*(2), 451-462; [9] Charette, M.P., and J.B. Adams (1975), *Proc. Lunar Sci. Conf. 6th,* 2281-2289; [10] Gold, T., et al. (1976) *Proc. Lunar Sci. Conf. 7th*, p. 901-911; [11] Hapke, B., et al (1975) *Moon*, 13, 339-354; [12] McKay, D.S., et al. (1972) *Proc. Lunar Sci. Con;f. 3rd,* p. 983-994; [13] Grier *et al.* (2001) *J. Geophys. Res. 106*(E12)*,* 32847-32862 [15] Stickle et al. (2016) *Proc. Lunar Sci. Conf.*, Abstract #2928.

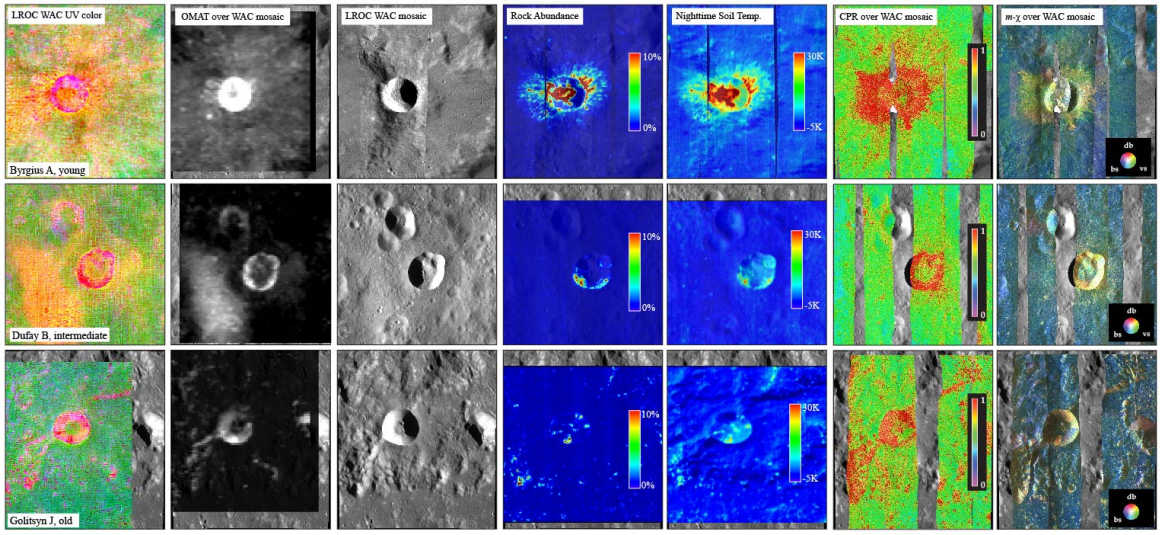

Figure 1. (top) Byrgius A (19.7 km, 24.6°S, 63.5°W), a young highlands crater, (middle) Dufay B (19.8 km, 8.3°N,171°E), an "intermediate" aged highlands crater, (bottom) Golitsyn J (19.5 km, 27.9°S, 102.9°W), an "old" highlands crater. The columns show the appearance of the crater across wavelengths, from UV (WAC UV, left) to radar (Mini-RF radar,right).

A THREE-BILLION-YEAR HISTORY FOR THE LUNAR DYNAMO. S. M. Tikoo[1-4], B. P. Weiss[2], D. L. Shuster[3,4], C. Suavet[2], H. Wang[2], and T. L. Grove[2], [1]Department of Earth and Planetary Sciences, Rutgers University, Piscatwaway Township, NJ 08854 (sonia.tikoo@rutgers.edu), [2]Department of Earth, Atmospheric and Planetary Sciences, Massachusetts Institute of Technology, Cambridge, MA 02139, [3]Department of Earth and Planetary Science, University of California, Berkeley, CA 94720, [4]Berkeley Geochronology Center, Berkeley, CA 94709.

Introduction: Lunar paleomagnetic studies indicate that the Moon generated a core dynamo with surface field intensities of ~20-110 μT between at least 4.25 and 3.56 billion years ago (Ga) [1-4]. The field subsequently declined to <~4 μT by 3.19 Ga [5], but it has been unclear whether the dynamo had ceased by this time or just greatly weakened in intensity. To investigate whether the lunar dynamo was still active after 3.56 Ga, we conducted a new analysis of regolith breccia 15498, a young rock that is capable of providing exceptionally high-fidelity paleomagnetic records.

Sample Description and Age: 15498 consists of clasts mainly derived from mare basalt fragments that are welded with basaltic composition melt glass [6-7]. We determined a 3.310 ± 0.024 Ga $^{40}Ar/^{39}Ar$ plateau age for one mare basalt clast, which places an upper limit on the lithification age of the breccia. Our thermochronometry modeling of the clast's thermal history suggests that 15498 formed between ~1-2.5 Ga. This range is consistent with trapped Ar data that indicate a ~1.3 Ga lithification age for the rock [8]. Our rock magnetic studies indicate that FeNi grains within the melt glass matrix are, on average, superparamagnetic to pseudosingle domain and are therefore excellent magnetic recorders.

Natural Remanent Magnetization (NRM): 12 mutually oriented melt glass matrix subsamples were collected from the interior of the breccia and were stepwise demagnetized using either alternating field (AF) or thermal methods. After removal of secondary magnetization components by AF levels of ~50 mT or temperatures of ~200°C, all subsamples exhibited a unidirectional, high coercivity (HC) and high temperature (HT) component blocked up to AF levels of at least 290-420 mT and temperatures up to 660-750°C (**Fig. 1**).

Paleointensity: We conducted Thellier-Thellier [9] paleointensity experiments on 6 out of the 12 matrix glass subsamples following the in-field, zero-field, zero-field, in-field (IZZI) protocol [10], including periodic checks for sample alteration. We obtained high-quality paleointensity values of 5 ± 2 μT (mean ± 1 σ) from the HT components.

Discussion: The highly stable, unidirectional nature of the HC/HT components and our paleointensity results collectively indicate that the melt glass matrix of 15498 records a primarily thermoremanent magnetization acquired during initial cooling in an ambient paleofield of

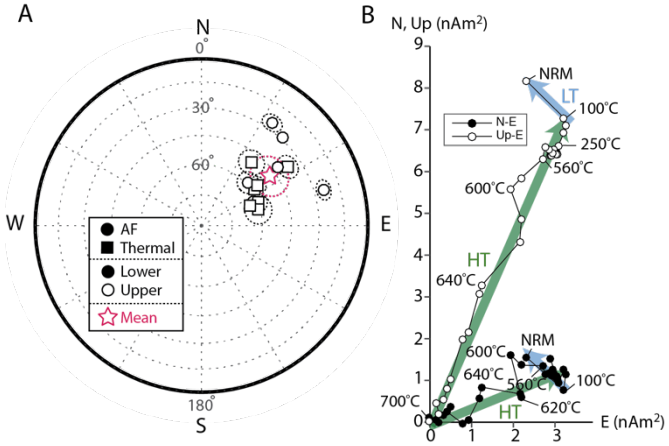

Fig. 1. (A) Equal area plot of HC/HT directions for 15498 subsamples. (B) Vector endpoint diagram showing thermal demagnetization steps for subsample 313e. LT and HT components are denoted with blue and green arrows, respectively.

~5 μT. This paleointensity is at least an order of magnitude stronger than lunar crustal fields at any Apollo landing site and external field sources like the Earth, Sun, and galactic magnetic fields [11].

The most likely mechanisms capable of generating ~5 μT fields at the lunar surface at ~1-2.5 Ga are impact fields and a core dynamo. Because the slow (several hours) primary cooling timescale of 15948 excludes a transient (<1 s) impact field origin for the observed TRM, our data strongly indicate that the glass matrix portion of 15498 preserves a dynamo record. No single dynamo mechanism proposed thus far (convective or mechanical) can explain the strong fields inferred for the period before 3.56 Ga while also allowing the dynamo to persist in such a weakened state beyond ~2.5 Ga [4]. Therefore, our results suggest that the dynamo was powered by at least two distinct mechanisms operating during early and late lunar history.

References: [1] Garrick-Bethell I. et al. (2009) *Science, 323,* 356-359. [2] Shea E. K. et al. (2012) *Science, 335,* 453-456. [3] Suavet C. et al. (2013) *Proc. Natl. Acad. Sci. USA, 110(21),* 8453-8458. [4] Tikoo S. M. et al. (2014) *Earth Planet. Sci. Lett., 404,* 89-97 [5] Weiss B. P. and Tikoo S. M. (2014) *Science, 346,* 1246753. [6] Mason B. (1972) *The Apollo 15 Lunar Samples,* 137-139. [7] Ryder, G. (1985) *Catalog of Apollo 15 Rocks*. [8] Fagan et al. (2013) *LPSC XLIV,* Abstract #2392. [9] Thellier E. and Thellier O. (1959) *Ann. Geophys.* 15, 285-376. [10] Tauxe L. and Staudigel H. (2004) *Geochem. Geophys. Geosyst.*, *5(2)*, Q02H06. [11] Dyal P. et al. (1974) *Rev. Geophys. Space Phys., 12(4),* 568-591.

THE AGE OF THE CRISIUM IMPACT BASIN. C. H. van der Bogert[1], H. Hiesinger[1], and P. Spudis[2], [1]Institut für Planetologie, Westfälische Wilhelms-Universität, Münster, Germany (vanderbogert@uni-muenster.de); [2]Lunar and Planetary Institute, Houston, TX, USA.

Introduction: Fragments of Crisium impact melt were presumably collected by the Luna 20 sample return mission, and the radiometric age for a feldspathic, KREEP-poor sample is reported as 3.895±0.017 Ga [1]. Earlier radiometric analyses suggested an age of ~3.84 Ga [2-4]. However, Swindle et al. [1] argue that the sample they analyzed is more likely to represent Crisium than the others. Updated Apollo 17 sample ages, thought to represent Crisium, range from 3.88 to 3.93 Ga [5]. Based on stratigraphy, Wilhelms [4] proposed that Serenitatis is younger than Crisium, which would set the lower age limit for Crisium to < the proposed age of Serenitatis: 3.87±0.012 Ga [6] or 3.825±0.048 Ga [5]. Neukum [7] reported crater densities for Crisium that yield an absolute model age of 3.99 Ga. However, more recent work by Spudis et al. [8] and Fassett et al. [9] indicates that Serenitatis may be older than Crisium, consistent with Baldwin [10,11]. Thus, the Serenitatis age could instead be an upper limit for the age of Crisium.

Recent geological mapping identified remnants of the Crisium basin impact melt sheet, based on their morphology and composition [12]. Some of the exposures exhibit cracked and fissured morphologies consistent with those at both fresh craters (e.g., Tycho and King craters [13]) and older impact melts (e.g., Orientale [4,14]), and show embayment by subsequent mare basalt flows [12,15]. Their compositions, determined from Clementine data, indicate that they have less FeO (~8.3 wt. %) than the surrounding basalts (>15 wt. %), attesting to their affinity to lunar highlands compositions [15]. We measure the crater size-frequency distributions (CSFDs) of these newly documented exposures to expand our understanding of the age of the Crisium basin and its position in the basin chronology.

Results: Our preliminary results, taken from the largest and most prominent of the melt deposits identified by Spudis and Sliz [15], indicate that Crisium basin formed at 3.85±0.05 Ga, using the production and chronology functions of [16] and fit using Poisson timing analysis [17] (***Fig. 1***). This result is consistent with the younger of the radiometric ages derived from samples thought to originate from Crisium. Our result is younger than that derived via crater statistics [7]. Even if we fit the CSFD using a cumulative fit and the functions of [7], we derive an age of 3.87+0.044-0.063 Ga. This age is closer to the radiometric age determined by Swindle et al. [1], but still younger than the absolute model age of [7] and younger than the oldest Ap17 sample ages. Finally, if we apply our newly derived $N(1)$ to the graphical representation of the lunar cratering chronology, the positioning of the Crisium point moves lower and better fits the Neukum et al. (2001)[16] lunar chronology function.

Conclusions: The identification of impact melt units associated with Crisium basin allows independent evaluation of its formation age using CSFDs. Our results indicate that Crisium basin formed between 3.85 and 3.87 Ga, rather than closer to 4 Ga. Impact melt units are interesting and important sites (e.g., [12,18]), which if directly sampled can provide additional calibration points for the lunar chronology [7,16,19,20].

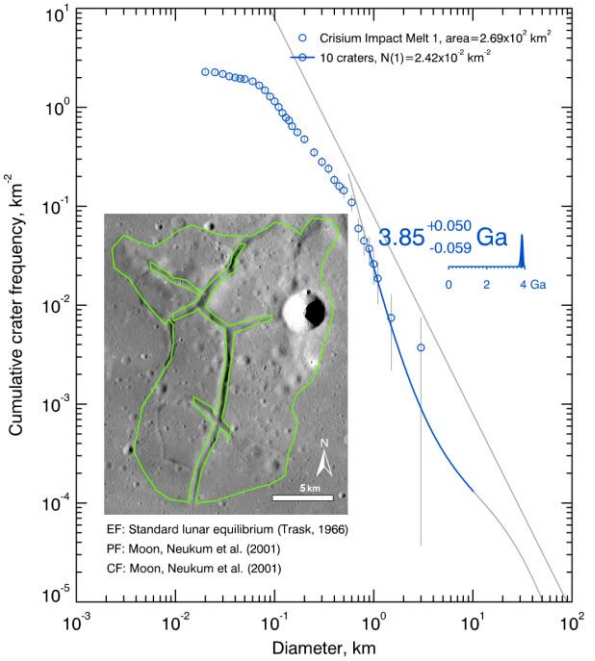

Figure 1. *CSFD and derived AMA for the largest exposure of the Crisium impact melt deposit identified by Spudis and Sliz (2017)(inset, SELENE mosaic).*

References: [1] Swindle et al. (1991) *PLPSC* 21, 167-181. [2] Cardogan and Turner (1977) *Philos Trans R Soc London* A284, 167-177. [3] Deutsch and Stöffler (1987) *GCA* 51, 1951-1964. [4] Wilhelms (1987) *USGS Prof Pap* 1046-A, 71 pp. [5] Schmitt et al. (2017) *Icarus*, 10.1016/j.icarus.2016.11.042. [6] Podosek et al. (1973) GCA 37, 887-904. [7] Neukum (1983) *NASA TM-77558*, 153 pp. [8] Spudis et al. (2011) JGR 116, 10.1029/2011JE003903. [9] Fassett et al. (2012) *JGR* 117, 10.1029/2011JE003951. [10] Baldwin (1987) Icarus 71, 1-18. [11] Baldwin (1987) Icarus 71, 19-29. [12] Spudis and Sliz (2017) *GRL*, 10.1002/2016GL071429. [13] Howard and Wilshire (1975) *J Res USGS* 3, 237-251. [14] Scott et al. (1978) *USGS Map* I-1034. [15] Sliz and Spudis (2016) *LPSC* 47, 1678. [16] Neukum et al. (2001) *Space Sci Rev* 96, 55-86. [17] Michael et al. (2016) *Icarus* 277, 279-285. [18] Ryder et al. (1989) *EOS* 70, 1495-1509. [19] Stöffler and Ryder (2001) *Space Sci Rev* 96, 9-54. [20] Stöffler et al. (2006) *New Views of the Moon, Rev Min Geochem* 60, 519-596.

PETROLOGIC CONTEXT AND DATING OF 4.2 GA OLD ZIRCON IN LUNAR IMPACTITES – 67955 REVISITED. D. M. Vanderliek[1] H. Becker[1], A. Rocholl[2], [1]Freie Universität Berlin, Institut für Geologische Wissenschaften, Malteserstr. 74-100, 12249 Berlin, Germany (dennisvdl@zedat.fu-berlin.de), (hbecker@zedat.fu-berlin.de), [2]Geoforschungszentrum Potsdam, Telegrafenberg, 14473 Potsdam, Germany (alexander.rocholl@gfz-potsdam.de).

Introduction: Early isotopic dating of lunar rocks led to the hypothesis of a spike in the impactor flux between 3.95 and 3.85 Ga in the inner solar system (lunar cataclysm or late heavy bombardment, e.g. [1-5]). Ages of 4.2 to 4.0 Ga were less common in previous studies of Apollo and Luna samples and lunar meteorites. However, the interpretation of the age data may be biased by resetting of chronometers during impact events and an overall sampling bias of Apollo samples caused by the proximity to the relatively young Imbrium basin (e.g. [6-7] and references therein). To obtain new evidence that may help to address these issues, in-situ U-Pb age data for Zr bearing minerals in well-characterized ancient lunar impactites are useful (e.g. [7-10]). Here, we provide further evidence from zircons for one or several large impact events at ca. 4.2 Ga [7].

Material and Methods: A thin section of the well-characterized breccia 67955 was investigated. The modal composition was determined by QEMSCAN (Quantitative Evaluation of Minerals by Scanning Electron Microscopy) and additional characterization methods were applied (e.g., Raman spectroscopy). U-Pb dating of 7 zircons was performed at the GFZ Potsdam using a CAMECA IMS 1280 HR instrument.

Results and Discussion: Three texturally different domains occur in thin section 67955,48. A granulitic domain (D1) is homogeneous, characterized by up to 3 mm long and 1.5 mm wide plagioclase crystals and interstitial olivine (Ol), orthopyroxene (Opx), clinopyroxene (Cpx) and locally apatite (Ap)., A brecciated domain (D2) comprises various rock clasts embedded in an apatite-bearing, fragment-rich matrix (D3). Troilite locally occurs as interstitial grains up to 30 µm ø (D1) or as speckles in some clasts (D2), but not in the matrix (D3). Minor amounts of Fe-Ni metal occur in all three domains. Some clasts underwent up to two different fracturing events before their final assemblage. Clasts show variable proportions, sizes and textures of Old, Cpx, Opx and Plg. Zircons are rare, anhedral and small in size (3 to 15 µm) and predominantly occur clasts in the clast-rich domain. Few zircons occur in the matrix. A few zircons show concentric to irregular zoning in BSE/CL images. Some display inclusions (possibly Plg). The mean of seven $^{207}Pb/^{206}Pb$ ages is 4.209 ± 0.014 Ga (2sd). Within-run uncertainties are better than 0.018 Ga (2sd). Our results agree well with in-situ U-Pb ages on zirconolite and apatite from the same sample [7], interpreted as reflecting impact events at 4.22 Ga and 3.9 Ga [7].

Conclusions: The three different domains in 67955,48 vary in texture and composition. All contain Fe-Ni metal, suggesting that they represent impactites. The predominance of apatite in the matrix (D3), its distribution in clusters or around clasts indicates that the matrix was not formed by fragmentation of the clasts. The absence of troilite in the matrix and its presence in clasts further supports this hypothesis. Textural and compositional variations of the different clasts imply that portions of this rock comprise different rock types that were mixed and welded together. Due to textural variations we interprete the different zircons to have been formed by crystallization in different impact melt settings. Most likely this requires one [7] or several large impacts at 4.2 Ga. Crystallization of the zircons at ~4.2 Ga predated the fracturing processes and formation of the clast-rich domain, which may have occurred at 3.9 Ga [7]. Our data reiterates that zircons from lunar impactites can provide critical information on the bombardment history of the Moon prior to 3.9 Ga.

References: [1] Cohen, B.A., Swindle, T.D., Kring, D.A. (2005) *MAPS* 40, 755-777. [2] Ryder, G. (2002). *J. Geophys. Res. Planets* 107, 6-1-6-13. [3] Stöffler, D., Ryder, G., Ivanov, B.A., Artemieva, N.A., Cintala, M.J., Grieve, R.A.F. (2006) *Rev. Mineral. Geochem.* 60, 519-596. [4] Tera, F., Papanastassiou, D.A., Wasserburg, G.J. (1974) *EPSL* 22, 1-21. [5] Norman, M.D. (2009) *Elements* 5 23-28. [6] Fernandes, V.A., Fritz, J., Weiss, B.P., Garrick-Bethell, I., Shuster, D.L. (2013) *MAPS* 48, 241-269. [7] Norman, M.D., Nemchin, A.A. (2014) *EPSL* 388, 387-398. [8] Nemchin, A.A., Pidgeon, R.T., Healy, D., Grange, M.L., Whitehouse, M.J., Vaughan, J. (2009) MAPS 44, 1717-1734. [9] Pidgeon, R.T., Nemchin, A.A., van Bronswijk, W., Geisler, T., Meyer, C., Compston, W., Williams, I.S. (2007) *GCA* 71, 1370-1381. [10] Grange, M.L., Nemchin, A.A., Timms, N., Pidgeon, R.T., Meyer, C. (2011) *GCA* 75, 2213-2232.

IMPACT GEOLOGY OF FRESH SIMPLE CRATERS ON MOON I .Varatharajan[1] and U. Sruthi[2], [1]Institute for Planetary Research, German Aerospace Center DLR, Rutherfordstr. 2, Berlin–Adlershof, Germany (indhu.varatharajan@dlr.de), [2]Centre for Earth Evolution and Dynamics, University of Oslo (sruthi.uppalapati@geo.uio.no),

Introduction: The detailed mapping of fresh simple craters for their structure, geometry, morphology, and mineralogy will help us to understand the early stage modification processes of simple craters on earth and other planetary surfaces. Though terrestrial craters are studied in detail through field geology, these craters have undergone continuous weathering since their formation. One such example is Lonar crater on Earth which is formed in ~65 Ma old Deccan flood basalts at 19°58′N, 76°31′E, near Lonar village in Buldhana district of Maharashtra State in India [1]. The detailed mapping of both geologic and mineralogic units of these freshly preserved craters will give us a window to understand the early impact scenario of Lonar crater (Fig. 1).

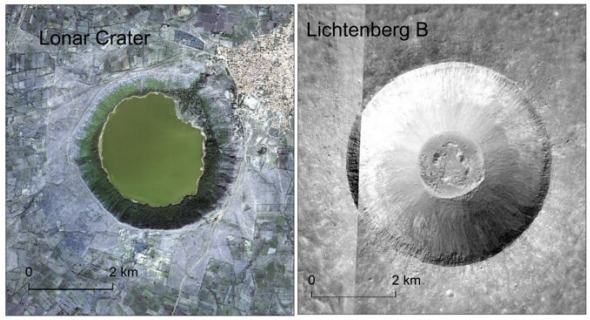

Figure 1. a) Quickbird extent map of Lonar crater, b) LROC NAC image showing Lichtenberg B (M1103959207RE).

Datasets used: The Lunar Reconnaissance Orbiter (LRO) Narrow Angle Camera (NAC) datasets having ~0.5 m/pixel spatial resolution and Chandrayaan-1 Moon Mineralogy Mapper (M3) hyperspectral datasets having spatial resolution of 140 m/pixel are used to study the morphology and mineralogy of the impact features.

Results: In this study, we identified 37 craters out of ~1349 craters of lunar surface that falls under the diameter of 3-6 km which displays freshly preserved impact structures. Interestingly, all of the 37 craters are found in the lunar nearside. 30 out of 37 are formed in the basaltic terrain (Fig. 2).

One of these craters is Litchenberg B which has a diameter of ~5 km located at 33.25°N, 61.52°W. It is a fresh crater formed at the boundary of two lava flows in Oceanus Procellarum, namely P9 (~3.47 Ga) and P53 (~1.68 Ga) [2]. This crater preserves various morphological features including melts, fractures, boulders, slumping of wall, the crater floor polygons, detailed ejecta morphology with wrinkled symmetrical crescent ridges, and the rock outcrops in the crater wall showing the successive thin lava flows of Oceanus Procellarum as old as ~3 Ga (Fig. 3). We estimated the absolute model age of this crater using Crater Size-Frequency Distribution (CFSD) and found to be ~17.9±0.6 Ma.

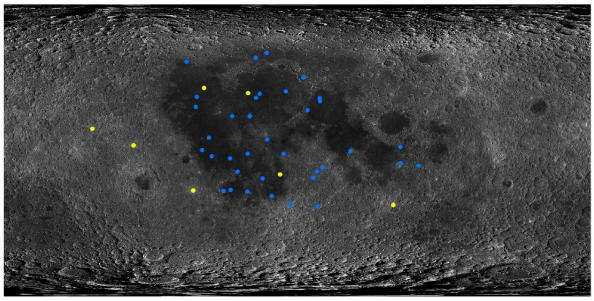

Figure 2. Blue dots represent the distribution of freshly preserved craters having diameter ~3-6 km; yellow dots are the fresh craters which are outside the range of 3-6 km crater diameter.

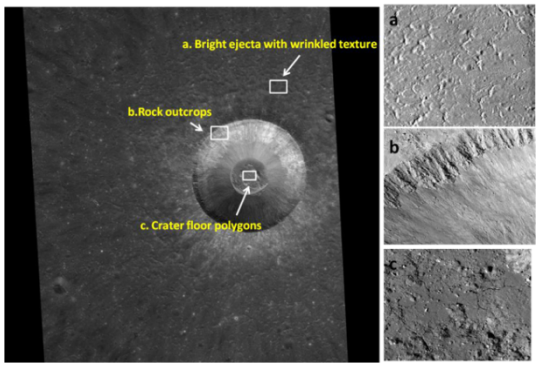

Figure 3. LROC NAC image of Lichtenberg B showing the details of a) wrinkled bright ejecta, b) rock outcrops in the crater wall, and c) melt cracks in the floor.

Conclusions: Morphologically, Lichtenberg B is comparable to the Lonar crater as both are formed in the flood basalts in Oceanus Procellarum and Deccan plateau respectively. Thus the studies of Lichtenberg B (and other fresh simple craters) and Lonar will improve understanding of the formation of simple craters in basaltic targets.

References: [1] Kumar, P. S. (2005) JGR, 110, B12402, [2] Hiesinger H. (2003) JGR, 108, E7, 5065.

INVESTIGATION OF LUNAR SPINELS AT SINUS AESTUUM. C. M. Weitz[1], M. I. Staid[1], L. R. Gaddis[2], S. Besse[3], and J. M. Sunshine[4], [1]Planetary Science Institute, 1700 E Fort Lowell, Suite 106, Tucson, AZ 85719 (weitz@psi.edu), [2]Astrogeology Science Center, U. S. Geological Survey, 2255 N. Gemini Drive, Flagstaff, AZ 86001; [3]Camino Bajo del Castillo s/n, Ur. Villafranca del Castillo, 28692 Villanueva de la Canada, Madrid, Spain; [4]Dept of Astronomy, University of Maryland, College Park, MD.

Introduction: Recent remote sensing observations by the Moon Mineralogy Mapper (M^3) on the Chandrayaan-1 spacecraft and the Spectral Profiler (SP) on the SELENE Kaguya orbiter have identified spinels in numerous locations across the Moon [1-3]. SP data analyzed by [3] was used to identify a visible-wavelength absorption feature around 0.7 μm along with a strong 2 μm absorption only at Sinus Aestuum (SA). They attributed the 0.7 μm feature to the presence of a Fe- or Cr-bearing spinel rather than the Mg-spinel more commonly identified on the Moon [2]. The Fe- or Cr-rich spinels in the SA region are associated with widespread, dark pyroclastic deposits [1,3,4].

In this study, we analyzed M^3 data for spinel locations at SA, and then examined visible images from the Lunar Reconnaissance Orbiter (LRO) Narrow Angle Camera (NAC) and Wide Angle Camera (WAC), as well as the Kaguya Terrain Camera (TC) and Multiband Imager (MI) images to correlate these spinel signatures to surface morphologic features. We extracted M^3 spectra of several spinel locations and attempted to understand what was creating the signatures throughout SA. Finally, we examined the locations where SP data showed visible-wavelength features in the spinel spectra and compared them to locations where M^3 data showed a 0.7 μm feature.

Observations: We examined 128 of the strongest and largest spinel signatures in widespread sites across the highlands and some mare of Sinus Aestuum. In all cases, we identified an impact crater in association with the spinel signature. The crater diameters ranged from ~100 m to ~4 km, which corresponds to transient crater excavation depths of ~25-1000 m [5,6], although for the larger craters (i.e., >1 km diam.) the spinels were observed along the upper crater walls rather than in the ejecta, suggesting shallower depths for the spinels. The majority of spinel deposits are associated with DMD on the highlands.

We identified several larger (>1 km diameter) highland impact craters that exhibit spinel signatures along the interior crater rim. The spinel is best identified in fresh exposures of the regolith, such as along the crater interior walls where mass wasting on the steeper slopes exposes immature regolith containing the spinels. For all these craters, there is no obvious source layer for the spinel observed along the crater walls.

We identified nine larger spots where we found a spinel signature in the highlands but outside of the mapped DMD. Examination of NAC and TC images for these nine locations showed a small (100-400 m diameter) impact crater correlated to the spinel signature. The remaining spinel spots are associated with four larger (3.5-11 km diameter) impact craters (Gambart B, Gambart G, Gambart L, and Schroter D) and one smaller crater (350 m diameter) in the mare. All four larger craters have low reflectance debris along portions of their interior walls that corresponds to the spinel signatures. The dark spinel-bearing materials are observed starting near the top of the walls and spread down towards the crater floors. Spectra taken from the crater surroundings show small remnant highland materials are present within or beneath the mare, and it appears that the spinel signatures actually occur in highland materials rather than in the mare.

Discussion: Our new M^3 results indicate that Fe- or Cr-spinels with 0.7 μm absorptions are mixed into most of the DMD across the Sinus Aestuum highlands. The discrepancy between spinel detections made by SP and M^3 is simply a function of the more limited spatial distribution of the SP data compared to M^3 data across the SA region. Consequently, our M^3 analysis provides a more comprehensive understanding of the spinel distribution at SA. The M^3 spectra extracted from spinel-rich locations show a visible-wavelength absorption, consistent with the SP results. Not all spinel spectra exhibit a strong visible-wavelength absorption, however, especially those spectra taken from slightly older craters.

The spinel deposits are strongly correlated to the distribution of pyroclastic deposits, indicating the two materials were most likely emplaced together as part of an explosive volcanic eruption. Although the spinels and pyroclastics may have once existed as a homogeneous deposit on the highlands, mixing by craters and regolith development over billions of years has created a heterogeneous distribution of both spinels and pyroclastics within the highlands of SA, and buried the deposit beneath younger lava flows on the mare.

References: [1] Sunshine J. M. et al. (2010) *LPSC 41*, Abstract #1508; [2] Pieters C. M. et al. (2011) *JGR 116*, 1-14. [3] Yamamoto S. et al. (2013) *Geophy. Res. Letts. 40*, 4549-4554. [4] Sunshine J.M. et al. (2014) LPSC 45, Abstract #2297. [5] Melosh J. (1989) *Impact Cratering, A Geologic Process*, Oxford Univ. Press. [6] Gaither T.A. et al. (2014) *LPSC 45*, Abstract 1933.

RECENT ADVANCES IN LUNAR MAGNETISM. M. Wieczorek[1], B. Weiss[2], D. Breuer[3], M. Fuller[4], J. Gattacceca[5], J. Halekas[6], L. Hood[7], F. Nimmo[8], R. Oran[2], M. Purucker[9], K. Soderlund[10], and S. Tikoo[11]; [1]Obs. Côte d'Azur, France (mark.wieczorek@oca.eu), [2]Massacusetts Institute of Technology, USA [3]Deutsches Zentrum für Luft- und Raumfahrt (DLR), Germany, [4]Univ. Hawaii, USA, [5]CEREGE, France, [6]Univ. Iowa, USA, [7]Univ. Arizona, USA, [8]Univ. California Santa Cruz, USA, [9]NASA Goddard Space Flight Center, USA, [10]Univ. Texas at Austin, USA, [11]Rutgers Univ., USA.

Introduction. Before the Apollo missions, it was often thought that the Moon was a primordial, undifferentiated relic of the early Solar System. It was thus a great surprise when the Apollo subsatellites and surface magnetometers detected magnetic fields originating from the lunar crust.

The initial paleomagnetic analyses of the Apollo samples indicated that some rocks cooled in the presence of a magnetic field whose intensity was similar to Earth. However, the ages of these samples were unevenly distributed, and the paleointensities were uncertain. Magnetic field measurements made from equatorial orbits led to the discovery of many strong magnetic anomalies. The origin of the these anomalies, however, was complicated by the fact that most were not correlated with known geologic process, and the equatorial distribution of the orbital data left the majority of the Moon's crust unexplored. Lastly, the origin of the magnetizing field was debated, with both internal core-generated and external fields being considered.

Tremendous advancements have been made towards understanding lunar magnetism since the close of the Apollo era. Global magnetic field mapping has been achieved from orbit by the Lunar Prospector and Kaguya spacecraft. The limitations associated with lunar rocks as paleomagnetic recorders have been quantified. Models for the distribution of lunar magnetic anomalies have been proposed. The size and composition of the lunar core is now better understood, and a wide range of mechanisms for powering an internal core-dynamo field have been investigated.

In this contribution, our current understanding of lunar magnetism will be reviewed. Advances made in the past decade since the publication of the first *New Views of the Moon* book [1] will be emphasized.

Paleomagnetism. New paleomagnetic analyses have strengthened the case that the Moon once had a long-lived global magnetic field with Earth-like field strengths. These new analyses place important constraints on the paleointensity fidelity by providing minimum retrievable field strengths [2]. From a suite of modern measurements, 40-110 μT surface field strengths were present from at least 4.25 to 3.56 Ga, after which the surface strength decreased rapidly to less than 10 μT at 3.3 Ga [3]. These samples recorded their natural remanent magnetization too slowly to have been magnetized by transient impact-generated fields and require a long-lived field such as that generated by a core dynamo. The time when the dynamo started and stopped, however, is currently unknown, in large part due to a lack of suitable young and ancient samples.

Crustal Magnetism. Magnetometer data collected by the polar orbiting Lunar Prospector and Kaguya spcecraft have permitted the construction of global magnetic field maps of the Moon [4,5,6]. Some impact basins possess weak anomalies in their interiors, where an impact melt sheet should be present [7]. The largest concentration of anomalies is however located on the farside on the northern rim of the South Pole-Aitken impact basin. These anomalies may represent the remanents of the iron-rich projectile that formed this basin [8], ejecta deposits antipodal to the largest nearside basins [9], or dikes that were later emplaced in the crust [10]. Many strong anomalies have no correlation with geologic processes, and given that most lunar rocks possess low abundances of metallic iron, the origin of these anomalies remains enigmatic.

Core dynamo modeling. Both the crustal magnetic field and paleomagnetic analyses suggest that the Moon once possessed a core dynamo. Possible scenarios for powering a dynamo include thermal convection as the core cooled quickly after lunar formation, later core crystallization, precession of the mantle spin axis, and impact-induced changes in lunar rotation. Thermal convection is a relatively short-lived process, operating during the first few 100 million years of lunar evolution [11]. Once the core begins to crystallize, between about 4-4.4 Ga [12], buoyancy driven chemical convection can power a dynamo for about a billion years [13]. More exotic energy sources have also been proposed to power the lunar dynamo. Precession of the solid mantle spin axis can power a prolonged dynamo between about 4.25 to 2.7 Ga [14], and changes in rotation of the lunar spin axis following large basin forming impact events can potentially power short-lived dynamos for 10s of thousands of years [15].

References. [1] Wieczorek et al. (2016), [2] Tikoo et al. (2014), [3] Weiss and Tikoo (2014), [4] Richmond and Hood (2008), [5] Purucker and Nicholas (2010), [6] Tsunakawa et al. (2015), [7] Hood (2011), [8] Wieczorek et al. (2012), [9] Hood et al. (2013), [10] Purucker et al. (2012), [11] Konrad and Spohn (1997), [12] Laneuville et al. (2014), [13] Scheinberg et al. (2015), [14] Dwyer et al. (2011), [15] Le Bars et al. (2011).

NEW RESULTS FROM THE CHANG'E-3 OPTICAL INSTRUMENTS. Y. Z. Wu[1], Z. C. Wang[2], Y. Lu[3], [1]Key Laboratory of Planetary Sciences, Purple Mountain Observatory, Chinese Academy of Sciences, Nanjing 210008, China (wu@pmo.ac.cn). [2]Department of Earth Sciences, Nanjing University, Nanjing 210023, China, [3]School of Geographic and Oceanographic Sciences, Nanjing University, Nanjing 210023, China.

Introduction: The Chinese CHANG'E-3 (CE-3) spacecraft landed in northern Mare Imbrium, east of the rim of a ~110 Ma crater currently named Zi Wei (44.12°N, 19.51°W). The *in situ* detection was performed by various instruments on the "Yutu (Jade Rabbit)" rover which travelled for ~114 m within 2 months. Here we present the results from four optical instruments on the rover and lander. The two optical instruments onboard the rover are the VIS/NIR Imaging Spectrometer (VNIS) and the Panoramic Cameras (PCAM), and the other two onboard the lander are the terrain camera (TCAM) and the descent camera.

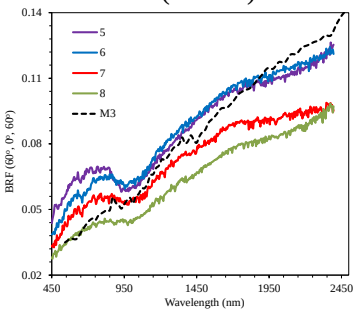

Fig. 1. The VNIS spectra of 4 sites. Site 5 is the closest to the lander and Site 8 is the furthest away.

Space weathering revealed by the VNIS: Four measurements of the regolith (sites 5, 6, 7 and 8; Fig. 1) were made by the VNIS. Reflectance increasing after spacecrafts landed have been observed for CE-3, Apollo, Luna, etc [1-4]. These studies suggest that smoothing of surface roughness is the main cause of the observed increase in reflectance and exposure of less mature soil was rejected because the maturity of core samples within the first tens of centimeters of regolith depth do not change significantly. The four spectra show that the reflectance, absorption strength, visible slope, and optical maturity (OMAT) all increase for sites closer to the lander, it suggests that:

1) brightness increases after the spacecraft landed are due to removal of the finest, highly weathered particles, not smoothing of the surface.

2) the uppermost surficial regolith is much more weathered than the regolith immediately below.

3) the finest fraction is much more mature than the coarser fraction.

4) the effects on the spectral slope caused by space weathering are wavelength-dependent: increasing the near-infrared continuum slope (VNCS) while decreasing the visible slope. That is, the *in situ* spectra reveal an opposite trend in the visible slope with respect to space weathering to the previously known trend. It is consistent with the ultraviolet observations for the Moon [5] and asteroids [6] and extends to the visible bands.

Young tectonism around CE-3 landing site: Recent studies found a lot of young tectonic activities on the moon [7-9]. The descent camera, PCAM, and LROC NAC all show small wrinkle ridges passed the Zi Wei crate (Fig. 2). To the north of Zi Wei, a younger crater (~50 Ma) was disturbed by the ridge, indicating the ridge is younger than 50 Ma.

By our global survey [10], the youngest ridges are mostly distributed inside Mare Imbrium, suggesting this area experienced more protracted thermal and structural evolution. The youngest wrinkle ridges also imply that the moon is probably active today.

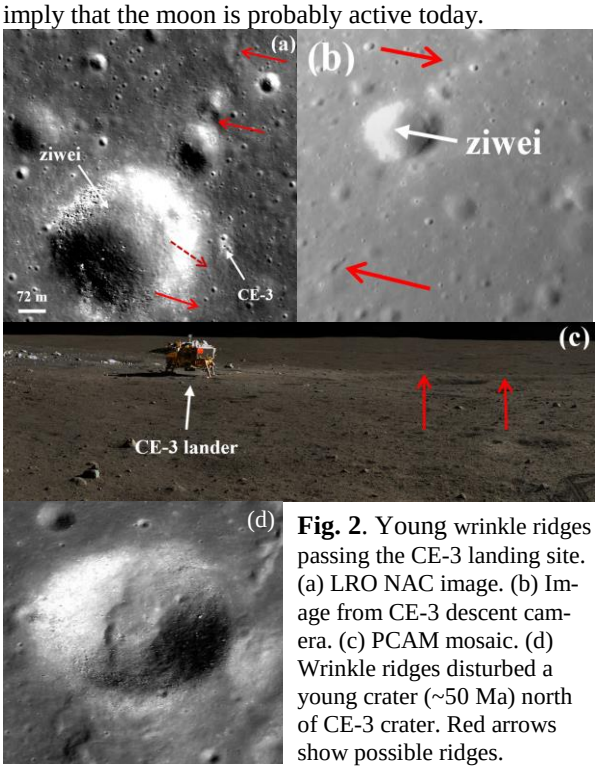

Fig. 2. Young wrinkle ridges passing the CE-3 landing site. (a) LRO NAC image. (b) Image from CE-3 descent camera. (c) PCAM mosaic. (d) Wrinkle ridges disturbed a young crater (~50 Ma) north of CE-3 crater. Red arrows show possible ridges.

References: [1] Kaydash V. et al. (2011) *Icarus*, 211(1), 89-96. [2] Shkuratov Y. et al. (2013) *Planet Space Sci.*, 75(1), 28-36. [3] Clegg R. N. et al. (2014) *Icarus*, 227(1), 176-194. [4] Clegg R. N. et al. (2016) *Icarus*, 273, 84-95. [5] Denevi B. W. et al. (2014) *JGR*, 119(5), 976–997. [6] Hendrix A. R. and Vilas F. (2006) *Astron. J*, 132(3), 1396. [7] Watters T. R. et al. (2012) *Nature geosci.*, 5, 181-185. [8] Williams N. R. et al. (2016) *LPSC, XLVII*, 2808. [9] Clark J. D. et al. (2017) *LPSC, XLVIII*, 1001. [10] Wu Y. Z. et al. (2016) *LPSC, XLVII*, 1406.

LUNAR METEORITES: A GLOBAL GEOCHEMICAL DATASET. R. A. Zeigler[1], K. H. Joy[2], T. Arai[3], J. Gross[4], R. L. Korotev[5], F. M. McCubbin[1]. [1]NASA – Johnson Space Center, Houston TX 77058, [2]SEAES, University of Manchester, Manchester, UK; [3]Planetary Exploration Research Center, Chiba Institute of Technology, Chiba, Japan. [4]Rutgers University, Piscataway, NJ 08854; [5]Washington University in St. Louis, St. Louis MO, 63130.

Introduction: To date, the world's meteorite collections contain over 260 lunar meteorite stones representing at least 120 different lunar meteorites. Additionally, there are 20-30 as yet unnamed stones currently in the process of being classified. Collectively these lunar meteorites likely represent 40-50 distinct sampling locations from random locations on the Moon. Although the exact provenance of each individual lunar meteorite is unknown, collectively the lunar meteorites represent the best global average of the lunar crust. The Apollo sites are all within or near the Procellarum KREEP Terrane (PKT), thus lithologies from the PKT are overrepresented in the Apollo sample suite. Nearly all of the lithologies present in the Apollo sample suite are found within the lunar meteorites (high-Ti basalts are a notable exception), and the lunar meteorites contain several lithologies not present in the Apollo sample suite (e.g., magnesian anorthosite).

Chapter Summary: This chapter will not be a sample-by-sample summary of each individual lunar meteorite. Rather, the chapter will summarize the different types of lunar meteorites and their relative abundances, comparing and contrasting the lunar meteorite sample suite with the Apollo sample suite. This chapter will act as one of the introductory chapters to the volume, introducing lunar samples in general and setting the stage for more detailed discussions in later more specialized chapters.

The chapter will begin with a description of how lunar meteorites are ejected from the Moon, how deep samples are being excavated from, what the likely pairing relationships are among the lunar meteorite samples, and how the lunar meteorites can help to constrain the impactor flux in the inner solar system. There will be a discussion of the biases inherent to the lunar meteorite sample suite in terms of underrepresented lithologies or regions of the Moon, and an examination of the contamination and limitations of lunar meteorites due to terrestrial weathering.

The bulk of the chapter will use examples from the lunar meteorite suite to examine important recent advances in lunar science, including (but not limited to the following: (1) Understanding the global compositional diversity of the lunar surface; (2) Understanding the formation of the ancient lunar primary crust; (3) Understanding the diversity and timing of mantle melting, and secondary crust formation; (4) Comparing KREEPy lunar meteorites to KREEPy Apollo samples as evidence of variability within the PKT; and (5) A better understanding of the South Pole Aitken Basin through lunar meteorites whose provenance are within that Terrane.

Chapter changes since the NVM II 2016 Workshop: There are no significant changes to the content of the chapter since the 2016 NVotM 2 conference.